Cellulose Nanocrystals (CNCs) Nanocomposite Films for Sustained Release of CNCs and Enhanced Anti-biofouling Property

by

Tong Liu

A thesis submitted in partial fulfilment of the requirements for the degree of

Master of Science

in

Civil (Cross-disciplinary)

Department of Civil and Environmental Engineering

University of Alberta

Abstract

Cellulose nanocrystals (CNCs) are nanoparticles with high aspect ratios and excellent surface tunability and are processed from renewable bioresource. CNCs possess unique surface and colloidal properties, which makes it efficient flocculant agents to separate colloidal sized bacteria from their aqueous dispersion. Efforts were made to utilize this property to develop disinfecting technology suitable for biomedical applications, particularly for biofilm prevention on indwelling catheters. Fabrication of nanocomposites that incorporate CNCs and other biopolymers offers a new opportunity to develop CNCs based antifouling materials with long-lasting performance, low toxicity, and minimized environmental problems. In this study, nanocomposite films incorporating natural rubber (NR) latex and CNCs were developed to achieve sustained release of CNCs into the aqueous solutions and to ultimately improve the antifouling performance against biofilms. The nanocomposite films were prepared by a facile approach of casting and evaporation. The obtained nanocomposite films were characterized by various analytical techniques. The release behaviours of CNCs from the nanocomposite films was studied by fluorescein labeling techniques based on the use of 5-(4, 6-Dichlorotriazinyl) aminofluorescein (DTAF), and the release process in various aqueous mediums was modeled by modified first-order mass transport model. Materials characterizations were conducted to understand the nanoparticles (CNCs) release mechanisms: the intermolecular interactions between the CNCs and NR latex were studied by FT-IR, the morphology and microstructure were observed by scanning electron microscope (SEM); the mechanical and thermal properties of the nanocomposite films were tested by dynamic mechanical analysis (DMA).

In the second part, the obtained NR/CNCs nanocomposite films were incorporated with silver particles to further enhance their long-term antifouling performance. NR/CNCs nanocomposite films were used as template materials for the synthesis and deposition of nano to micro-sized silver particles. A green synthesis approach based on reaction between the nanocomposite films and silver nitrate solution were employed. The impact of CNCs contents, green synthesis reaction time, on the silver particles formation were evaluated. The silver release behavior of the silver particle modified nanocomposite films were studied by a seven-day silver release test facilitated by ICP-OES. The antifouling performance of all nanocomposite films was evaluated by bacteria adhesion assays conducted under static and continuous flow settings.

Preface

The research for this thesis was conducted under the supervision of Dr. Yaman Boluk and Dr. Yang Liu at the University of Alberta. Part of research covering chapter 3, 4 and 5 has been published as Gong, X.; Liu, T.; Zhang, H.; Liu, Y.; Boluk, Y. "Release of cellulose nanocrystals particles from natural rubber latex composites into immersed aqueous media". *ACS Applied Bio Materials* 4.2 (2021): 1413-1423. The publication was co-first-authored by me and Dr. Xiaoyu Gong. I was in charge of performing experiments and data analysis, and composing the manuscript, while my supervisors provided guidance and comments on the manuscript writing. Dr. Xiaoyu Gong participated in experimental design, manuscript compositions and minor portion of the experimental analysis.

Dedication

I dedicate this work to my family, friends and senior fellows in academia who support me in every endeavor I seek.

Acknowledgement

First of all, I would like to express my sincere gratitude to my supervisors, Dr. Yaman Boluk and Dr. Yang Liu for giving me an opportunity to develop academically in this exciting research project. Their timely guidance, kind support, and valuable inspirations never ceased to motivate me to become a better researcher.

I would like to thank all members of the two research groups I was part of, especially Dr. Xiaoyu Gong, Dr. Huixin Zhang, and Dr.Yussef Esparza. Special thanks to Mr. Jonathan Stolz, Mr. Karthik R Shivakumar, Ms. Anika Benozir Asha, Mr. Casey Rusin, Dr. Huijuan Sun, Ms. Anqi Mou, and Ms. Xin Zou, who helped me with the experiments and offering me advice regarding to my research. Their support has made my MSc studies an unique academic journey.

In addition, I want to thank Ms. Shiau-Yin Wu in Nanofab for helping me on the FE-SEM analysis and trainings, and Dr. Nasser Tahbaz for helping me with the TEM analysis.

Last but not least, I would like to express my greatest gratitude and appreciation to my mother, who offered me unconditional support both spiritually and materially for my seven-year studies in Canada. Her guidance and support have always motivated me to explore my values both in life and in my career. Without her, I would not have gone this far in life and in academical study.

Table of Contents

List of Tables

List of Figures

List of Abbreviations and Symbols

CAUTIs	Catheter Associated Urinary Tract Infections
EPS	Extracellular Polymeric Substances
NPs	Nanoparticles
CNCs	Cellulose Nanocrystals
NR	Natural Rubber
phr	Parts Per Hundred Rubber
DTAF	5-(4,6-dichlorotriazinyl) aminofluorescein
E. Coli	*Escherichia coli*
S. Aureus	*Staphylococcus aureus*

Chapter 1 INTRODUCTION

1.1 Introduction

Urinary catheterization is a typical in-hospital post-operative procedure. A catheter tubing that provides passage for urine collection is inserted into the patient's urinary bladder through urethra and remain in-situ, typically for over 7 days (Lawrence & Turner, 2005; Nacey & Delahunt, 1993; Singha et al., 2017). When urine is drained, bacteria from the urine, can migrate, diffuse, and adhere on the inner wall of catheter tubing, leading to the biofilm formation. Biofilms facilitate the survival of bacteria in a hostile environment and provide increased resistance against host's defenses responses and antimicrobials. Infections affecting the urinary tracts due to biofilms formed on catheters are commonly known as catheter associated urinary tract infections (CAUTIs). These infections significantly increase the patient's morbidity and the associated medical expenses and can only be effectively treated by the removal of catheters. In 2011, there were over 56000 cases of CAUTIs in US alone, with the total annual costs of the treatment being as high as $1.8 million (Umscheid et al., 2011). Effective and long-lasting biofilm preventative technologies are needed to reduce biofilm related infections and minimize the catheterization failures.

Conventional biofilm preventative materials can be classified as antimicrobial and antifouling materials. Antimicrobial materials suppress biofilm formation by killing microbes that approach the surface and in the surrounding aqueous environment. Clinically, however, the use of antimicrobials could lead to many concerns and complications such as the development of microbial resistance, environmental contaminations due to the emission of harmful materials, and the toxicity to human due to the biocidal diffusion (Seabra & Durán, 2015; Singha et al., 2017). In

comparison, antifouling materials reduce the biofilm formation by inhibiting the initial bacterial adhesion. Modifications to achieve antifouling surfaces involve in the use of hydrophilic antifouling coatings based on polymers such as PEG and poly(zwitterions) and surface micropatterning methods (Damodaran & Murthy, 2016; Singha et al., 2017). Both methods have shortfalls. PEG and polyzwitterions based coatings have limited long-term stability and can irreversibly degrade with prolonged use. Surface micropatterning are challenged with limited applicability and processing complexity (Damodaran & Murthy, 2016). The limitations of these materials have driven the exploration of more efficient and long-lasting biofilm preventative materials. Ideal anti-biofouling materials should not only possess low material toxicity, good biocompatibility, and long-term stability, but also incurs low fabrication challenges, and minimized environmental impact (Kenawy et al., 2007).

Cellulose nanocrystals (CNCs) are renewable, biodegradable, and nontoxic nanomaterials processed from natural biomass (Dufresne, 2013; E. J. Foster et al., 2018). CNCs possess excellent surface tunability, unique optical and colloidal properties and are biocompatible to be used in biomedical applications. CNCs are efficient flocculant for colloidal sized bacteria. At volume concentration of as low as 0.1%, anionic CNCs particles having ~100 nm in length and ~12 in geometric aspect ratio can flocculate, and phase separate bacteria from their colloidal dispersions by up to 99%, consequently reducing the bacterial adhesion on surfaces (Sun et al., n.d., 2012, 2015). With these characteristics, CNCs based materials have great potential to be used for biofouling prevention and are potential alternatives to current antimicrobial and antifouling materials.

Natural rubber processed from *Hevea Brasiliensis* tree is a naturally occurring polymer, which consists of poly(cis-isoprene) and minor components of protein, carbohydrates and phospholipids (Mooibroek & Cornish, 2000; Nawamawat et al., 2011). Natural rubber has excellent flexibility and strength, and good resistance to water and certain chemicals (Lawrence & Turner, 2005). Because of the excellent matrix forming property, NR latex was used to fabricate controlled drug release (delivery) systems for a wide variety of therapeutic compounds (Danna et al., 2016; Donizetti et al., 2009; Herculano et al., 2010; Miranda et al., 2017; Pichayakorn et al., 2012). Previous studies have demonstrated the promising long-term release capacity of these drug delivery systems. By modifying the surface characteristics and properties like hydrophilicity and pore characteristics, it was possible to control the drug release process and to achieve controlled and long-term release of the compounds.

Dispersions of CNCs in various NR systems have been investigated with a focus on reinforcing and crosslinking properties for addressing divers applications such as composite materials, tires and adhesives (Lawrence & Turner, 2005; Mooibroek & Cornish, 2000). Homogeneous dispersion of CNCs was successfully achieved in various types of NR matrices and has resulted in substantial increase of the material's performance, including the mechanical, barrier and swelling properties. Thus, CNCs incorporated NR nanocomposite films offer a potential opportunity not only for enhancing the materials' processability through effective improvement of various properties, but also allows for controlled delivery of CNCs to provide effective, and long-term biofilm prevention (E. J. Guidelli et al., 2011; É. J. Guidelli et al., 2013).

1.2 Hypothesis

Compositing CNCs into natural rubber latex is an approachable way to fabricate drug delivery systems for controlled release of CNCs. Polymeric nanocomposite films that incorporate CNCs and NR can be prepared by mixing and casting aqueous suspensions of the two components, followed by solvent evaporation and film conditioning. Incorporation of hydrophilic fillers in NR latex at high concentration can drastically increase the water sensitivity of the films, resulting in an improved water permeation into the films (Mariano et al., 2016; Tian et al., 2017; Yin et al., 2018). Diffusion of aqueous solvent within the polymer matrix causes nanocomposite films to swell, which generates micro-openings on the surface of the material (Langer, 1990; Pichayakorn et al., 2012; Yin et al., 2018). Relaxations of polymers during swelling creates micro-channels in the bulk of materials, which provides efficient pathways for CNCs to migrate from the inner portion to the surfaces of the pores and micro-opening.

Pore size and density are key surface characteristics that determines the drug release behavior in the NR latex based drug delivery systems (Herculano et al., 2010; Miranda et al., 2017) With optimal control of these characteristics, release behaviors can be optimized. Casting/ evaporation method offers advantage over other processing methods as it allows for easy control over the pore characteristics. This can be simply achieved by modifying the processing conditions such as casting temperature, water evaporation time, and polymerization temperature.

Incorporating silver particles into the nanocomposite system is a promising approach to enhance the antifouling performance of the film. Silver is a common antibacterial agent, which has proven effectiveness against a wide range of infections associated bacteria, including *Escherichia Coli*, *Staphylococcus Aureus* and *Pseudomonas Aeroginosa* (Krishnaraj et al., 2010). Nano to micro sized silver particles (< 1000 nm) possess great surface-to-volume ratio and high reactivity

to bacterial cellular components, and can delivered silver ions into the surrounding microenvironment through controlled Ag^+ dissolution and oxidation of elemental silver (Damm et al., 2007; J. Li et al., 2019; Pugliara et al., 2015). NR latex is an excellent material to synthesize and grow metallic AgNPs. NR latex contains bio-reductant compounds, which can be used to reduce ionic silver to elemental silver under high energy treatment such as heating and irradiation process. The process is known as green synthesis. The presence of CNCs in the nanocomposite films can further affect AgNPs synthesis process as CNCs provide additional binding sites for silver nanoparticles. The high binding affinity of silver surface to the sulphate ester groups promotes the deposition of AgNPs on CNCs. Thus, it can be hypothesized that the NR/CNCs nanocomposite films is a great candidate template material to grow surface embedded silver particles and with the control of CNCs contents, the morphological characteristics of silver particles can be well controlled (Liu et al., 2011; Lokanathan et al., 2014).

1.3 Research Objectives

The overall objective of this work is to develop a CNCs based nanocomposite film that can suppress biofilm formation through long-term and sustained release of CNCs and antibacterial silver. The specific objectives are outlined below.

1. To prepare nanocomposite films using cellulose nanocrystals and natural rubber latex.
2. To develop appropriate mathematical models to characterize the release of CNCs from nanocomposite films in aqueous mediums.
3. To investigate the impact of physiochemical conditions (ionic strength, pH) on the CNCs release process.

4. To characterize the nanocomposite films with focuses on mechanical properties (DMA, tensile testing), morphological studies (SEM, TEM, AFM), and structural analysis (ATR-FT-IR)

In the second part, NR/CNCs nanocomposite films were used as reacting template to synthesize silver particles. Additional objectives are implemented as follow.

1. To synthesize and deposit nano to micro-sized silver particles on the NR/CNCs nanocomposite films using green chemistry approach.
2. To analyze the effect of CNCs on the characteristics of surface embedded silver particles (i.e. particles size, morphology)
3. To evaluate the Ag^{+} release capacity of the silver particles embedded nanocomposite films in the aqueous mediums
4. To evaluate the antifouling performance of all synthesized nanocomposite films under static and continuous flow settings

1.4 Thesis organization

Chapter 1 presents the detailed background information, hypothesis, and the research objectives of this study. Chapter 2 details a complete and broad literature review. This section contains the introduction of current biofilm preventative strategies and their applications on biomaterials, the roles of CNCs and silver nanoparticles on bacteria adhesion prevention, preparation techniques for CNCs based nanocomposite materials, and a brief review on relevant drug release models. Chapter 3 presents materials and methods for the synthesis and characterizations of NR/CNCs nanocomposite films and silver particles embedded NR/CNCs nanocomposite films. In chapter 4, results and discussions of the experimental studies was detailed: The release behaviors of CNCs in aqueous solutions was characterized using modified mass transport models; The surface properties, dynamic mechanical characterizations, and intermolecular interaction within the NR/CNCs nanocomposites are discussed as well as the silver release behaviors of the silver particles embedded NR/CNCs nanocomposite films. Furthermore, the antifouling performance of all nanocomposite films was discussed. Chapter 5 summarized the thesis study and provides the future recommendations regarding to the improvement of nanoparticle release and antifouling performance of the nanocomposite materials.

Chapter 2 LITERATURE REVIEW

2.1 Bacterial adhesion and biofilm formation

2.1.1 Biofilms

The microbial biofilm is a self-producing consortium comprised of aggregated bacteria secreting extracellular polymeric substances (EPS). The biofilm plays an important role in the pathogenesis of biofilm-related infections and is responsible for 80% of hospital acquired infections (Kenawy et al., 2007). Bacteria responsible for catheter biofilm development are primarily gram negative bacteria, which include *Escherichia Coli, Pseudomonas Aeruginosa, Bacilius Proteus*, and *Bacilius aerogenes* (Stoodley et al., 2002). Bacteria biofilm forms on a surface in a process consisting of three phases, namely, (1) the initial reversible adhesion (2) irreversible attachment, (3) maturation and dispersion. In the first stage, planktonic bacteria in the liquid environment adhere on a surface through a weak, reversible interaction of Van Der Waal forces, electrostatic attraction, hydrophobic interaction or target specific binding (An & Friedman, 1998). In the second stage, bacteria aggregate and reinforce their attachment through appendage anchorage. In the third stage, bacteria communicate with each other through the gene transfer and secrete extracellular polymeric substances (EPS) to strengthen their aggregation. Matured biofilms can degrade, collapse, and release motile planktonic bacteria into the surrounding microenvironment. A new cycle of biofilm formation process is then started (Gupta et al., 2016).

Biofilms provide increased protections and resistance against antimicrobials and the host immunome system response, primarily through three possible mechanisms: 1) the reduced antimicrobial transport within the biofilm due to the presence of EPS; 2) the presence of antimicrobial resistant phenotypes called persister cells that are in the dormant state; 3) the change

of the microenvironment in the biofilm due to the accumulations of the waste and acidic metabolic compounds (Lewis, 2007) . Due to these protective mechanisms, biofilm associated bacteria have increased resistance against antimicrobials and most antimicrobials have little to no effect in eradicating biofilms that have already formed. The removal of matured biofilm replies exclusively on the strategies that work to disrupt biofilm structure or inhibit the growth of bacteria in biofilms.

Inhibitory strategies that target each phase of the biofilm formation process were listed in Figure 2.1. Preventative strategies taking effect at various stages of the biofilm formation process range from anti-adhesion surface coatings to the disruption of biofilm structure like QS signal interference, and benign bacteria interference.

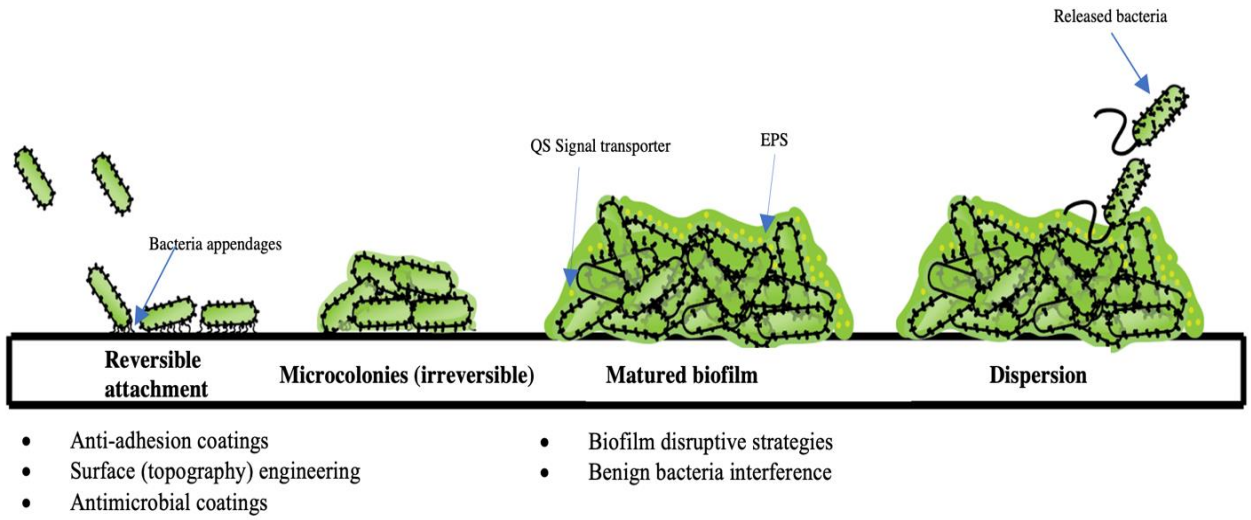

Figure 2.1. Inhibition strategies for each phase of the biofilm formation process.

2.1.2 Antimicrobial approach

Antimicrobials are materials that carry out biocidal activity against a wide range of microbial pathogens, which include bacteria, fungi, and protozoa, and virus. They can be classified based on their functions against the microbes. For instance, agents that act to kill microbes are

referred as microbiocidal agents, agents that inhibit microbial growth are termed as biostatic (Singha et al., 2017). Current efforts to advance antimicrobial technologies for applications on urinary catheters mainly focuses on the innovations of long-lasting, effective antimicrobial urinary catheter coatings. Antimicrobial coatings can be categorized based on their schemes of actions into, 1) release of antimicrobials 2) contact-active killing 3) the disruption of biofilm structure, and 4) benign bacteria interference (Francolini et al., 2017; Singha et al., 2017; Yang et al., 2012).

Antimicrobial agents commonly studied for urinary catheter coating applications are outlined in Figure 2.2. Only silver coatings and antibiotics coatings are FDA approved for urinary catheter applications (Singha et al., 2017).

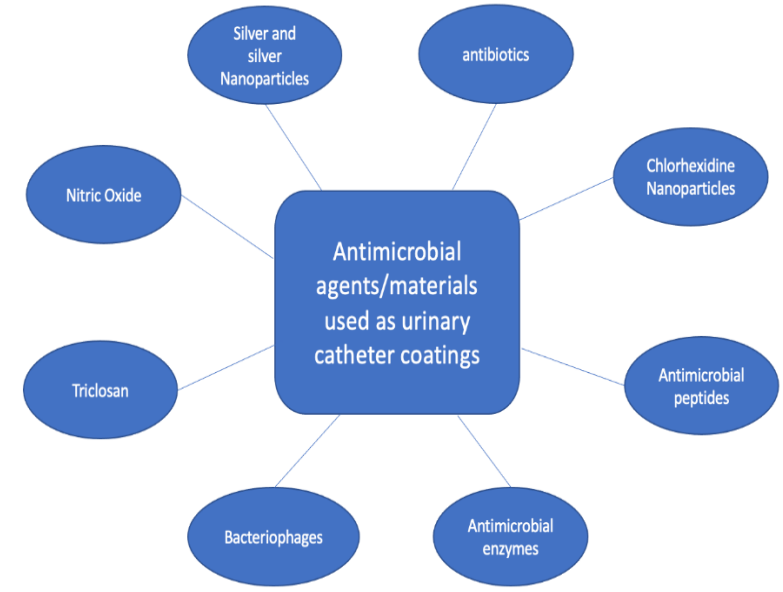

Figure 2.2. Antimicrobial agents used on urinary catheters

The release based antimicrobial coatings are designed for sustained release of antimicrobials in sufficient concentrations at a potential colonization site. The most common

antimicrobial coatings using this scheme are silver coatings, antibiotics coatings, surface modifications by bactericidal enzymes and bacteriophages. Despite their promising antibacterial activity, they all have shortfalls. For example, silver impregnated catheters become ineffective in inhibiting biofilm growth with the exhaustion of silver. The use of antibiotics coatings can lead to the development of microbial resistance. Bactericidal enzymes and bacteriophage coatings are subject to denaturation and the loss of biological activity under extreme conditions (Singha et al., 2017).

Contact killing coatings perform biocidal activity through their surface exposed antimicrobial groups. Such type of materials is usually fabricated by immobilizing antimicrobials on its surface through chemical conjugations or physical adsorption (Francolini et al., 2017). Contact-killing coatings are considered promising alternative to release-based coatings as they do not emit biocidal agents to the bodily fluids and do not exhaust with long-term usage. The performance of contact killing coatings, however, can be compromised by a series of factors, which include non-specific bindings, insufficient AMPs surface densities, ineffective molecular orientations, and pH sensitivity issues. The typical antimicrobials used for contact killing coatings are antimicrobial peptides (AMPs), carbon nanotubes, and graphene oxides (Singha et al., 2017).

Biofilm disruption coatings are designed to destroy biofilms that have already formed on the catheters. Disruption of matured biofilms can be achieved by biochemically induced biofilm degradation and inhibition of biofilm growth. The typical biofilm disruptive strategies used on urinary catheter coatings include enzyme-based EPS dissociation approach, quorum sensing (QS) signal interference approach, and nitric oxide releasing coatings (Singha et al., 2017).

Benign bacteria interference is another approach that recently attracts attention. Benign bacteria disrupt pathogenic biofilms through several mechanisms, including competitions for nutrients and colonization sites, inhibition by antibacterials, and the regulations of biofilm gene expression (Darouiche & Hull, 2012). Benign bacteria can be introduced into the catheter systems by either inoculating the patient's bladder with benign bacteria strains or coating urinary catheters with pre-established benign biofilms before catheterization (Horwitz et al., 2015; Lopez et al., 2011).

2.1.3 Antifouling strategies

Bacteria adhesion initiates with the anchorage of its adhesin proteins on a surface. Antifouling materials like antifouling hydrophilic polymers, resists the protein adsorption and subsequent bacteria adhesion through electrostatic, and/or steric repulsions. Creating antifouling surfaces on indwelling medical devices can be achieved by either chemically modifying the surface compositions or physically altering the surface topography (Damodaran & Murthy, 2016; Francolini et al., 2017).

2.1.3.1 Hydrophilic coatings

The most common antifouling hydrophilic coating materials for catheter coating applications include 1) hydrophilic polymers, 2) Poly (ethylene glycol) (PEG) based polymers, 3) zwitterionic polymers. These polymers possess strong water-binding affinity due to their unique surface chemistry and macromolecular structure. For example, antifouling properties of PEG are related to surface hydration and steric hinderance. PEG molecules assume brush-like configurations at the surface/water interface and form a hydration layer via hydrogen bonding around molecular chains to restrict bacteria approach to the surface (Roosjen et al., 2004). As their

counterpart, Polyzwitterionic coatings resist non-specific protein adsorption through both electrostatic repulsion and steric hindrance. Polyzwitterionic polymers bears equimolar number of homogeneously distributed cationic and anionic groups on their molecular backbones, which renders them neutral in charge. Compared to PEG based materials, zwitterions have a broader structural diversity and greater freedom for molecular design and material selections. Zwitterionic polymers can be designed to switch between cationic forms and anionic forms, which allows them to perform simultaneous antifouling and antibacterial actions. For example, (Mi & Jiang, 2014) designed an antibacterial surface based on zwitterionic poly (carboxybetaine) ester precursor. The designed poly (zwitterion) surface was able to hydrolyse with prolonged exposure to aqueous solution. This type of materials kills bacteria attached on the surface at the initial in-vitro stage through its cationic ethyl ester groups, which switch to anionic carboxylates via a controlled hydrolysis process to resist dead bacteria from the surface and further prevent planktonic bacteria from attaching.

2.1.3.2 Modifications of surface topography

Alternatively, antifouling properties can be introduced into surfaces by altering the surface topography, typically in a physical technique known as surface micro-patterning. Surface topography in μm scale affects the attachment of cells. Materials can be engineered with desirable surface topography and texture to lower the surface energy, which impairs the attachment of bacteria (Damodaran & Murthy, 2016; Francolini et al., 2017). Biomimetic micropatterning technologies have recently attracted attentions. One of the most successfully reproduced bio-inspired antifouling micropatterning designs are lotus inspired “superhydrophobic” self-cleaning surfaces. Fabricated surfaces contain micro-scaled mould structure, decorated with nano-scaled hydrophobic “waxy” surface. Air trapped inside the cavities between convex cones prevents the

wetting of surfaces, making the material superhydrophobic. The contact angle of 90° to 150° can be achieved with this design. Generally, fabrication of superhydrophobic materials involves surface etching or incorporation of materials such as nanoparticles, mesoporous polymers, and sometimes, chemical modifications (Damodaran & Murthy, 2016; Francolini et al., 2017; Loo et al., 2012). The major challenge for this type of technologies is the limited applicability of micropatterned surfaces in fabrication. Due to the harsh processing conditions and complicated fabrication procedures, micropatterning technologies are less widely used in medical industry than hydrophilic coatings (Damodaran & Murthy, 2016).

2.2 Nanomaterials with anti-adhesion and antibacterial properties

2.2.1 Nanoparticles (NPs)

Nanoparticles (NPs) are materials with size in nanometer range (1 to 100 nm) Due to their small size and large surface-to-volume ratio, NPs possess unique physical and chemical properties that are not commonly found in their macroscopic counterparts (Dizaj et al., 2014; Rai et al., 2009; Wang et al., 2017). Important properties such as particle morphology, physical structures, and surface chemistry can be tailored to obtain desirable chemical or biological properties for antimicrobial applications. Commonly reported antimicrobial NPs include metal and metal oxide NPs, fullerene (C_{60}) NPs, carbon nanotubes (CNT), and polymeric NPs (Dizaj et al., 2014; Q. Li et al., 2008). The mechanism of biocidal action is mainly due to their direct contact with the microbes through membrane structures, which cause the loss of cellular integrity, disruption of cellular metabolisms, and eventually cell death. Surface composition, particle size and transport are the three major factors that contribute to the NP toxicity to bacteria (Wang et al., 2017).

Introducing polymeric NPs into the bacterial colloidal system have been proposed recently as a strategy to separate bacteria from solution and reduce the initial bacterial adhesion on a surface (L. L. Foster et al., 2019; Sun et al., n.d., 2012) . Bacterial interaction with certain cationic polymers potentially leads to the change of bacterial aggregation and growth behaviors. For examples, colloidal sized bacteria can interact with smaller polyelectrolytes through a series of aggregating mechanisms such as polymer bridging, charge neutralization, and depletion flocculation (L. L. Foster et al., 2019). Aggregated bacteria have lower diffusion coefficient than single bacteria cell and therefore could experience reduced convective-diffusive transport to the solid surface, resulting in reduced bacterial initial adhesion (Sun et al., n.d., 2015). Based on the flocculation mechanisms, polymers that promotes bacterial aggregations can be classified as adsorbing polymers and non-adsorbing polymers.

2.2.1.1 Adsorbing polymers

Destabilization of a bacterial colloidal system occurs when the bacterium-bacterium inter-molecular forces became unbalanced (Lekkerkerker & Tuinier, 2011). In a stable colloidal system, Bacteria are inert, negatively charged particles. The interaction between two bacteria are dominated by electrostatic repulsive interactions, which prevents them from clustering (Liang et al., 2007). When small, charged polymers are being introduced, the repulsive forces between bacteria are gradually overcome by steric attractive forces, resulting in the destabilization of the colloidal system. Bacterial aggregations due to the presence of adsorbing polymers occurs mainly through three mechanisms, which are charge neutralization; polymer bridging and mutual dehydration (Harris & Mitchell, 1973). Polymer are adsorbed onto bacterial surface through Brownian motion and attractive forces like electrostatic and hydrophobic interactions. They then

form macromolecular chains that extend out and bridge adjacent bacterium from the surrounding environment, leading to the floc formation (Harris & Mitchell, 1973; Larsen et al., 2008).

Both non-ionic and cationic polymeric NPs can flocculate a bacterial system through adsorption induced mechanism. For example, (Larsen et al., 2008) demonstrated that cationic chitosan nanoparticles can flocculate colloidal sized *Escherichia Coli,* through polymer bridging. In this study, cationic chitosan nanoparticles were synthesized by ionic gelation with sodium triphosphate (TTP). The nanoparticles (380 nm in diameter) were highly positively charged (zeta potential = +51.1 mV) and can cluster over 90% of bacteria within seconds in a solution at neutral condition. (Treweek & Morgan, 1977) investigated the role of high molecular weight Polyethyleneimine (PEI) in bacterial aggregation. High molecular weight PEI showed more promising flocculation inducing effect against *E. Coli* bacteria than low molecular weight PEI. Larger PEI molecules not only neutralized the negative charges at the adsorption sites, but also caused local charge reversal on the bacterial surfaces through the presence of longer, surface attached cationic polymer tails. In comparison, less effective bacteria coagulation was caused by the reduction of electrostatic double layer energy induced by the adsorption of small PEI polymers on the bacteria surfaces (Treweek & Morgan, 1977).

2.2.1.2 Non-adsorbing polymers

With appropriate solution chemistry, the presence of repelling polymers can destabilize the colloidal system of larger bacterial particles. This process occurs as a result of depletion interactions between the bacteria cells and likely charged polymeric nanoparticles (Jenkins & Snowden, 1996). Figure 2.3 schematically illustrates the depletion flocculation of two colloidal

particles in the presence of non-adsorbing (repelling) polymers. On the diagram, large colloidal particles are represented as hard spheres, each with a radius of R, in a solution of polymer. Each colloidal particle is surrounded by a depletion layer, where the polymer coils cannot enter. For colloidally stable particles, the polymer concentration at the inter-particle space is equal to the bulk's concentration. The depletion mechanism is triggered when two particles come close to each other with their depletion volume overlapped. For particles separated by a distance less than the diameter of the polymer coils, their depletion becomes overlapped, which causes the imbalanced osmotic pressure. The exclusion of polymer from the depletion regions maximizes the entropy of the system, eventually forcing the two particles to coagulate.

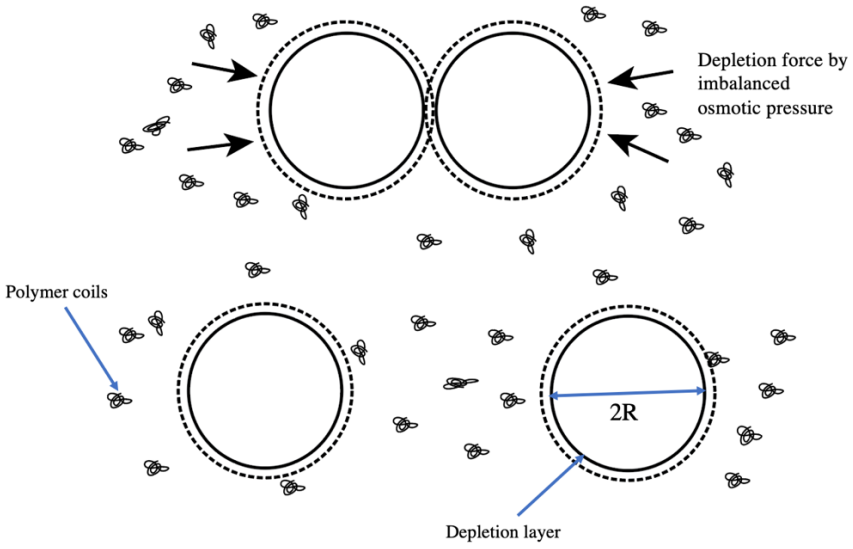

Figure 2.3. Schematic of depletion-flocculation

When small particles such as CNCs are introduced into the dispersion of colloidal sized bacteria, depletion interaction can be triggered, which leads to the exclusion of small particles from the gaps between bacteria cells, consequently resulting in bacteria flocculation. (Eboigbodin et al.,

2005) revealed that rod-like *Escherichia coli* bacteria can be phase separated through depletion mechanism by sodium polystyrene sulfonate particles . (Sun et al., 2012, 2015) reported that both *Escherichia coli K12* and *Pseudomanas. Aeruginosa* bacteria system can be destabilized in the presence of cellulose nanocrystals, as shown in Figure 2.4. Based on models proposed by (Lekkerkerker & Tuinier, 2011), CNCs possess ideal geometric characteristic and colloidal properties to be efficient depletion inducers for spherical colloidal particles having diameter of ~ 1000 nm. It was reported that bacteria flocculation occurs at a wide range of pH (5.2 - 7.2) and ionic strength (1mM to 50 mM) and the optimal bacterial aggregation occurs at pH of 7.2 and ionic strength of 10 mM (Sun et al., 2015). Furthermore, in the same system, bacteria deposition on the silica surface was significantly reduced at neutral condition, which was considered as the direct result of the reduced number of planktonic bacteria due to the bacteria sequestration.

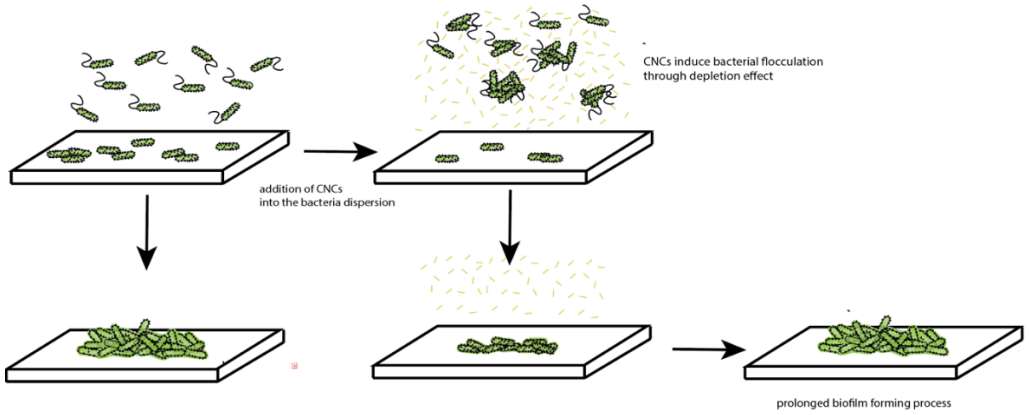

Figure 2.4. Delay of biofilm formation at presence of CNCs

2.2.2 Cellulose nanocrystals (CNCs)

Cellulose is the one of the most abundant naturally occurring biopolymer on Earth. Based on an estimation from Leith and Whitaker's in 1975, crops had a global standing stock of 1.841 ×

10^{12} tons with an annual production of 1.7×10^{11} tons. With a rough estimate of 50% of its weight being cellulose, the total standing stock of cellulose would have been 9.2×10^{11} tons in 1989, with an annual increase of 8.5×10^{10} tons (Duchesne & Larson, 1989). Figure 2.5 shows the chemical structure of cellulose I. Cellulose is composed of linear homopolysaccharides of 1,4 linked β-anhydro-glucan with cellobiose as repeating units. The base unit (cellobiose) contains hydroxyl groups, which contributes to its crystalline structure. A parallel, highly order crystalline structure is resulted from polysaccharides chains being stacked up closed by hydrogen bonding (Phanthong et al., 2018).

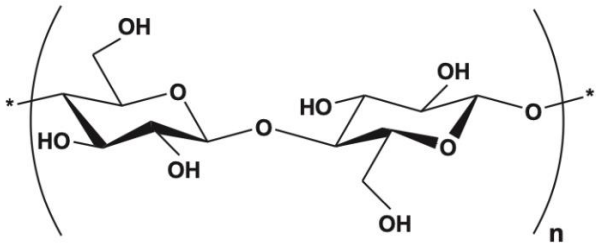

Figure 2.5. Structure of cellobiose in cellulose I

Cellulose nanocrystals (CNCs) is commonly prepared by sulfuric acid hydrolysis of the cellulose I in a controlled mode (Dufresne, 2013). The acid hydrolysis process removes the amorphous region (low crystallinity regions) from cellulose molecules, breaking the cellulose chains into small, rod shaped, fragmented "crystals" particles (CNCs) (Dufresne, 2013). During the sulfuric acid treatment, anionic sulphate ester groups are introduced into the CNCs molecules as surface functional groups, which contributes to their hydrophilic nature and good dispersibility in aqueous mediums (Dufresne, 2013; Phanthong et al., 2018).

2.2.2.1 Antimicrobial and antifouling properties

Several studies have reported that CNCs possess intrinsic antibacterial property. (Du et al., 2015) investigated the biotoxicity of pristine CNCs nanoparticles against *Escherichia Coli* bacteria using bioluminescent *E. Coli* as biomarker. Significant reduction of *E. Coli* was observed at CNCs concentration of above 300 mg/L and the antibacterial effect was found to be concentration dependent. In another study, it was reported that CNCs coated PVDF surface were able to inactivate *Escherichia Coli* bacteria that are attached on the surface. Bacteria depositions were reduced by approximately 90% on the CNCs coated surface in the first 3 hours, indicating CNCs have a great potential to be used as antifouling agents in coating applications. The mechanisms of CNCs' antibacterial activity were not widely agreed upon. However, both (Du et al., 2015) and (Noronha et al., 2021) suggested that their biotoxicity was potentially related to the physical membrane stress and the loss of cellular integrity triggered by CNCs penetrating into the bacteria cells. CNCs' intrinsic characteristics such as high surface area, needle-like morphology, are critical factors contributing to this mechanism.

The potential antifouling properties of CNCs were explored by (Sun et al., n.d., 2012, 2015). Its anti-adhesion activity is considered as a direct result of CNCs' depletion effect in the bacterial system. It was reported that the depletion interactions between like-charged bacteria can be significantly enhanced by the addition of negatively charged CNCs into the system (Sun et al., n.d., 2012, 2015). When CNCs (Length = 90 ± 10 nm, diameter = 8 ± 1 nm, zeta potential = - 51.5 ± 0.8 mV) were dispersed in the aqueous suspension of *Pseudomonas. Aeruginosa* (average length = 1.2 μm, radii = 0.22 μm), effective bacteria phase separation was triggered at CNCs concentration of less than 0.1 volume %.within 24 hours of incubation. In the bacterial system

with *Pseudomonas Fluorescens* (hydrodynamic diameter = 0.88 μm), CNCs could inhibit bacterial initial adhesion to a solid surface under both static and hydrodynamic flow conditions. its efficacy is dependent upon several factors such as bacteria EPS coverage, physiochemical conditions (pH, ionic strength) and the medium flow rate in the system. Higher EPS coverage can enhance the bacterial aggregation as surface EPS leads to greater steric interactions, consequently promoting the polymer bridging between bacteria. More aggressive hydrodynamic flow condition imposed stronger fluid drag effect on bacterial deposition, which further enhance the anti-adhesion activity of CNCs. The efficiency of CNCs depletion effect largely depends on the physiochemical conditions of the bacterial-CNCs colloids as both pH and ionic strength could affect their DLVO interactions in the bacterial systems. maintenance of the ideal solution chemistry for CNCs-bacteria interactions is critical for the effective bacteria separation (Sun et al., 2015).

2.2.3 Silver nanoparticles (AgNPs)

Silver nanoparticles (AgNPs) are clusters of silver atoms with size of 1 to 100 nm (Rai et al., 2009). AgNPs are widely used as an additive in plastic and coatings applications. Silver nanoparticles possess great chemical inertness, high stability, and minimal toxicity to human compared to other inorganic antimicrobial NPs, which makes them excellent materials of choice for applications requiring long-lasting antimicrobial performance (Dizaj et al., 2014; Rai et al., 2009; Singha et al., 2017). Silver nanoparticles act as a reservoir of antibacterial agents and release Ag+ ions progressively into the surroundings through water mediated oxidation (Damm et al., 2007). Ag^{+} penetrate and bind with the bacterial cells wall, resulting in the rupture of bacterial membrane structure and disruption of bacterial DNA reproduction, thereby causing bacteria death (Rai et al., 2009; Singha et al., 2017).

Like most NPs, the antimicrobial efficacy of silver nanoparticles can be controlled by tuning the particle size and particle morphology. For the same mass of the silver nanoparticles, the bacterial cytotoxicity replied on the surface area and the portion of silver atom being exposed for biological interactions. (Pal et al., 2007) compared the antimicrobial performance of triangular, rod-shaped, and spherical AgNPs. Truncated triangular AgNPs exhibited the greatest antimicrobial performance. It was found that 1 μg of Truncated triangular AgNPs was able to completely inhibit bacteria growth in the inoculated agar plate, while 50 to 100 μg of spherical AgNPs were required to achieve the same result. The enhanced bactericidal activity of triangular AgNPs was ascribed to their high surface atom density and superior reactivity towards the bacteria cellular components. The influence of particle size on the AgNPs' antimicrobial activity was demonstrated by (Bera et al., 2014). Fluorescent AgNPs of 1.5 nm demonstrated superior antimicrobial effect compared to larger particles. As particles gets smaller, their specific surface area increase, which allows for faster dissolution of ionic silver and higher reactivity with the bacteria cells.

2.3 Preparation of CNCs based nanocomposites

2.3.1 CNCs based nanocomposites

Polymeric nanocomposites refer to materials comprised of inorganic or organic nanoparticles dispersed in a polymer matrix. Polymeric materials reinforced with nanofillers demonstrated remarkable mechanical, thermal and barrier properties compared to conventional composites fabricated at microscale (Mariano et al., 2014). Cellulose nanocrystals is one of the best materials to be used as nanofillers in polymeric nanocomposites as these nanoparticles are chemically stable, lightweight, easily processible, and have great potential to induce significant

reinforcing effect with tuneable surface chemistry. (Arias et al., 2015; Dastjerdi et al., 2017; Dufresne, 2017; Flauzino Neto et al., 2016; Morelli et al., 2016).

2.3.1.1 Mechanical property

The mechanical strength of the CNCs outperforms many traditional reinforcing materials such as glass fibre and steel. The specific young's modulus of CNCs (ratio of young's modulus to density) is 85 J/g, much higher than that of glass fibre and steel, which are around 25 J/g (Mariano et al., 2014). Due to the presence of hydroxyl groups on the particle's surface, CNCs have strong tendency to self-associate through hydrogen bonding in the host matrix. Intermolecular interactions between CNCs particles results in the formation of stiff and continuous nanocrystal networks surrounding the host matrix, which leads to substantial improvement of strength and stiffness. This phenomenon is only expected to occur at above the critical volume concentrations of the nanofillers phase, known as percolation threshold. In a few polymer composite system like poly (S-co-BuA) films, percolation effect can also stabilize composite modulus at extreme condition of high temperature (500K) (Mariano et al., 2014). Percolation threshold is generally related to the density, shear modulus of filler materials, and the geometric aspect ratio (Length/cross-sectional diameter) of the filler nanoparticles. Figure 2.6 shows the evolution of Young's modulus as a function of aspect ratio of the CNCs used to process the nanocomposites. A weak, positive correlation between the CNC's aspect ratio and the strength of the nanocomposites existed. In general, materials incorporated with nanoparticles of higher aspect ratio have lower percolation thresholds as these nanoparticles can easily form percolative networks through stronger interfacial interaction with the matrix (Favier et al., 1995; Mariano et al., 2014).

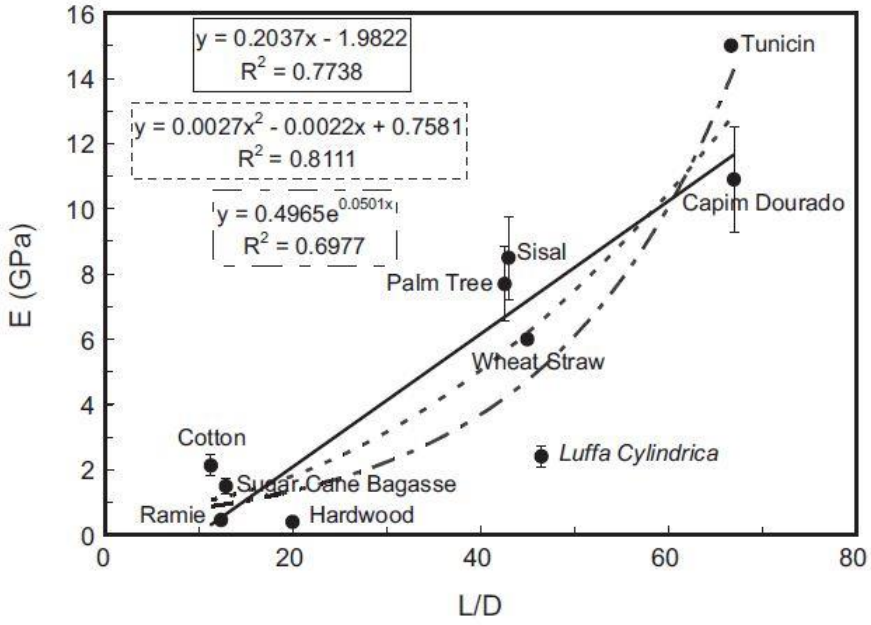

Figure 2.6. Evolution of Young's modulus as a function of aspect ratio of CNCs constituting the nanocomposites adapted from (Bras et al., 2011) with authors' consent.

2.3.1.2 Water permeability and swelling properties

Water permeability, and barrier properties are important properties that determine the applicability of a nanocomposite material as urinary catheter tubing. Good barrier properties are required for urinary catheter to resist water permeation and solvent erosion for extended durability Cellulose nanoparticles could improve the barrier properties of their composite system. Due to their small size and large surface area, dispersion of CNCs in the host matrix increases the tortuosity of the pathway for water molecules to transport within the composite, resulting in the reduced water permeability and increased water resistance (Mariano et al., 2014).

For most nanocomposite films, water permeability largely depends on the hydrophilicity of the composite materials, and the materials microstructure. For example, for hydrophilic matrices such as carrageenan, chitosan, glycerin plasticized carboxymethyl cellulose, and plasticized starch,

incorporation of CNCs could decrease the water uptake and limit the water diffusivity within the materials. This can be ascribed to the formation of three-dimensional nanoparticles/matrix network because of the strong interactions between CNCs particles and between CNCs and the polymer matrix. These rigid crystal structure could stabilize the composite matrix, preventing it from swelling, which limits the permeation of the water molecules (Dufresne, 2000). For hydrophobic matrices such as poly (vinyl acetate) (PVAc), poly(methyl methacrylate) (PMMA), and natural rubber (NR), however, the introduction of CNCs could increase the water uptake and enhance their permeation into the materials. The improved water diffusion towards the hydrophilic CNCs particles and weak interfacial regions are responsible for this phenomenon.

2.3.2 Processing strategies for CNCs based nanocomposites

The performance of CNCs-based polymeric nanocomposites depends on the dispersion of CNCs in the composites and the compatibility of CNCs to the matrix materials. CNCs can self-associate by hydrogen bonding to form nanocrystal agglomerates in the matrix, which compromise its nanometric effect and limits the potential of various properties enhancement. Therefore, to process CNCs into high performance nanocomposite materials, it is essential to disperse CNCs homogeneously in the continuous phase of matrix. Such systems are usually formed during the processing of the nanocomposites, which makes the processing techniques important (Dufresne, 2013; Mariano et al., 2014).

Common methods to prepare CNCs based nanocomposites are present in Figure 2.7. Dry processing includes melt compounding and nanoparticles impregnations. These methods are less frequently used due to the inherent incompatibility and thermal stability issues of CNCs. For wet processing, water is the most common processing medium. To process nanocomposite incorporating latex or hydro-soluble polymers, aqueous suspensions of CNCs and hydro-soluble

polymers or polymer latex are mixed and casted, followed by evaporation of liquid phase (Dufresne, 2013, 2017).

For polymers that are not dispersible in water or aqueous medium, polar liquid media such as dimethyl sulfoxide (DMSO), N,N-dimethyl sulfoxide (DMF), N-methyl pyrrolidine (NMP) can be used to disperse nanoparticles. In this scheme, the aqueous suspension of CNCs is mixed with polymer dispersion that involves one solvent miscible with water. The mixture of the solvents with dispersed by nanoparticles is then casted to obtain the CNCs reinforced nanocomposites. Alternatively, solvent exchange can be used to suspend CNCs into a low polarity or non-aqueous medium for subsequent surface modifications or solution of monomers for further in-situ polymerization. For example, (Siqueira, Bras, et al., 2010) chemically grafted CNCs with long chain isocyanate by solvent exchange methods. The aqueous suspension containing CNCs was progressively solvent exchanged in liquid medium of decreasing polarity (acetone, toluene) by successive centrifugation and redispersion operations. Sonication is used to eliminate agglomeration from each procedure.

Surface modifications are commonly used techniques to improve the nanoparticles' dispersibility in non-polar processing media and to enhance their compatibilization with the hydrophobic matrix. The purpose of surface modifications is to reduce the surface energy of the CNCs nanoparticles to mix with non-polar liquid media or hydrophobic materials. This can be achieved by either physically coating CNCs surface with surfactants or chemically grafting CNCs with non-polar moieties (Dufresne, 2013, 2017). Processing surface modified CNCs into composites can lead to two conflicting effects. The use of surface modified CNCs could improve the dispersion of fillers nanoparticles in the continuous non-polar matrix phase, which makes the properties of the nanocomposites optimizable. On the other hand, surface modified CNCs are less

likely to associate due to the loss of polar surface groups, which could ultimately limit the potential of mechanical reinforcement.

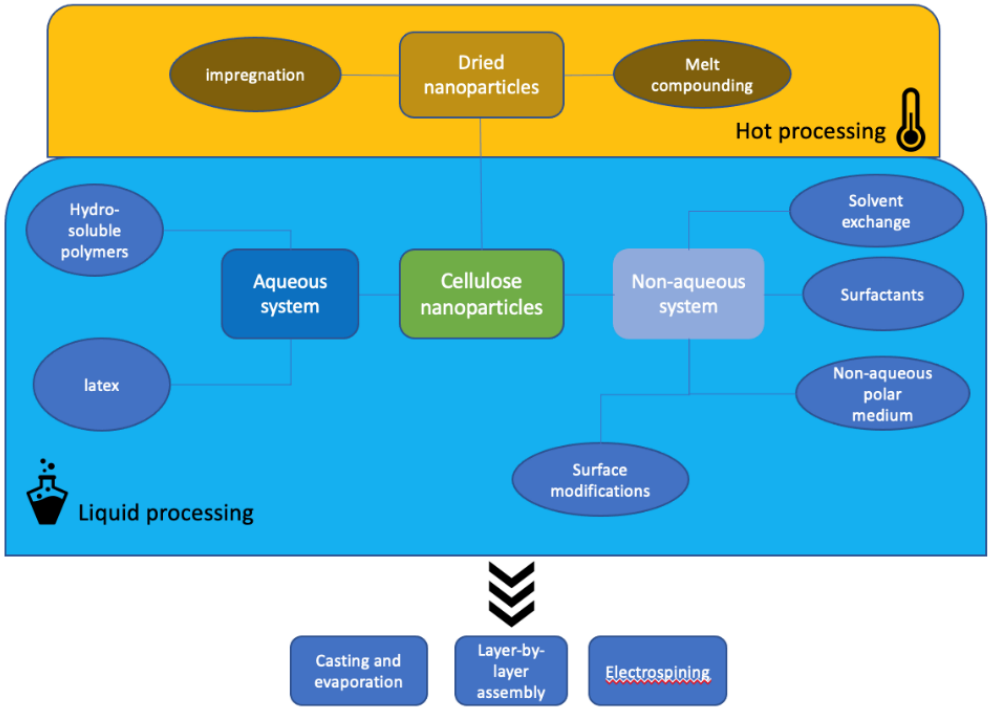

Figure 2.7. Strategies for the processing of CNC reinforced nanocomposites

2.3.3 Processing of Natural rubber/CNCs nanocomposites

2.3.3.1 Casting and evaporation

Casting/evaporation technique is one of the most practiced techniques to process NR/CNCs based nanocomposites. In aqueous latex, NR latex particles are hydrophobic particles coated by a layer of negatively charged shells comprised of proteins and phospholipids. The presence of these charged protein groups makes these latex particles highly negatively charged (zeta potential = -60 mV to -80mV) at neutral to alkaline condition (Sanguansap et al., 2005). Stable and homogeneous dispersion of NR latex and CNCs particles can be yielded by blending the two aqueous dispersions at optimal ionic strength and pH (Mekonnen et al., 2019).

Figure 2.10 schematically illustrates the processing schemes of NR/CNCs nanocomposite films prepared by casting/evaporation method. The aqueous suspension of CNCs is first blended with NR latex. The mixture is then casted, followed by water evaporation at above the glass transition temperature of the matrix polymer, typically at range of 40 °C to 50 °C (Bras et al., 2010; Dufresne, 2017; Pasquini et al., 2010; Siqueira, Abdillahi, et al., 2010; Zhang et al., 2014). The film can be further conditioned in the environment with appropriate humidity to ensure that water contents in the film is equilibrated to the atmospheric conditions (Bras et al., 2010; Cao et al., 2018). Highest mechanical performance was reported in literature where nanocomposites were processed by slow water evaporation process. Slower solvent evaporation provides ideal condition for nanoparticles to interact in the suspension by Brownian motion as the viscosity of the liquid medium is low. The coagulation of latex particles could then promote the CNCs interaction to form percolative networks.

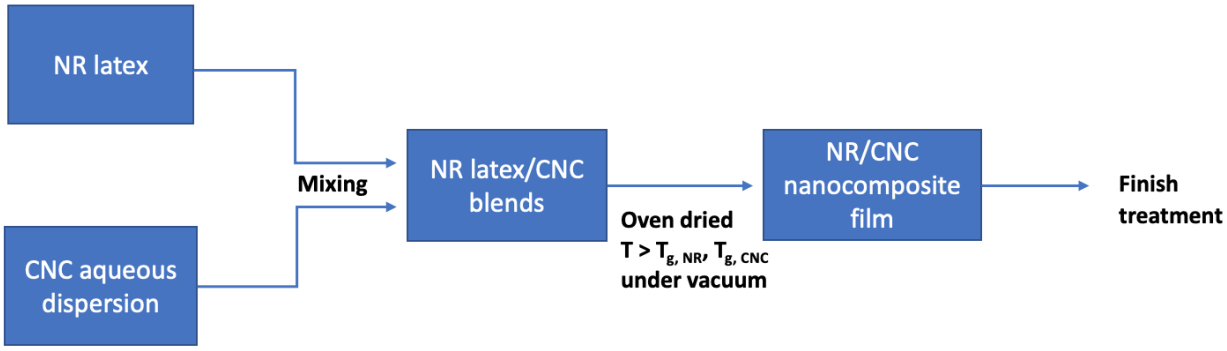

Figure 2.8. Casting and evaporation process for preparation of NR/CNC nanocomposite films

Table 2.1 summarizes the properties, processing information of NR/CNCs nanocomposite films prepared by casting/evaporation method in literature. Mechanical properties are important factors to evaluate the incorporation of nanofillers and filler-matrix molecular interactions. Tensile strength (σ), elongation at break, and elastic modulus (E') are crucial parameters to assess the

mechanical reinforcements brought by the nanofiller incorporations. Tensile strength is the maximum stress a material can withstand until it stretches and breaks. It has units in MPa. Elongation, commonly used to assess the flexibility of a film, is the extent to which film can stretch before break point (Rhim & Lee, 2004). Three parameters that affect the mechanical properties of CNCs reinforced nanocomposites are the dimension and morphology of the filler nanoparticles, the processing methods, and the microstructure of the composite and filler/matrix interaction (Mariano et al., 2014).

The morphological characteristics of CNCs particles, like length, and aspect ratio (L/D) are key factors that determine the potentials of mechanical reinforcement in the nanocomposites (Bras et al., 2011). In general, introduction of CNCs with higher aspect ratio yields to better mechanical reinforcement. CNCs with higher aspect ratio tends to have stronger hydrogen bonding interactions and can create stronger interfacial adhesions with the matrix, reinforcing the materials (Bras et al., 2011; Yin et al., 2018). Thus, with high aspect ratio, lower filler content is required to achieve percolation effect. Stronger filler/matrix interaction can improve the mechanical reinforcement and extensibility of the materials. For example, Mariano et al. (2016) synthesized a dual cross-linked NR/CNCs composite materials using epoxidized natural rubber (ENR) and carboxylate modified tunicate CNCs (mt-CNCs). The nanocomposite was cross-linked with both covalent bonding and reversible hydrogen bonding to improve the filler/matrix interfacial adhesions. The dual cross-linking networks facilitated the energy dissipation from matrix to load-bearing fillers nanoparticles when acted upon by shear stress. Mechanical properties were improved significantly. With addition of only 3 phr of mt-CNCs, the tensile strength, and strain at

failure were increased to 3.07 MPa and 568%, respectively. The improvement was even more significant than composite loaded with 5phr of unmodified CNCs.

Sedimentation phenomenon adds another complication to the mechanical properties of the NR/CNCs nanocomposites. Sedimentation of CNCs occurs during the casting and water evaporation stage and can be ascribed to the translational motions of CNCs during the water evaporation (Helbert et al., 1996). (Flauzino Neto et al., 2016) reinforced NR films with high aspect ratio CNCs (L/D = ~103) using casting/evaporation method. SEM results indicated multilayered structure containing different concentrations of CNCs was formed across the film and a CNCs concentration gradient was resulted with settling layers having highest CNCs content (over the CNCs loading concentration). Percolation effect occur in the CNCs rich layer, leading to significant improvement of mechanical properties even at below the percolation threshold (Helbert et al., 1996). With 2.5 wt.% of CNCs addition, the storage tensile modulus at 25 °C was increased by 20-folds.

Matrix material	Aspect ratio of CNCs (L/D)	Percentage of CNCs loading for the best property enhancement	Relative rubbery storage tensile modulus at 25 °C	Roles of CNCs	Reference
NR	~ 8.5	5 w/w %	E' increases by 4.33-fold	Mechanical reinforcer	(Zhang et al., 2014)
NR	~13	10 w/w %	E' increased by 5.3-fold	Enhancement agents: • mechanical properties • barrier properties • biodegradability	(Bras et al., 2010)
NR	~67	10 w/w %	E' by 256-fold	Mechanical reinforcer	(Siqueira, Abdillahi, et al., 2010)
NR	~76	10 w/w %	Rubbery E' increased by 69 folds	Mechanical reinforcer	(Pasquini et al., 2010)
NR	~ 80	20 phr[1]	E' increased by 487.5-fold at 25°C	• Mechanical reinforcers • Shape memory inducer	(Yin et al., 2018)
NR	~ 100	5 w/w %	E' increased by 20-fold at 25°C	Mechanical reinforcer	(Flauzino Neto et al., 2016)
Oxidized NR	~ 21.5	3 w/w %	E' increased by 5.28-fold	Enhancement agents • mechanical properties • thermal properties	(Mariano et al., 2016)

Table 2.1. NR/CNCs nanocomposites prepared by casting/evaporation method

[1]parts per hundred rubber

2.3.3.2 Melt compounding approach

Melt compounding procedures like extrusion or injection molding is a conventional method for thermoplastic processing. In the extrusion process, dried nanoparticles are dispersed directly into the molten polymer under high temperature and pressure. The extruder provides shear stress and heating, which promotes the dispersion of nanofillers in the polymer blends (Oliveira & Beatrice, 2019). Higher shear stress reduces the size of agglomerates during melt processing and promotes the re-structuring of the filler nanoparticles in the matrix. Under applied shear, larger agglomerates are broken into smaller ones, dispersed in the matrix polymers. The polymer further distributes the shear flow to the smaller agglomerates, breaking them into individual particles. Upon cooling, these particles re-form their connections with the matrix, forming better dispersed systems (Oliveira & Beatrice, 2019). The advantages of this methods include the good dispersion of nanoparticles, eco-friendliness, simplicity to process, and low cost (Oliveira & Beatrice, 2019). In nanocomposite systems involving natural rubber, thermoplastic processing is mainly conducted for molding and vulcanization purposes. For example, (Visakh et al., 2011) fabricated a NR based nanocomposite membrane reinforced with bamboo pulp derived CNCs, The materials were synthesized by a two-step process involving the masterbatch of CNCs in NR latex and the nano-compounding process by compression molding and vulcanization at 150°C.

(Xu et al., 2012) addressed the mechanical properties weaknesses of NR containing silica impurities by partially replacing the silica impurities with 3-aminopropyl-triethoxysilane (KH550) modified CNCs (modified CNCs) as a nanofiller. The CNCs suspension, modified CNCs suspension were mixed in the NR latex and co-coagulated with aids of $CaCl_2$ solution and the coagulum was further compounded with NR latex in a two-roll mill to obtain the composite sheets. The rubber compound sheets were then compressed and vulcanized at 143°C to obtain the final

vulcanized NR/modified CNCs nanocomposites (Xu et al., 2012). KH550 reinforced the cross-linking of the nanocomposite by chemically reacting with both CNCs and rubber, resulting in stronger interfacial interaction between the modified CNCs fillers and matrix materials. The introduction of KH550 modified CNCs led to improvement of a list of mechanical properties including elongation at break, tensile strength, modulus at 300%, and the tear strength.

2.3.3.3 In situ polymerization

In in-situ polymerization strategy, nanofillers particles are dispersed in a solution containing monomers precursors and in-situ polymerization was carried out using appropriate techniques, followed by solvent evaporation to obtain nanocomposites. The homogenous dispersion of nanofillers in the monomer solution ensures that the polymer forms between the nanofillers in the nanocomposite materials resulting in a good dispersion of nanoparticles. Surface modifiers may be added to disperse the nanoparticles and aid in the polymerization process. By using this method, it is possible to incorporate nanofillers at higher contents without causing aggregations (Oliveira & Beatrice, 2019).

(Kedzior et al., 2018) explored the potentials of CNCs in commercial adhesive and coating applications and present a strategy to incorporate CNCs into the core of latex particles of Poly (methyl methacrylate) (PMMA). Both surface modifications of CNCs and mini-emulsion polymerization were applied. To compatibilize CNCs with hydrophobic MMA monomers, CNCs were first grafted with a poly (butyl acrylate) (PBA) through a two-step "grafted from" techniques via surface-initiated atom transfer radical polymerization. PBA-grafted CNCs was then dispersed into the solution of methyl methacrylate (MMA) monomers, followed by the addition of initiators and subsequent mini-emulsion polymerization. The encapsulation of PBA-g-CNCs in the PMMA latex particles were demonstrated by the increased particle size from 204 nm to 248 nm. The zeta

potentials of all PMMA latex particles remains negative, indicating good colloidal properties was maintained throughout the reaction. (Mallakpour & Naghdi, 2018).

2.4 Polymeric drug release systems

"Drug release" refers to the transport of a solute from its initial position in the polymeric system to the outer structure of the polymer, and then to the bulk of aqueous medium (Fu & Kao, 2010). For polymeric materials the mechanism of drug release is mainly dependent on the drug diffusion, dissolution, and degradation of the matrix. Based on the solubility of matrix polymers, polymeric drug release systems can be simply classified as degradable polymeric systems and non-degradable polymeric systems.

2.4.1 Non-degradable polymeric systems

Non-degradable drug release systems are commonly prepared using water-repellent polymers such as rubber, polyurethanes, polydimethylsiloxane (PDMS), and poly(ethylene vinyl acetate) (PEVA) (Fu & Kao, 2010). Examples of non-degradable polymeric drug delivery systems used on implantable medical devices include silver dopped urinary catheters, antibiotics loaded dental implants, and skin wound dressing and tissue adhesives (Fu & Kao, 2010).

Non-degradable polymeric systems can be typically divided into "Reservoir" type systems and monolithic "matrix" type systems. The mechanisms of the drug release in these systems are illustrated in Figure 2.10. In monolithic system, drug molecules are homogeneously distributed throughout the polymer matrix. The polymer matrix acts as rate-controlling medium, regulating the transport of the drug. The drug release process in such systems is governed by Fickian diffusion, which is influenced by the drug concentration gradient, diffusion distance, and degree of swelling. With this design, and the rate of the release process becomes dependent on the concentration of

drugs being encapsulated in the polymer matrix. Thus, the sustained release can be achieved by increasing the concentration of drug encapsulated in the pellets. In comparison, “Reservoir” type systems contain drug depot covered by an inert membrane acting as rate-controlling barrier for drug release process. In such design, the rate of drug release is related to the thickness of the membrane and the permeability of drug through the membrane. The main advantage of this system is that the rate of drug release can be maintained at a constant rate (zero order release kinetics), which is favored by most controlled release applications. The concentration gradient does not impact the rate of release. However, the diffusion of high molecular weight compounds in such systems can be difficult, which could limit its applicability among high MW drugs.

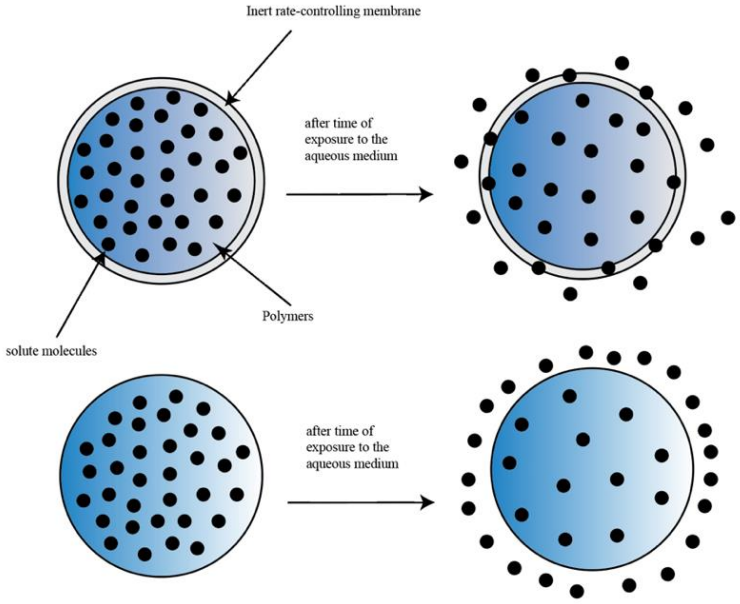

Figure 2.9. Schematic of the drug release mechanisms a) “reservoir” type systems and b) monolithic “matrix” type systems

2.4.1.1 Natural rubber (NR) based polymeric systems

Drug release systems using natural rubber as matrix were extensively studied for their potentials applications in drug therapies and regenerative medicine. NR has been shown to stimulate cellular adhesion, formation of extracellular matrix, and promote wound healing process in various types of tissues. Examples of using NR latex matrices to deliver drugs are listed in Table 2.2. NR based composites incorporated with drugs were commonly prepared by blending the drug solution with NR latex or latex/polymer blends. The mixture is then polymerized under casting and solvent evaporation process. Characteristics such as surface pore size and pore density, hydrophilicity of the membrane components, and the material processing temperature are the typical parameters that affect the release behaviors of the drug delivery systems.

(Herculano et al., 2010) used NR latex to fabricate metronidazole releasing membranes as dermatological formations for potential applications in treating rosacea. The composite membranes were polymerized at different temperature (-100 °C to 40 °C) to create pores of different density and sizes on the materials. Total cumulative metronidazole release was increased from 11.86 mg to 15.41 mg in 200 mL aqueous medium when the pore sizes diameter range increased from 1.17 to 3.17 μm to 0.49 to 5.12 μm. It was speculated that surface pores and cavities could facilitate the drug migration from inner portions of the membrane to the materials' surface, leading to higher release of the metronidazole. (Miranda et al., 2017) fabricated a bovine serum albumin (BSA) releasing membranes. A contradictory trend was observed. Higher BSA was released from membrane containing less pores. In this study, the pore formation was associated with higher degree of cross-linking in the matrix, which leads to denser BSA-matrix structure, compromising the BSA release from the membrane.

Hydrophilicity of the matrix materials can also affect the release process. (Pichayakorn et al., 2012) developed a nicotine transdermal patch based on using deproteinized natural rubber latex blended with hydrophilic polymers. Poly (Vinyl Alcohol), methyl cellulose, sodium carboxymethyl cellulose, as well as hydrophilic plasticizers were used. The increase of polymer contents and the addition of plasticizers accelerated the nicotine release, and this phenomenon was ascribed to the enhanced matrix hydrophilicity. Increased water uptake and enhanced swelling behavior promote the erosion of the patches, creating porous channels for the diffusion of nicotine, thereby promoting the release process.

Table 2.2. Drug release systems based on natural rubbers

Drug compounds	**Molecular weight** (g/mol)	**Fabrication approach**	**Release kinetics & Release performance**	**Characteristics that impact the release behaviors**	**Reference**
nicotine	162.2	• De-proteinized NRL blended with polymers, plasticizers and nicotine • casting and evaporation in hot air oven at 70±2 °C	• Higuchi model • First order model	• Hydrophilicity • Surface pores and cavities	(Pichayakorn et al., 2012)
metronidazole	215.2	• Solution blending of NRL and metronidazole • Casted and polymerized at different temperature for 2 h • Air dried for 2 days	• Bi-exponential model	• Pore density • Pore size • Morphology of the surface	(Herculano et al., 2010)
Silver nanoparticles (AgNPs)	N/A	• NRL blended with AgNPs solution • Casting and evaporation at 40 °C	• Sustained release up to 48 h	• Nanoparticle size	(É. J. Guidelli et al., 2013)
Sodium diclofenac	318.13	• NRL blended with Sodium diclofenac	• Bi-exponential model • 59.6% of fractional release in 74 h	• Hydrophobicity of the matrix	(Aielo et al., 2014)

		• Casting and evaporation at room temperature			
ciprofloxacin	331.4	• Casting and evaporation at room temperature	• Korsmeyer-Peppas model	N/A	(Dias Murbach et al., 2014)
oxytocin	1007.19	• NRL blended with oxytocin solution • Freeze dried at -40 °C for 8 h	• Korsmeyer-Peppas model	N/A	(de Barros et al., 2016)
Bovine serum albumin (BSA)	66463	• Deproteinized NRL blended with BSA Solution • Casting and evaporation at different temperature	• Double rectangular hyperbola model • 68.4% of fractional release in 18 days	• Pore size • Pore density • Polymer chain organization	(Miranda et al., 2017)
Fluconazole	306.27	• NRL blended with fluconazole solution • Casting and evaporation for 2 days at 28 °C	• Bi-exponential model • 45% of fractional release in 48 h	N/A	(Yonashiro Marcelino et al., 2018)

2.4.2 Empirical models

Empirical models that are developed based on the transport mechanisms and the release behaviours and are listed in Table 2.3. When the solvent diffusion rate is significantly greater than the polymer relaxation rate ($t_r >> t_d$), the transport mechanism is termed as Fickan diffusion driven. Conversely, when the polymer relaxation rate is significantly greater ($t_r << t_d$), the mechanism is considered non-Fickian or case II transport controlled (relaxation controlled). A n parameter in the range of 0 to 0.5 indicated analogous transport behaviours (Fu & Kao, 2010), ($t_r \approx t_d$). (Kosmidis et al., 2003). Mathematical models can be derived based on one or two of the dominant mechanisms.

Table 2.3. Common empirical models for drug release kinetics

Model name	Mathematical expression	Transport Mechanism	Reference
Zero order	$\frac{Q_t}{Q_\infty} = kt$	Case II (relaxation controlled) transport	(Fu & Kao, 2010)
First order	$\frac{Q_t}{Q_\infty} = A[1 - \exp(-bt)]$		(Unagollaa & Jayasuriyaa, 2018)
Higuchi	$\frac{Q_t}{Q_\infty} = kt^{\frac{1}{2}}$	Fickian diffusion	(Fu & Kao, 2010)
Ritger-Peppas	$\frac{Q_t}{Q_\infty} = kt^n$	Case II transport, n =1 Fickian transport, n =0.5 Non-Fickian transport, 0.5 < n < 1	(Fu & Kao, 2010)
Peppas-Sahlin	$\frac{Q_t}{Q_\infty} = k_1 t^n + k_2 t^{2n}$	Non-Fickian diffusion	(Fu & Kao, 2010)
Alfrey	$\frac{Q_t}{Q_\infty} = k_1 t + k_2 t^{\frac{1}{2}}$	Non-Fickian diffusion	(Fu & Kao, 2010)

Chapter 3 EXPERIMENTS AND CHARACTERIZATIONS

3.1 Materials and methods

3.1.1 Materials

Cellulose nanocrystals (CNCs) were prepared from sulfuric acid hydrolysis of hardwood kraft pulp feedstock by Alberta Innotech according to the method previously reported (Ngo et al., 2018). The obtained CNCs aqueous suspensions were colloidally stable and the zeta potential of CNCs aqueous suspension (1 g/L) was determined to be -51.7 ± 0.5 mV, using a Zetasizer Nano-ZS ZEN3600 (Malvern Instruments Ltd, UK). Natural rubber latex extracted from natural rubber tree (*Hevea Brasiliensis*) with a solid content of 62% was purchased from Holden's Latex Corp. Table 1 shows the composition of natural rubber latex suspension sample as received. 5-(4, 6-Dichlorotriazinyl) aminofluorescein (DTAF) and sodium hydroxide (NaOH) were purchased from Thermo Fischer Canada and used directly without any purification. Silver nitrate (ACS reagent, > 99%), Lubria-Bertani (LB) agar and trypticase soy agar (TSA) were obtained from Sigma-Aldrich Canada Ltd. (Oakville, ON, Canada) and used as received. Synthetic urine concentrate (catalog:8362-5) was purchased from RICCA chemical company. The reagent contains sodium chloride, calcium chloride, urea, and magnesium sulphate hexahydrate and has a pH of 7.80 to 8.00 at 25 ℃.

Table 3.1. Composition of NR latex suspension.

Ingredients	CAS No.	Functions	Weight (wt.%)
Poly (isoprene)	9006-04-6	main ingredient	62
$(NH_4)OH$	1336-21-6	chemical stabilizer	<0.3
Ammonia	7664-41-7	chemical stabilizer	<0.005
Tetramethylthiuram disulfide	137-26-8	curing agent	<0.049

3.1.2 Preparation of the NR/CNCs nanocomposite films

Nanocomposite films were prepared by mixing and casting of CNCs suspensions with NR latex at various weight ratios followed by evaporation of the liquid phase. Specifically, CNCs suspensions were prepared by dispersing desired amount of CNCs in deionized water (DI water) with the aid of magnetic stirring for 4 h, followed by sonication for 15 min. The obtained CNCs suspensions were then added dropwise into the natural rubber latex and the mixtures were magnetically stirred at 150 rpm for 2 h. The weight ratios of CNCs to NR at 3.0 wt.%, 6.0 wt.%, and 12 wt.% were used, respectively. The NR/CNC films were then fabricated via casting the mixtures into glass petri dishes and dried in an oven at 50 °C for 24 h following with further conditioning at 55°C for 3 days. The samples are named according to the content of CNCs in the nanocomposite films, as NR/CNCs-3, NR/CNCs-6, and NR/CNCs-12, respectively. Meanwhile, neat NR film were prepared with NR latex accordingly.

3.1.3 Synthesis of silver particles on the nanocomposite films

Silver particles were synthesized and incorporated onto the NR/CNCs nanocomposite films following the method proposed by Danna et al (2016) with modifications. The method was based

on the reaction between NR/CNCs nanocomposite films and silver nitrate solution. Specifically, a rectangular (2.5 cm × 2.5 cm × ~ 0.15 cm) film of neat NR or NR/CNCs nanocomposite (3.0 wt.%, 6.0 wt.% and 12.0 wt.%) was immersed in an aqueous solution (15 mL) of $AgNO_3$ solution (1mM) at 80 °C for designated time periods. The films were collected from the solution at different reduction time, which are 60 min and 120 min, and dried overnight in the desiccator to remove the moisture. The specimens were named based on the green synthesis reduction time as, NR/CNCs-3-AgNP60, NR/CNCs-6-AgNP60, NR/CNCs-12-AgNP60, NR/CNCs-3-AgNP120, NR/CNCs-6-AgNP120, NR/CNCs-12-AgNP120 respectively.

3.1.4 Transmission electron microscopy (TEM)

The morphology of NR/CNCs suspension was observed by transmission electrical microscopy (TEM, Morgagni 268, Philips-FEI, Hillsboro, USA) operating at an accelerating voltage of 80 KV. In addition, CNCs suspension, and NR latex were also studied for comparisons. All the samples were negatively stained with 2 $^{w}/_{v}$% sodium phosphotungstate (pH 7.4) and the ImageJ image-visualization software developed by the National Institute of Health dimensions was used for image analysis.

3.1.5 Scanning electron microscope (SEM)

The morphology of NR/CNCs films and silver nanoparticles was characterized using Zeiss Sigma FE-SEM. The dried samples were carbon coated with Leica ACE600 carbon coater. The coating thickness was 5 nm, at a pulse rate of 0.1 nm/min. The samples were visualized by field emission mode with an accelerating voltage of 5 to 10 kV. The images were further processed and analyzed using ImageJ.

3.1.6 Fourier Transform Infrared Spectroscopy (FT-IR)

Fourier transform infrared (FTIR) spectra of the pristine materials CNCs and NR, NR/CNCs-3, NR/CNCs-6, and NR/CNCs-12 as well as all the silver particles modified nanocomposite films were measured on the FT-IR iS50 spectrophotometer. The equipment operates at build-in ATR module with air set up as the background spectra. The scan range is set from 400 cm^{-1} to 4000 cm^{-1}. Spectra were recorded as the average of 128 scans at 4 cm^{-1} resolution and 25 ℃.

3.1.7 Dynamic mechanical analysis (DMA)

Dynamic Mechanical Analysis (DMA) were conducted to measure the tensile strength and thermomechanical property of the nanocomposite films. DMA TA instrument Q800 was used to perform the test. Tensile strength test was carried out at tension (film) mode. Samples were prepared as rectangular strips with lengths of about 11mm, whereas the thickness and width of the films were measured before each experiment. The films were placed in the desiccator containing silica gel to be fully dried. The tensile properties (stress-strain relationship) of nanocomposite films were measured at controlled force of 0.010N and 25°C. The frequency dependence of storage modulus and loss modulus was measured in multifrequency mode at isothermal condition (37°C), constant strain amplitude (15µm), and preload force of 0.010N. Furthermore, temperature sweep test was conducted to analyze the thermomechanical properties of the films. The dynamic storage modulus (E') and loss modulus (E'') were measured as a function of temperature from 25°C to 150°C at a constant heating rate of 3°C/min and controlled strain of 50 µm and a controlled frequency of 1 Hz.

3.1.8 Quantification of CNCs release from films

3.1.8.1 Fluorescein labeling of CNCs

To quantify the released CNCs from the nanocomposite films, CNCs were labeled with DTAF fluorescein and monitored using UV-vis spectrometer. DTAF with an absorbance/emission peaks at 488 nm/516 nm was used to modify the surface of CNCs according to the method previously reported with modifications (Abitbol et al., 2013). To be specific, 7.5 mg of DTAF and 0.2 g of NaOH were directly added into 25 ml of 2.0 wt.% CNCs aqueous suspension. NaOH was used to adjust the pH to above 11. The mixture was then magnetically stirred in dark for 24 h, following with dialysis against DI water to remove the excess reactants and salts. The conductivity of the dialysate was monitored regularly until it became constant. The DTAF labeled CNCs (DTAF-CNCs) was then freeze dried in LabConco freeze dryer to obtain the solid DTAF-CNCs for preservation. FTIR and UV-vis spectra of DTAF-CNCs and CNCs were measured to confirm the grafting of fluorescein, and to determine the degree of labeling on the CNCs particles. Detailed procedure of the quantification of CNC release from the nanocomposite films is depicted in Figure 3.1.

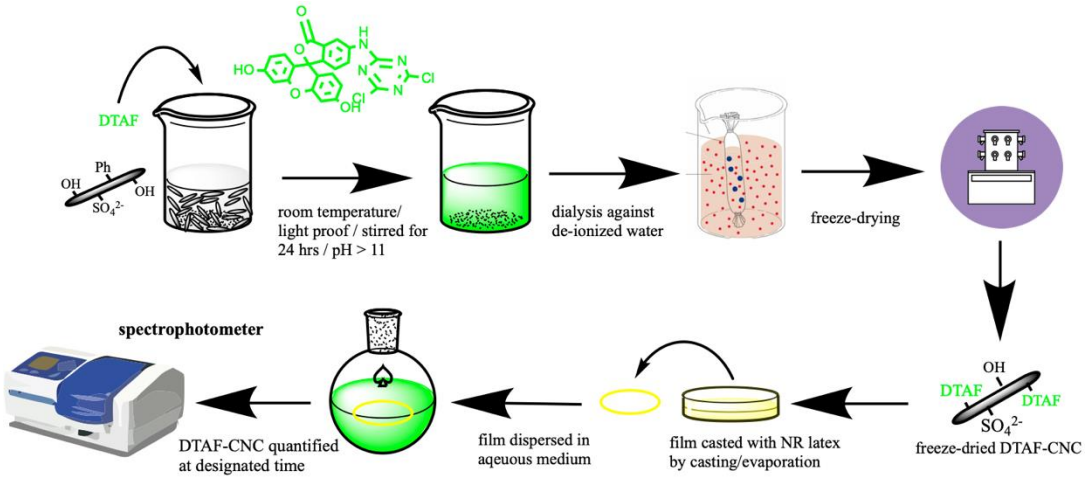

Figure 3.1. The scheme of CNCs release study using fluorescently labeled CNCs.

3.1.8.2 CNCs release into aqueous solutions.

Fluorescence labeled NR/CNCs nanocomposite films were prepared using DTAF-CNCs and natural rubber according to method in section 3.2.2. Three DTAF-labeled samples (NR/CNCs-3, NR/CNCs-6, and NR/CNCs-12) were obtained. To study the effect of pH and ionic strength on the release behavior of the nanocomposite films, the release of DTAF-CNCs in DI water, 200 mM NaCl solution, and PBS buffers with different pHs (6.0, 7.4, and 9.0) was quantified in the procedures as follow: circular films (2.5 cm in diameter) were immersed into 40 ml of release medium in sealed glass vessels, respectively, following with continuous shaking at 120 rpm and 37 °C. 2 ml of the medium was then collected at every two hours and replenished with the same volume of fresh medium. The amount of DTAF-CNCs in the medium were quantified by measuring the absorbance at 488 nm using a DR 3900 UV-vis spectrophotometer. In the meantime, a standard curve (absorbance vs. concentration) of DTAF-CNCs dispersion in each medium was established by measuring the absorbance of the DTAF-CNCs at 488 nm in the linear range of concentration. The concentrations of the DTAF-CNCs in the medium were acquired at designated time for further calculation to determine the cumulative release of DTAF-CNCs.

3.1.9 Quantification of silver release from nanocomposite films

3.1.9.1 Preparation of release medium

To quantify the silver nanoparticles potentially released into the physiological fluids, the silver release capacity of the nanocomposite films was tested with de-ionized water. The nanocomposite films (NR/CNCs-3-AgNP120, NR/CNCs-6-AgNP120, NR/CNCs-12-AgNP120) with equal surface area ($1.25\ cm\ \times 3.00\ cm\ \times 0.100\ cm$) were submerged in 15 mL of de-ionized water in sealed test vessels held at 37°C. A 1.5 mL of release media were collected at designated time points (8 hours, every day from day 1 to day 7) and replaced with DI water. The

release medium from each sample was then diluted to 15 mL with DI water and filtered using sterile syringe with 1 μm pore size. Two drops of concentrated nitric acid were added into the medium for stabilization and storage.

3.1.9.2 Silver release quantification

Silver composition of the release media was quantified using inductively coupled plasma-optical emission spectroscopy (ICP-OES). Before the testing, the pH of the sample media (15 mL) was adjusted to below 2 by acid digestion using concentrated nitric acid. The sample media were then analyzed using Thermo iCAP6300 Duo (N. America) inductively coupled plasma-optical emission spectrometer (ICP-OES) to detect concentration of silver ions.

3.1.10 Evaluation of Bacteria Antifouling Performance

3.1.10.1 Bacteria strains and cultures

Escherichia coli (*E. Coli)* (ATCC 25922) and *Staphylococcus aureus* (*S. aureus*) (ATCC 25923) were obtained from Fisher Scientific Inc. and were used as model bacteria for bacteria adhesion assay. Lubria-Bertani (LB) Broth, trypticase soy broth (TSB) were used for the cultivation of *E. Coli* and *S. Aureus*, respectively. LB agar and trypticase soy agar (TSA) were used to prepare agar plate.

3.1.10.2 Preparation of bacteria suspensions

To prepare the bacteria suspensions, a single inoculum was taken from grown bacteria colony on the agar plate (LB agar and TS agar plate). 25 mL of sterile LB broth and TSB were inoculated with various bacterial cultures. The inoculated media were then placed in the shaker incubator, operating at 37°C, and 120 rpm for 20 hours for the bacteria to grow into stationary phase. After inoculation, bacteria cells were washed with sterile PBS solution for three times.

Bacterial suspensions were centrifuged at 3000 × g for 10 min at 4 °C and resuspended using PBS solution. The procedure was repeated in another two consecutive sessions. The freshly grown bacteria suspensions with cell concentration of 3.3×10^6 cell/mL were prepared by resuspending the bacteria pellet in PBS buffer, following the proper dilution with PBS for adjustment of OD_{600} (optical density at 600 nm absorbance) to 0.005.

3.1.10.3 Static condition

The sample materials with an equal dimension of 1 cm length × 1 cm width × 0.1 cm thickness were immersed into 3 mL of the bacterial suspension. All specimens were placed in enclosed polyisoprene tube containing prepared bacterial suspension. The containers were then incubated at 37 °C. This study is designed to investigate the antifouling performance of the nanocomposite materials against bacteria in liquid immersion under static condition.

3.1.10.4 Flow condition

The antifouling performance of the nanocomposite films with exposure to the bacteria in aqueous flows was evaluated using modified flow cell device. The device was assembled from the coupon evaluation flow cells (FC71-PC-3×0.5), purchased from BioSurface Technologies Inc. The device simulates the condition in the urinary catheter during the discharge of urine. It consists of a multi-port sampling flow cells connected with rubber tubes for liquid medium withdrawal and discharge. The flow cells contain two channels, each with three flow chambers of approximately 39 mm long by 13 mm wide by 0.34 mm deep. Each chamber is made from polycarbonate plastic and contains recessed wells in the bottom to adjust the specimens. Before each experiment, all components of experiment set-up were sterilized with autoclaving procedure.

The flow cells device was connected to a 2-litre reservoir containing flowing medium (synthetic urine contaminated with bacteria), kept at room temperature. the physiochemical

condition of the synthetic urine was provided in the materials section. Synthetic urine containing freshly grown bacteria with a cell concentration of 3.3×10^6 cell/mL was pumped from the reservoir through the modified flow cells chambers by a peristaltic pump operating at a pumping rate of 1.333 mL/min. The reservoir was replenished with freshly prepared medium on the daily basis to maintain consistent experimental conditions. 24 ℃ was used as the incubation temperature for this study as it allows for stable and slower bacteria growth on the sample surface compared to 37℃. *E. Coli* was used as template bacteria for this study. A 1-cm diameter disks was cut from each tested specimen and placed inside the flow cell chambers for bacteria exposure (NR films, NR/CNCs-6, NR/CNCs-12, NR/CNCs-6-AgNP120, NR/CNCs-12-AgNP120). At each designated test time (8 hours, 1 day, 2 days, 3 days, 5 days, 7 days), tested specimens were removed ascetically from the flow cell chambers for bacteria adhesion assay.

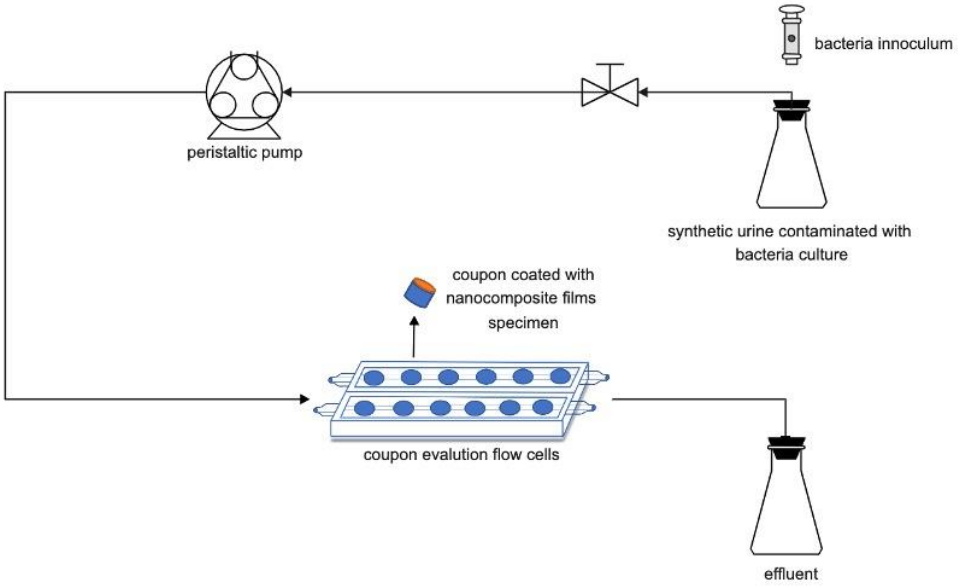

Figure 3.2. Experimental setup of bacteria adhesion assay conducted under continuous flow condition

3.1.10.5 Bacteria Adhesion Assay

At designated time, the sample films were removed from the suspension and washed gently with PBS × 1 buffer for 3 times to remove the unattached bacteria on the surface. Each time, the films were immersed into the PBS solution for 10 seconds. PBS solution (pH ~7.44) helps maintain the ideal osmosis for which bacteria can survive and reproduce. The films were then placed in 1 mL of PBS and sonicated for 3 minutes to remove the attached bacterial cells on the surface. The sonicated media were then diluted from 1 to 7 folds for the drop plate assay. 10 μL of diluted aliquots was dropped onto the agar plate at designated area of dilution factors by micropipette. Five to six identical drops were plated on each area designated with a concentration. After the contaminant medium is fully absorbed by the agar media, the petri dishes were inverted and incubated at 37 °C for 16 hours. The number of colonies were counted at each droplet. The result was only counted when number of colonies falls into the accepted range (5 < # of colonies < 30). Four to five experimental results were collected for each sample. The number of colony-forming units per unit area of film was then calculated using the formula below.

$$\frac{CFU}{unit\ area\ of\ films} = \frac{total\ count\ \times 100 \times 10^{d}}{a}$$

Where, a is the total surface area of the nanocomposite film that were in contact with the bacterial suspension, and d is the dilution factor.

3.1.11 Statistical Analysis

Samples prepared from three separated batches were analyzed for their properties. Experimental results were represented as the mean of three batches ± SD. Statistical evaluation was carried out by two-way analysis of variance (ANOVA) with replications, followed by multiple-comparison tests using Duncan's multiple-range test. All the analyses were conducted

using SAS statistical software (SAS Institute, Inc., Cary, NC) with a probability of $p < 0.05$ considered to be significant.

Chapter 4 RESULTS AND DISCUSSION

4.1 Morphological studies

4.1.1 Transmission electron microscope (TEM)

As shown in Table 3.1, the natural rubber (NR) latex with solid content of 62 wt.% was used as the matrix material for the casting and evaporation of the NR/CNCs composite films. Since the contents of the minor compounds were relatively low, their influence on the performance of the fabricated films was considered negligible. Figure 3.2 showed the appearance of the nanocomposite films containing CNCs at CNCs/NR weight ratio from 0-12 wt.%. Neat NR film appears to be transparent, and homogenous without apparent aggregations. When CNCs were added, the NR/CNCs nanocomposite films become increasingly non-transparent with visible aggregates in those prepared with higher contents of CNCs (pointed by arrows in Figure 4.1 d). These aggregates were formed, likely by the interactions between colloidal CNCs in the mixed suspension. When CNCs suspension was added into the latex, ionic strength of the dispersion is increased instantly, which causes the screening of the surface charges on CNCs, leading to the destabilization of the colloidal system. The aggregation then occurs through Brownian motion. Thus, CNCs display a poor dispersion in the natural rubber matrix at higher CNCs concentrations.

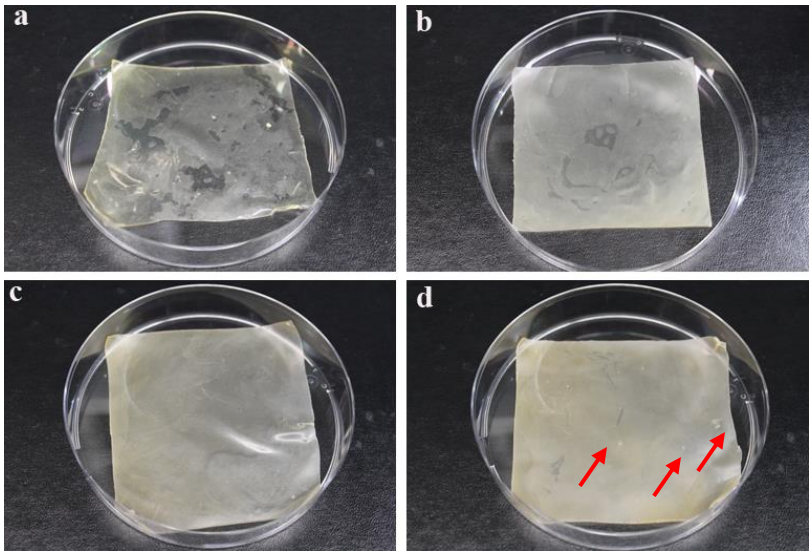

Figure 4.1. nanocomposite films: (a) neat NR film; (b) (c) (d) NR/CNCs nanocomposite films with the CNC content of 3 wt.%, 6 wt.%, and 12wt.%, respectively (petri dish diameter: 100 mm).

CNCs, natural rubber latex, and NR/CNCs suspensions were observed under the transmission electron microscopy (TEM). As shown in Figure 4.2 a), CNCs were homogenous and uniform in shape with narrow distribution of the length and width. Further analysis of the CNCs using the "Image J" software demonstrated the CNCs had an average length and width of 103±26 nm and 10±5 nm (n=50), respectively. Dispersion of CNCs in the de-ionized water results in colloidally stable suspension, which can be attributed to the presence of sulphate half ester groups on the particle surface. CNCs used in the current study possess a zeta potential of -51.7 ± 0.5 mV according to the zeta potential measurement conducted for CNCs aqueous suspension (1.0 g/L), which indicates that CNCs particles are negatively charged and colloidally stable in aqueous dispersion at low concentrations. The latex particles shown in Figure 4.2 b) were spherical with a hairy structure around the spheres. The adsorption of phospholipids and proteins onto the surface of the poly (isoprene) spheres gives rise to the formation of hairy shell structure that appear on the

latex particles (Mekonnen et al., 2019). Figure 4.2 c) and d) showed that most of the CNCs particles and natural rubber latex particles were widely distributed in the NR/CNCs suspension. However, a tendency of aggregation due to the presence of CNCs particles could be observed. At higher concentrations of CNCs, the inter-particle distance becomes shortened, which promotes the interaction between the particles by Brownian motions. CNCs particles form aggregates network structure in the NR/CNCs suspension, which could be resulted from the compromised electrostatic repulsion between the particles in the suspensions at the presence of charged macromolecules and inorganic salts (Beck-Candanedo et al., 2006; Phan-Xuan et al., 2016).

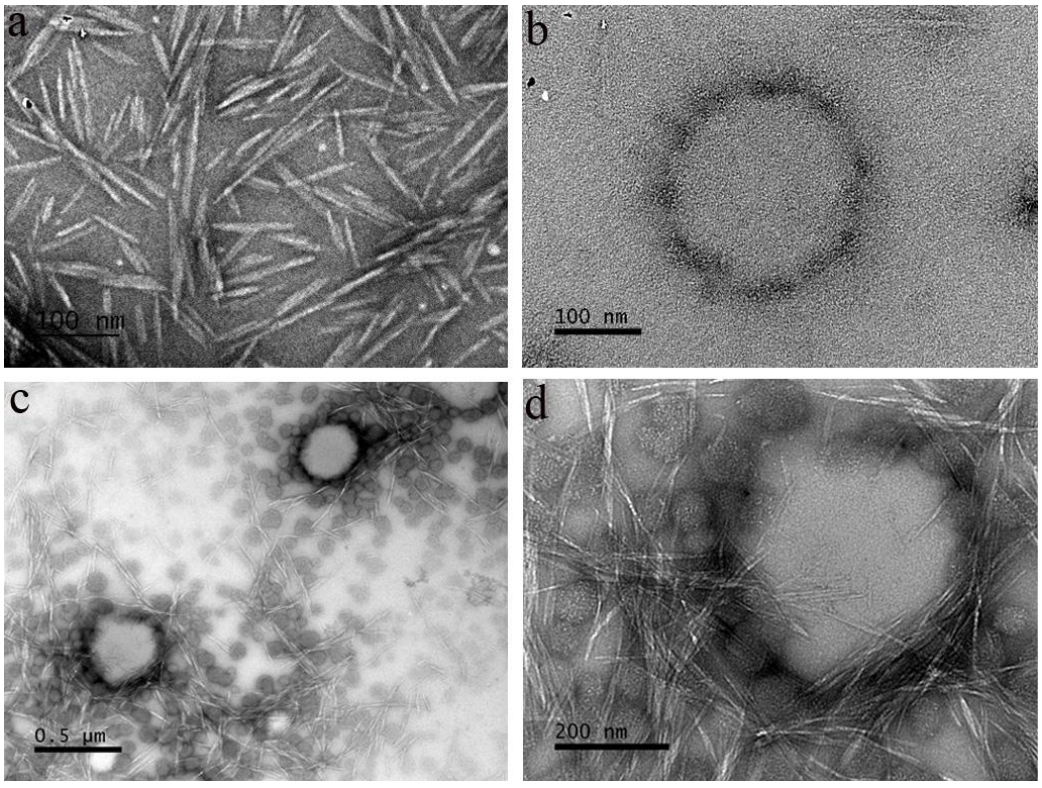

Figure 4.2. TEM images of (a) cellulose nanocrystals, (b) natural rubber latex, and (c,d) NR/CNC suspension.

4.1.2 Scanning electron microscope (SEM)

4.1.2.1 Natural rubber latex/CNCs nanocomposite films

The surface characteristics of solid NR/CNCs nanocomposite films were further studied using scanning electron microscopy (SEM). Figure 4.3 shows the surface of pristine NR film and NR/CNCs nanocomposite films with CNCs/NR weight ratio of 3 wt.% to 12 wt.%. Neat NR exhibits a smooth and pleated surface. Such characteristics were previously reported by (Zhang et al., 2014). The pleated structure was formed during the latex film formation process. During the casting and evaporation stage, latex particles are organized into a structure packed with polyhedron cells with hydrophobic interiors and hydrophilic walls (Joanicot et al., 1990). The polyhedron configuration leads to the macroscopic appearance of pleated layers.

For nanocomposite films incorporated with CNCs, the nanostructure of the nanocomposite films was hardly detected but a trace of macrostructure can be observed. Nanocomposite films with CNCs contents of 3 wt.% and 6 wt.% shows a relatively smooth surface with visible aggregates. It can be observed that CNCs are not visible as individual, rod like particles. They most likely stay within proteins and lipids components, which were embedded within the NR matrix structure. The aggregation of CNCs was due to the compromised colloidal stability of the polymer blends at higher CNCs concentration and the self-association of CNCs during the film processing. No clear trends of aggregate formation have been observed. However, as the concentration of CNCs increases from 3 wt.% to 6 wt.%, the aggregates are visibly bigger, indicating that higher contents of CNCs could promote the phase separation between CNCs and NR latex, resulting in CNCs forming more aggregates through hydrogen bonding.

NR/CNCs-12 film exhibits a rougher and patch-like characteristics with cracks forming in between the surface “patches”. SEM images revealed that the surface was randomly packed with

micro-sized “patches” that are non-uniform in size, with small “channels” separating them. In the water evaporation stage, higher contents of CNCs tend to interact with latex particles to form more viscous layer at the liquid/air interface, which hinders the water evaporation from the core of the matrix. Microcracks thus formed to facilitate the water evaporation on the surface of the films. Therefore, small channels were formed in between these patchy particles.

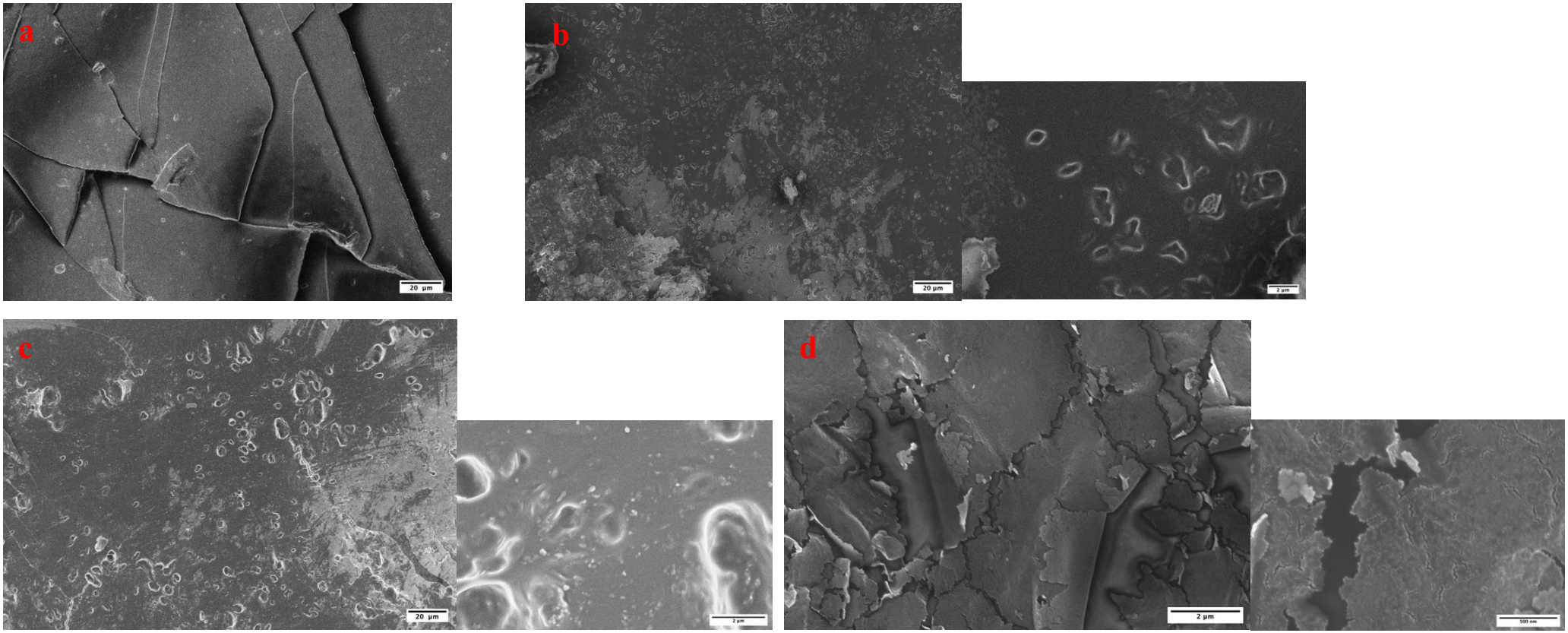

Figure 4.3. SEM images of top face of NR/CNCs nanocomposite films; a) unfilled NR b) NR/CNCs-3 c) NR/CNCs-6, d) NR/CNCs-12

4.1.2.2 Natural rubber/CNCs nanocomposite films embedded with silver particles

Figure 4.4 shows the appearance of silver particles embedded NR/CNCs nanocomposite films at different CNCs contents (0, 6, 12 wt.%) and reaction time (60, 120 min). The nanocomposite films undergo significant colour changes from yellow to brown and deep brown, which indicates the Ag particles synthesis was effective on the films.

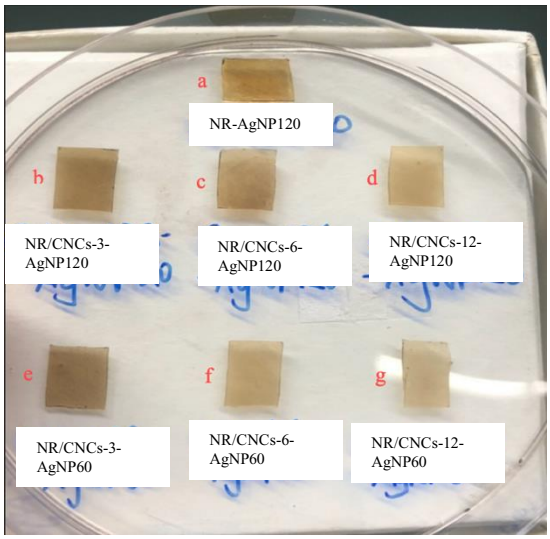

Figure 4.4. Appearance of Ag particles embedded NR/CNCs nanocomposite films: (a) NR-AgNPs120; (b)NR/CNCs-3-AgNP120 (c) NR/CNCs-6-AgNP120 (d) NR/CNCs-12-AgNP120 (e) NR/CNCs-3-AgNP60 (f) NR/CNCs-6-AgNP60 (g) NR/CNCs-12-AgNP60 (petri dish diameter: 100 mm).

Figure 4.5 shows the SEM images of NR/CNCs nanocomposite films embedded with silver particles. These images were chosen because the silver particles were clearly found. Nano to micro sized particles formed on the surface in the clusters as indicated by the red box. Further analysis of the particles by ImageJ software indicated that these particles have a size (length of the particles) ranging from 65 nm to 370 nm.

No distinctive pattern of silver particles distribution was observed. However, as the CNCs content increases, the size of silver particles varied, which indicated that the contents of CNCs in the films can impact the characteristics of the incorporated silver particles. In this study, it can be hypothesized that Ag particles were synthesized by electrostatic binding of Ag^+ on the negatively charged latex particles and CNCs surfaces, followed by reduction of Ag^+ to elemental silver by naturally occurring reductants from the NR latex and further particles growth The role of CNCs and its derivatives on the Ag particles synthesis and nanoparticles stabilizations have been well reported by literature (Liu et al., 2011; Lokanathan et al., 2014). CNCs and carboxyl functionalized CNCs (tempo-oxidized CNCs) demonstrated promising reducing property and were used as reducing agents to synthesize silver nanoparticles from silver nitrate precursor (Hoeng et al., 2015; Xiong et al., 2013).. Therefore, the contents of CNCs must be kept at an optimum to generate Ag particles with better size control and dispersity.

Table 4.1. The average size of the silver particles at various concentrations of CNCs and $AgNO_3$ exposure time

$AgNO_3$ concentration, 10^{-3} M	**CNCs concentration (wt.%)**	**$AgNO_3$ Exposure time (min)**	**Average particle size (nm)**	**Standard deviation (nm)**	**Total numbers of particles observed**
1.0	6	60	N/A	N/A	N/A
1.0	12	60	37.1	10.6	50
1.0	0	120	321	100	18
1.0	6	120	65.8	30	45
1.0	12	120	N/A	N/A	N/A

N/A* cannot be accurately measured

Table 4.1 summarizes the particle sizes of silver particles observed on the nanocomposite films. While individual silver particles do not have consistent shape, the particle size in length was measured based on the longest length of each individual particle in the clusters found on the films. The size of the silver particles changes with the time of reaction and the contents of CNCs. As the CNCs contents increased in the film, the average particle size decreased tremendously. This was probably because at higher CNCs contents, there were less NR latex on the surface, which lowered the reducing property of the films, leading to less silver nanoparticles deposited on the surface. In addition, it has been previously reported that CNCs can act as stabilizing agents to regulate AgNPs aggregation during its synthesis (Liu et al., 2011). CNCs contains anionic groups such as hydroxyl groups, carboxyl groups, which complex with Ag^{+} and Ag^{0} through electrostatic and/or coordination binding when it is used to mediate the AgNPs synthesis process. The binding with CNCs results in the passivation of silver nanoparticles and this prevents nanoparticle aggregation (Liu et al., 2011; Lokanathan et al., 2014; Suwan et al., 2019). It is also noteworthy that the silver particles present on all samples exhibited large polydispersity, with high relative standard deviations. The wide particle size distribution can be attributed to the variation of surface topography, the distribution of CNCs on the films prior to green synthesis treatment.

The synthesis of silver particles on the NR film in the absence of CNCs were also investigated. Interestingly, the average silver particles size on NR-AgNP120 were much higher than that on NR/CNCs-6-AgNP120, which was due to the absence of CNCs. In the absence of CNCs, aggregation of monomeric silver particles occurs more frequently on NR films probably due to the lack of steric hindrance and the higher contents of reductants compounds.

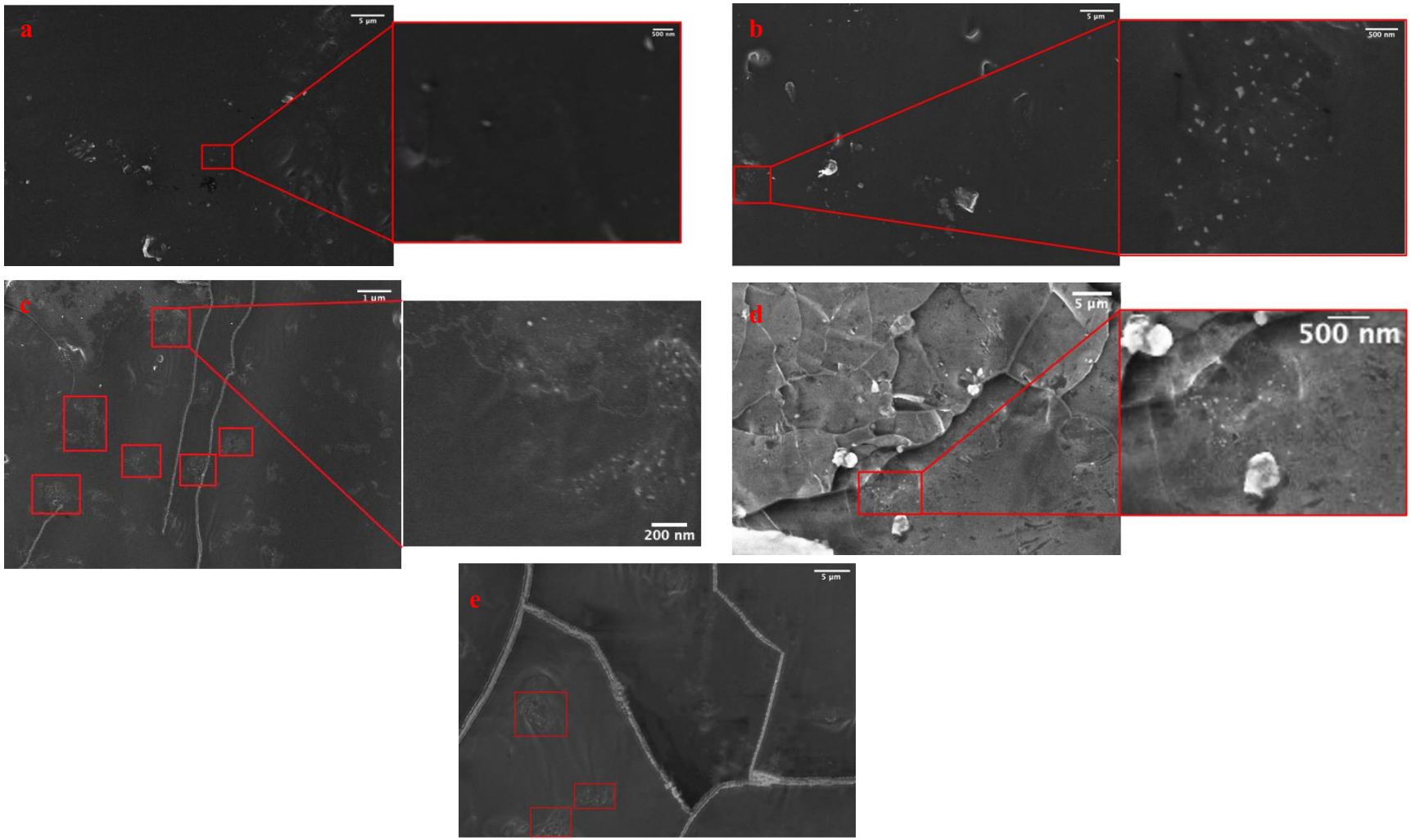

Figure 4.5. SEM images of silver particles embedded NR/CNC nanocomposite films of (a) NR/CNCs-6-AgNP60 (b) NR/CNCs-6-AgNP120 (c) NR/CNCs-12-AgNP60 (d) NR/CNCs-12-AgNP120 (e) NR-AgNP120

4.2 Structural Analysis (FT-IR analysis)

4.2.1 NR/CNCs nanocomposite films

To study the molecular interactions of the NR/CNCs nanocomposite films, NR/CNCs nanocomposite films were tested by ATR-FT-IR spectroscopy alongside with pristine CNCs and NR for comparison. The IR spectrum of neat NR film shows similar characteristics as reported in literature. The major components of NR latex are polymer of cis-1,4-isoprene, proteins, and phospholipids. As shown in Figure 4.6. a), Pristine CNCs showed characteristic absorbance at 3340 cm^{-1} (-O-H stretching), 2920 cm^{-1} (-CH_2 stretching), and 1250 cm^{-1} (C-O-C stretching), which is consistent with its structure. NR had a broad peak at 3290 cm^{-1} (-N-H stretching and -O-H stretching), which was ascribed to molecular vibration of free peptide, protein, and lipids in NR latex.

When CNCs were incorporated into NR latex, the IR spectra showed flatten peaks at 3290 cm^{-1} (-N-H stretching and -O-H stretching) and 1670 cm^{-1} (C=O stretching associated with amide I), indicating depletion of amide structure (Barth & Zscherp, 2002). The disruption of amide structure was caused by the interactions between CNCs and proteins shells of the latex particles. CNCs associate with amino acids through its highly negatively charged surfaces. It was noted the intensity of the peaks at 1250 cm^{-1} and 900 cm^{-1} increased in the NR/CNCs nanocomposite films compared with neat NR latex, which can be ascribed to the incorporation of CNCs in the film, resulting in increased C-O-C stretching. More interestingly, the intensity of the peak at 840 cm^{-1} in the NR/CNCs nanocomposite films increased compared with neat NR latex, which could be due to the formation of the CNCs-protein complex in the NR latex leading to the interruption of the stable colloidal system and the exposure of poly (isoprene) matrix on the surface (Danna et al., 2016).

.

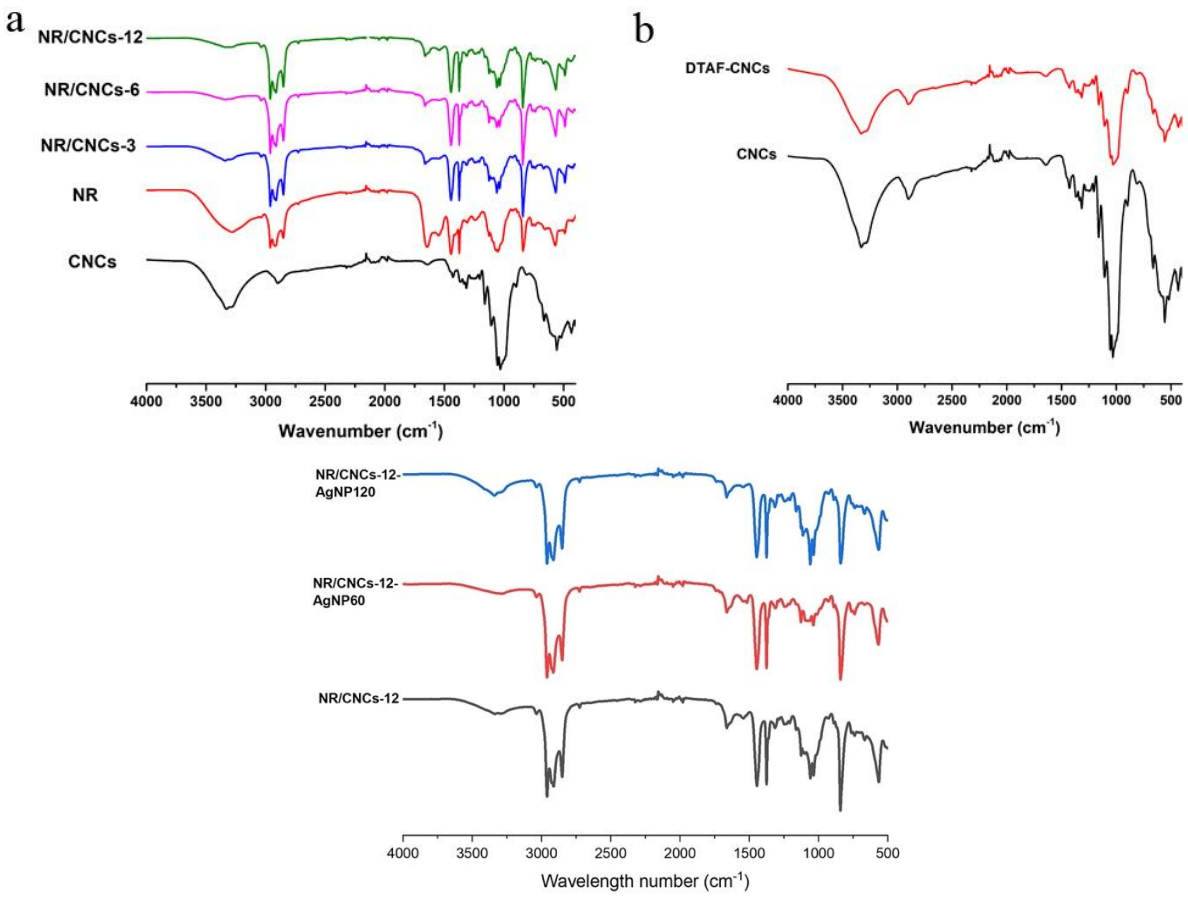

Figure 4.6. Fourier-transform spectra of a) neat NR, CNCs, and NR-CNCs nanocomposite films; b) DTAF-CNCs and unlabeled CNCs c) NR/CNCs nanocomposite and NR/CNCs-AgNPs films

4.2.2 NR/CNCs-AgNP nanocomposite films

A comparison between the IR spectra of NR/CNCs and NR/CNCs-AgNPs nanocomposite films was shown in Figure 4.6 c). The results indicated effective incorporation of the silver particles in the nanocomposite films. NR/CNCs-12-AgNP60 shows a flattened peak at 3290 cm^{-1} (-N-H stretching and -O-H stretching), which indicates the depletion of amide structure in the nanocomposite, which could be due to the fractioning of proteins in the nanocomposite films during green synthesis. This results further confirmed that reactions between silver ions and

reducing agents such as proteins and amino acids was involved in the silver particles synthesis process. Another distinctive difference on the IR spectrum is the decreased intensity of peaks at 1060 cm^{-1} and 1030 cm^{-1} on NR/CNCs-12-AgNP60. These characteristic peaks are associated with the structures of CNCs. The reduction of CNCs characteristics suggested the screening of CNCs surface structures, which can be ascribed to the reduction of Ag^{+} by CNCs and the binding of silver nanoparticles on CNCs backbones. These results confirmed that both CNCs and NR proteins are responsible for the reduction of Ag^{+} during the synthesis of silver particles.

4.2.3 DTAF-grafted CNCs

4.2.3.1 FT-IR spectroscopy

To verify the labelling of DTAF onto the surface of CNCs, DTAF-CNCs were tested on FTIR spectroscopy, in comparison to the IR spectrum of pristine CNCs (Figure 4.6 b)). It was noted the featured peaks of the DTAF-CNCs were similar to that of pristine CNCs. However, a significant decrease in the peak intensity was observed, especially at 3340 cm^{-1} (-O-H stretching), 2920 cm^{-1} (-CH_2 stretching), and 1250-1050 cm^{-1} (C-O-C stretching in pyranose and the glycosidic bonds), which was due to the labelling of DTAF onto the surface of CNCs.

4.2.3.2 UV-vis spectroscopy

Figure 4.7 shows the UV-*vis* spectra of CNCs in DI water, and DTAF-CNCs in both DI water and pH 7.4 PBS at a concentration of 1g/L. Unlabeled CNCs did not show any absorption peaks in the wavelength range of 350 to 700 nm. However, the DTAF-CNCs exhibited absorption at 488 nm both in DI water and pH 7.4 PBS, indicating DTAF had been successfully labelled onto the surface of CNCs. It was noteworthy that the intensity of the peak of DTAF-CNCs in PBS was stronger than that in DI water, which was due to the deprotonation of the DTAF at higher pH..

Figure 4.8 further demonstrated the absorbance of DTAF-CNCs at various concentrations in DI water and pH 7.4 PBS. It was observed the higher concentration of the DTAF-CNCs in the release mediums, the more pronounced absorbance could be detected. Compared to the pistine CNCs, the labelled CNCs showed significant absorbance at 488 nm, which indicated that DTAF has been successfully grafted onto the surface of CNC.

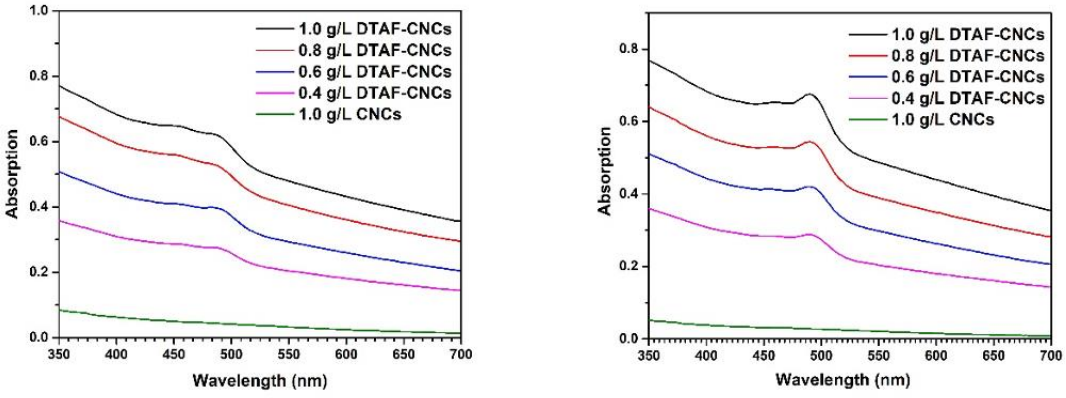

Figure 4.7 UV-*vis* spectra of DTAF-CNCs in DI water and PBS buffer (pH = 7.4).

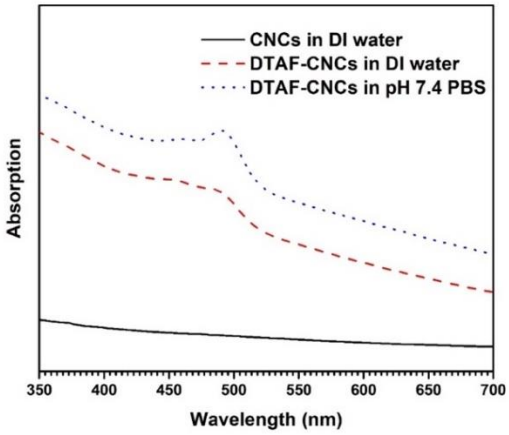

Figure 4.8. UV-*vis* spectra of CNCs in DI water (1g/L), DTAF-CNCs in DI water (1g/L) and DTAF-CNCs in pH 7.4 PBS (1g/L).

4.3 Mechanical properties of films

4.3.1 Tensile properties

The deformation of NR/CNCs nanocomposite films with various CNCs contents were analyzed by tensile test at 25 °C. Typical stress-strain curves of the films were shown in Figure 4.9. It was noted that the addition of CNCs into the NR matrix increased the tensile modulus of the nanocomposite films, as the initial slopes of the curves increased with the increase of CNCs content in the films, indicating the stiffening effect of CNCs on NR films. The tensile strength, tensile modulus, and the elongation at break of NR with the incorporation of 1.5 wt.% of CNCs were not significantly increased, while higher amount of CNCs significantly enhanced the mechanical performance of the nanocomposite films, which indicated a reinforcing threshold of CNCs in the NR/CNCs nanocomposite films existed. This increase in robustness could be due to the formation of a 3D percolative network of CNCs in the NR matrix. This phenomenon has been extensively reported in studies of CNCs-based nanocomposite materials (Bras et al., 2011; Flauzino Neto et al., 2016; Garcia de Rodriguez et al., 2006).

The obtained NR/CNCs nanocomposite films were excellent elastomers, as most of their elongation at break was closed to that of the neat NR film (260%). Specially, the elongation at break of the NR/CNCs nanocomposite film with 6 wt.% of CNCs was significantly increased to 416% of the neat NR film, which was superior to that of the neat NR film. The elongation at break is generally affected by the concentration of the nanofiller, the dispersion of the nanofiller, and the interaction between the nanofiller and the matrix (Khoshkava & Kamal, 2014). In this study, a

higher elongation at break on the NR/CNC-6 could be due to the incorporation of CNCs at optimal NR/CNCs weight ratio. At 6 wt.%, CNCs were able to reinforce the nanocomposite films better than NR/CNCs-3 and NR. The high elongation at break could insinuate that a better dispersion of CNCs was obtained at 6 wt.% compared to 12 wt.%. Optimal dispersion of CNCs in the nanocomposite enhanced the intermolecular interaction between CNCs and NR matrix, which further strengthened the structure of the film. Since bigger and more aggregates were visibly observed on the NR/CNCs-12, it can be concluded that CNCs were better dispersed in NR/CNCs-6 then in NR/CNCs-12. Therefore, the nanocomposite films with balanced ratio of NR and CNCs showed both increased elongation at break and good mechanical strength.

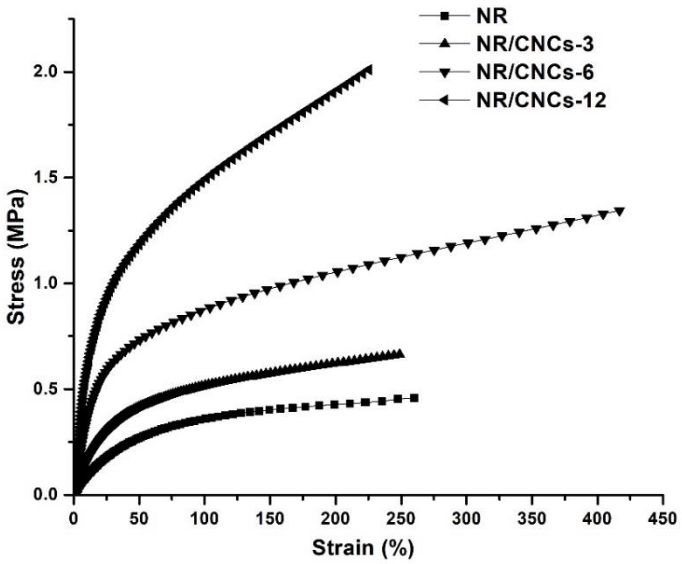

Figure 4.9. Stress-strain relationships obtained from tensile test for NR/CNCs nanocomposite films with various CNCs contents

Furthermore, Figure 4.10 shows the tensile strength and tensile modulus of NR/CNCs nanocomposite films as a function of CNCs content. The tensile strength increased significantly

with the addition of CNCs into the NR matrix, as the tensile strength of neat NR film was 0.46 MPa while that of NR/CNCs nanocomposite film with 12 wt.% of CNCs was 2.01 MPa, which was 4.37-fold enhancement. Additionally, the tensile modulus of the films increased by 24.44-fold from 0.009 MPa to 0.22 MPa as the CNCs content in the films increased from 0 to 12%, which was in accordance with the observation in Figure 4.8, indicating the significant mechanical reinforcement of CNCs in the NR/CNCs nanocomposite films. The excellent reinforcing effect of CNCs could be attributed to the formation of the percolated 3D network at higher concentration, which surpasses the traditional filler-matrix model. It was noted the tensile strength and tensile modulus only change significantly when the CNCs content was higher than 3 wt.%. This could imply that a threshold of CNCs concentration to form percolative network existed in the current study. At concentration lower than 3 wt.%, the percolative threshold was not reached and less mechanical reinforcement was introduced in the nanocomposite films (Habibi et al., 2010).

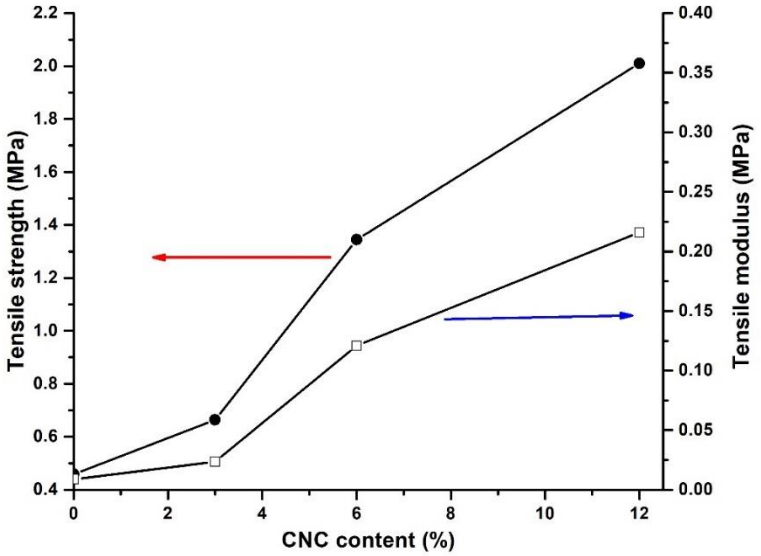

Figure 4.10. Tensile strength and tensile modulus of NR/CNCs nanocomposite films as a function of CNCs content.

4.3.2 Dynamic mechanical properties.

The thermal properties and thermomechanical properties are critical properties to determine the applicability of the fabricated nanocomposite films as urinary catheters. Dynamic mechanical thermal analysis (DTMA) was employed to investigate the thermomechanical behavior of the NR/CNC nanocomposite films. Figure 4.11 shows the evolution of storage modulus in logarithmic scale as a function of temperature in isochronal conditions at a frequency of 1 Hz. In this study, DTMA at amorphous region above the glass-transition temperature (T_g) was investigated. T_g of NR film were reported as around -50 °C, respectively (Bras et al., 2010). Thus, the entire temperature variation range of the DTMA occurred at the rubbery state. As observed, the variation of log (E') of all samples was quite stable and no rapid decrease was observed in a wide range of temperature (30-150 °C). This was ascribed to the highly entangled poly (cis-

isoprene) molecules in the NR latex. Above the T_g, the storage modulus of the films increased significantly with the addition of CNCs, further confirming the reinforcing effect of CNCs in the NR/CNCs nanocomposite films. As observed in the TEM images, CNCs tended to interact with the natural rubber latex particles through electrostatic binding. At CNCs concentration lower than the percolative threshold, CNCs interact with NR latex first and could not form a strong percolated network through self-association. However, when CNCs was added at high concentration, CNCs were more likely to evenly disperse in the NR/CNCs nanocomposite. CNCs became embedded on the matrix of the nanocomposite through electrostatic binding with NR latex, while forming strong percolative network via hydrogen bonding, which further enhanced the mechanical properties of the NR/CNC nanocomposite films.

Additionally, the frequency dependence of the storage modulus (E′) and loss modulus (E′′) of NR, NR/CNCs-3, NR/CNCs-6, and NR/CNCs-12 nanocomposite films were investigated. As shown in Figure 4.12, when compared with the neat NR film, the nanocomposite films were observed with larger storage modulus and loss modulus, indicating the reinforcing effect of CNCs in the NR/CNCs nanocomposite films. Additionally, the E' increased with the increasing frequency for all samples, which was due to the decreased time for molecular relaxation at high frequency. The increasing E' demonstrated the stiffness of the films at higher frequency. It was noted storage modulus (E') of the nanocomposite films reinforced with higher CNCs contents (12 wt.%) were significantly greater than that of the samples with lower CNC contents (3 wt.%), This, again can be ascribed to the formation of the continuous percolated network at CNCs concentration above percolative threshold. The NR/CNC nanocomposite films reinforced with higher content of CNCs (6 $^{wt.}$% and 12 $^{wt.}$%) exhibited elevated storage modulus due to the formation of continuous, rigid percolated network in the matrix. Furthermore, E' was significantly greater than E'' for all

samples. No crossover point appeared between the storage modulus and loss modulus curves during the heating process, indicating that the films displayed solid-like behaviour during DTMA.

Overall, dynamic mechanical analysis of NR/CNC composites did not show any results, which might suggest poor dispersion of CNCs. The reinforcing effect of CNCs in the NR/CNC nanocomposite films further strengthens the network. Generally, E″ is also very sensitive to agglomerates and will show weak spots in poor dispersions. Based on E″, it can be concluded that there were no such weak spots. As expected, due to the similarity of time and temperature effects, Figure 8a,b plots from the temperature and frequency sweeps show the opposite trends. E′ increased with the increase in frequency for all samples, which was caused by the decreased time available for the molecular relaxation at high frequencies, demonstrating the stiffness of the films at higher frequencies.

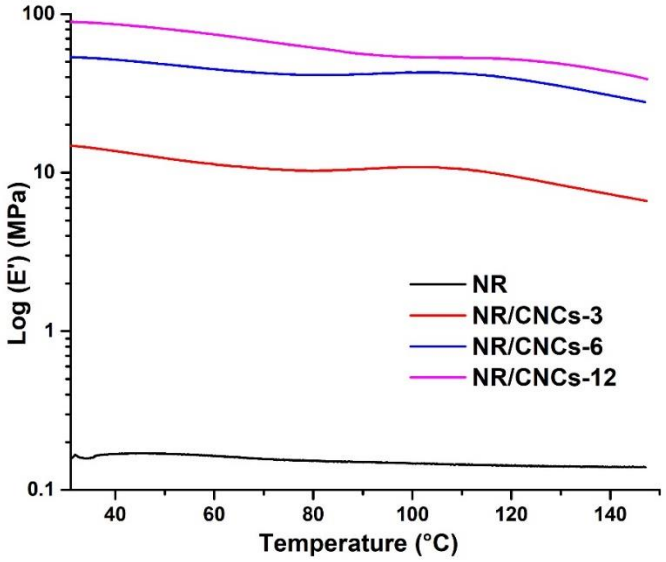

Figure 4.11. Evolution of storage modulus of NR and NR/CNC nanocomposite films as a function of temperature.

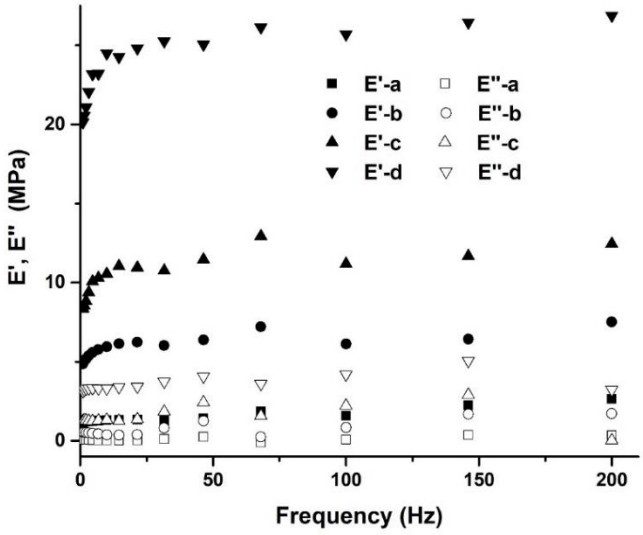

Figure 4.12. Frequency dependence of the storage modulus (E′) and loss modulus (E′′) of NR (a), NR/CNCs-3 (b), NR/CNCs-6 (c), and NR/CNCs-12 (d) nanocomposite films.

4.4 Studies of CNCs release behaviors

Figure 4.13 schematically illustrates the experiment of NR/CNCs nanocomposite immersion in aqueous solutions and release of CNCs particles by assuming there was no particles release from the surfaces of edges. The challenge was to quantify the amount of CNCs released from the nanocomposite films. Therefore, CNCs were firstly labelled with DTAF via chemical grafting techniques and then measured by UV-vis spectrometer for quantifications. To investigate the release profile of CNCs in various aqueous mediums, the standard curves of DTAF-CNCs in DI water, 200 mM NaCl solution, and PBS buffers with various pHs (6.0, 7.4, and 9.0) were linearly fitted in the range of 0-0.5 g/L (R^2=0.994-0.999, Figure SI-4), respectively. The relationship between the UV-vis absorbance of DTAF-CNCs and their concentrations was

established. The released DTAF-CNCs from the NR/CNCs nanocomposite films were then quantified accordingly.

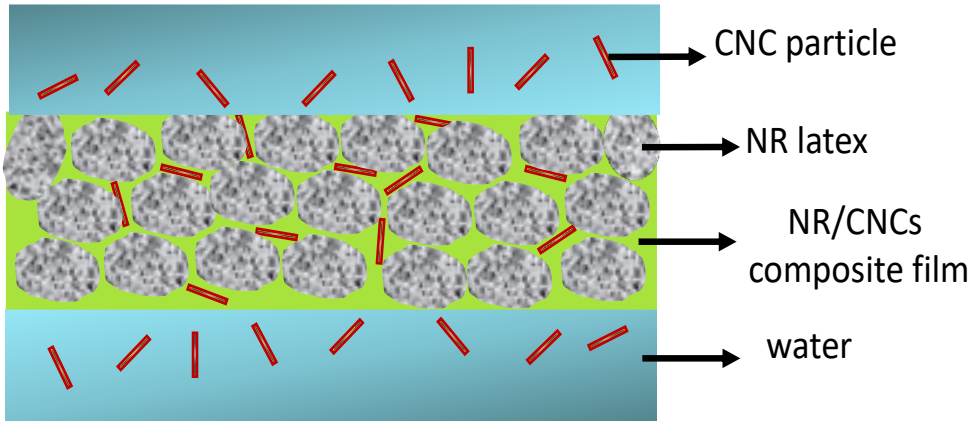

Figure 4.13. Schematic illustration of CNCs transport from NR/CNCs composite into immersed DI water

4.4.1 Release kinetics and behaviors

The cumulative release of CNCs per unit mass of films in different aqueous mediums was monitored at thirteen time points. All samples showed almost no release of CNCs particles during the initial stage ($\boldsymbol{t_0}$), which was likely due to the delay of CNCs diffusion from wetting process. After the lag time $\boldsymbol{t_0}$, a burst of release of CNCs was observed at around 20 hr. The burst release has been observed in various polymeric release systems during the early stage with most of the work focusing on drug delivery (Allison, 2008; Broaders et al., 2011; Hasan et al., 2007). So far, no successful theories have been proposed to understand the underlying mechanisms of burst release. However, the burst release phenomenon can be attributed to several reasons, including the processing conditions, surface characteristics of host materials, sample geometry, filler/excipient interactions, wetting process, and porosity of the material's structure (Huang & Brazel, 2001; Miranda et al., 2017; Siepmann & Siepmann, 2008)

The relationship of cumulative release per unit mass-time was mathematically modeled by the first order equation with the introduction of lag time parameter, $\boldsymbol{t_0}$. This model has been extensively used to monitor the mass transfer of different systems (Grolimund & Borkovec, 1999).

$$Q_t = Q_0(1 - e^{-K(t-t_0)})$$

where Q_t (g CNCs released/g CNCs in the prepared NR/ CNC composite) is the total amount of CNCs released at any time t (h) and Q_0 (g/g) is the ultimate amount of released CNCs at the infinite time from the NR/CNC nanocomposite films. K (h−1) is the rate constant, and t_0(h) is the lag time as prolonged wetting of the nanocomposite surface is needed for release of CNCs at the initial stage. For $t < t_0$, Q_t=0 and no CNCs release were observed, while for $t \geq t_0$, this equation was employed to simulate CNCs release behaviors from the NR/CNCs nanocomposite films.

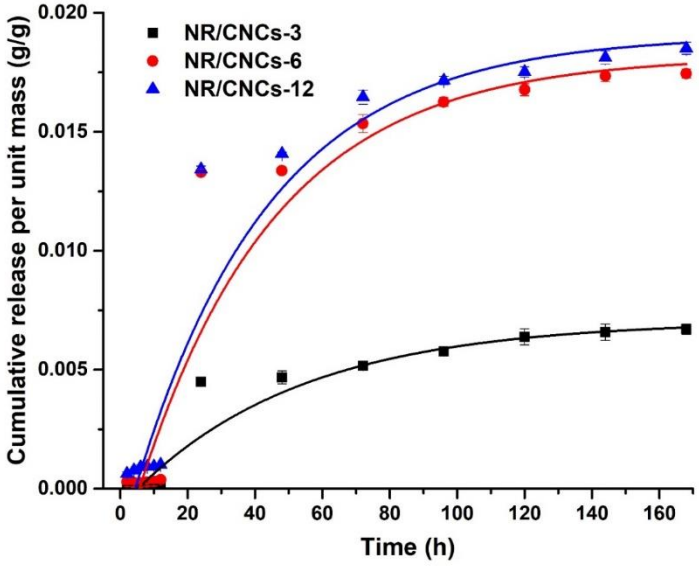

Figure 4.14. The cumulative release of CNCs per unit mass of the NR/CNCs nanocomposite films with various contents of CNCs in DI water. Legends show 3, 6, 12% of CNCs in samples,

respectively. The scattered plots show the experimental data, and the profile curves show the results simulated by the model

As summarized in Table 4.2, the samples in various release mediums showed acceptable values of r^2 (0.93624-0.98646), indicting a good fitting of the experimental data to predicted values. The value of Q_0, which demonstrated the cumulative release at infinite time, increased with increasing the content of CNCs in the nanocomposite films. For each sample studied in different release mediums, there was a clear trend that DI water maximized the release of CNCs from the nanocomposite films, while a pH of 7.4 mostly resulted in lowest Q_0. Therefore, it is worthwhile to investigate the effect of CNCs concentrations in the films, pH, and ionic strength of the release mediums on the release behaviors of CNCs from NR/CNCs nanocomposite films.

Table 4.2. The release kinetics of CNCs from NR/CNCs nanocomposite films in different mediums.

Samples	Release mediums	Release kinetics (First order)			
		r^2	K (h^{-1})	t_0(h)	Q_0 ($g.cm^{-2}.cm^{-1}$)
NR/CNCs-3	DI water	0.97765	0.02	8.26	0.01
	NaCl (200mM)	0.96971	0.02	6.97	0.01
	PBS6.0	0.96341	0.05	1.71	0.01
	PBS7.4	0.97606	0.03	3.65	0.01
	PBS9.0	0.96079	0.03	4.13	0.01
NR/CNCs-6	DI water	0.97031	0.02	6.66	0.02
	NaCl (200mM)	0.96539	0.02	5.75	0.01

	PBS6.0	0.93624	0.02	2.60	0.01
	PBS7.4	0.96513	0.04	3.39	0.01
	PBS9.0	0.96579	0.03	4.04	0.01
NR/CNCs-12	DI water	0.97273	0.02	6.68	0.02
	NaCl (200mM)	0.9557	0.02	4.03	0.01
	PBS6.0	0.98646	0.04	2.25	0.01
	PBS7.4	0.98131	0.04	1.98	0.01
	PBS9.0	0.97575	0.02	3.92	0.02

4.4.2 Effect of CNCs concentrations in nanocomposite films.

As shown in Figure 4.14, the release of CNC particles has been delayed on all samples by a time period, characterized as lag time, while the cumulative release per unit mass was around 0. K values of these three samples were not significant different (0.02024-0.02492). The same trend was observed while immersing NR/CNCs-3, NR/CNCs-6, and NR/CNCs-12 composites in NaCl (200 mM), PBS6.0, PBS7.4, and PBS9.0 solutions. Those results indicate that the amount of CNCs in the NR/CNC nanocomposite films did not significantly influence the release rate (K). However, the lag time decreased from 8.26 to 6.68 by increasing CNCs in NR/CNCs composites from 3 to 12.0% in DI water. The lag time of particle release from the nanocomposite films was longer at lower CNC concentrations. A denser hydrophobic barrier retarded the release of CNCs in the case of lower CNC concentrations. This trend nevertheless lessened while immersing the NR/CNC composites in other aqueous solutions. The lag time could be synergistically influenced by the content of CNCs, the pH, and the ionic strength. Additionally, the maximum cumulative release

of CNCs per unit mass increased with the increase of CNCs content, as shown in the Figure 4.14. However, there are significant difference between NR/CNCs-3 and its two counterparts. The maximum cumulative release of NR/CNCs-6 and NR/CNCs-12 was about 2-fold higher than that of NR/CNCs-3, which could be ascribed to the higher total amount of CNCs existed in the NR/CNCs-6 and NR/CNCs-12. It was noticed the maximum cumulative release of CNCs didn't show significant difference between the NR/CNCs-6 and NR/CNCs-12, which could be caused by the limited CNCs migration from the bulk of the nanocomposite films. As the content of CNCs increased, more CNCs are embedded in the inner section of the films, which are not accessible to the aqueous solution due to the barrier effect of NR matrix.

4.4.3 The effect of pH

Figure 4.15 shows the cumulative release of CNCs per unit mass of the NR/CNCs-3 nanocomposite film in different PBS buffers. It was noted in the Table 4.2 that the lag time t_0 of the release of CNCs in PBS buffers increased with the increase of pH, indicating an acidic condition could facilitate the release of CNCs from the NR/CNCs nanocomposite films, while a more alkaline medium could inhibit the release of CNCs. This could be explained by the sensitivity of NR to different pH conditions. NR has been reported to be more sensitive to acids than to alkaline (Sadaka et al., 2012). Therefore, the NR matrix in the NR/CNCs-3 nanocomposite film was relatively more susceptible to erosion by acidic aqueous environment than an alkaline environment. Thus, the lag time $\boldsymbol{t_0}$ of the release of CNCs in PBS 7.4 buffer and PBS 9.0 buffer was higher than that in PBS 6.0 buffer. Furthermore, it was noted the maximum cumulative release of CNCs per unit mass in PBS 6.0 buffer and PBS 9.0 buffer was higher than that in PBS 7.4 buffer. This could be explained by the synergistic effect of the stability of NR matrix and the electrostatic interactions between CNCs. As CNCs are negatively charged nanoparticles, they tend to form into

aggregates at an acidic condition due to the protonation of the surface functional groups and the screening of the surface charges, while they form a more colloidally stable dispersion at a relatively alkaline conditions due to the strong electrostatic repulsions between each other. A higher pH at 9.0 could improve the dispersibility of CNCs in the aqueous solution, promoting the release of CNCs from the films. Therefore, even though the NR matrix was relatively stable at higher pH, large amount of CNCs could still be released.

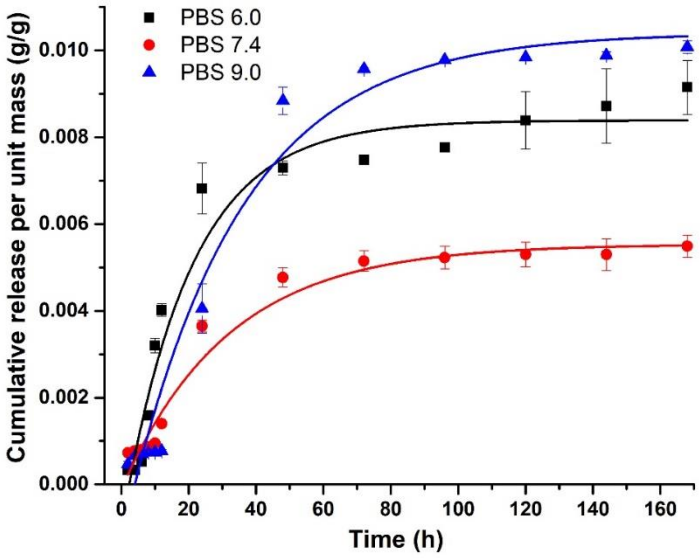

Figure 4.15.The cumulative release of CNCs per unit mass of the NR/CNCs-3 nanocomposite film in PBS buffers with different pHs. Legends show 3, 6, 12% of CNCs in samples, respectively. The scattered plots show the experimental data, and the profile curves show the results simulated by the model.

4.4.4 The effect of ionic strength.

Figure 4.16 shows the release plots of CNCs from the NR/ CNCs-12 nanocomposite film into DI water and the 200 mM NaCl solution. Release values from other NR/CNCs composites are

also summarized in Table 4.2. The lag times t_0 were shorter in the NaCl solution than in DI water for all the NR/CNCs composites. Penetration of the NaCl solution into NR/CNCs composite matrices was faster than with DI water. Therefore, the lag times were getting shorter in faster swollen matrices. On the other hand, the ultimate release of CNCs from NR/CNC nanocomposite films, except for NR/CNCs-3, decreased in salt solutions. This could be, again, due to the migration of NaCl solutions in nanocomposite matrices. CNCs are negatively charged nanoparticles, and adsorption of Na+ on the surface of CNCs can screen the surface charge of CNCs. Therefore, the CNCs in the NR/CNC nanocomposite films could aggregate due to the reduced electrostatic repulsion, thus resulting in a lower amount of ultimate particle releases.

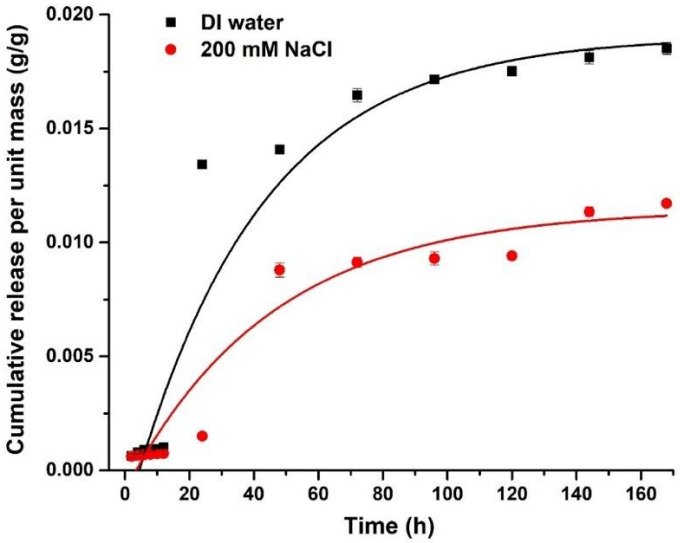

Figure 4.16. The cumulative release of CNCs per unit mass of the NR/CNCs-12 nanocomposite films in DI water and 200 mM NaCl solution. Legends show 3, 6, 12% of CNCs in samples, respectively. The scattered plots show the experimental data, and the profile curves show the results simulated by the model.

4.5 Silver release capacity

The mode of action of silver particles disinfection systems in the current study involves the dissolution of silver particles in the materials and the release of Ag^+ into the de-ionized water. Thus, to investigate the long-term antifouling potency of the silver particles embedded nanocomposite films, it is essential to evaluate the release of Ag^+ from the nanocomposite films in aqueous mediums. A seven-day silver release test was conducted to evaluate the capacity of nanocomposite films to release Ag^+ in aqueous mediums. Figure 4.17 displays the cumulative Ag^+ release in concentration per unit surface area of the films as function of time. The mechanisms of the release process were attributed to the desorption of surface bound Ag^0 solids and the oxidative dissolution of elemental silver in de-ionized water (Dobias & Bernier-Latmani, 2013).

A burst release of Ag^+ was observed on all samples within the first 24 h, which was ascribed to the rapid dissolution of silver particles deposited near and on the surface of the films. The rate of Ag^+ release gradually diminished after the burst release until it a reached plateau at day 7. The slow release could be associated with the slow Ag^+ diffusion through the matrix. With the exhaustion of silver particles on the surface, the rate of Ag^+ release was significantly affected by the diffusion of particles from the inner portion of the films (É. J. Guidelli et al., 2013; Maneerung et al., 2008). It was expected that the release of silver particles embedded at the deeper layers of the films was hindered by the hydrophobic matrix materials (Damm et al., 2007; Pugliara et al., 2015). High contents of NR restricted the permeation of water into the films, inhibiting the wetting of particles in the inner portion, thus slowing down the release process. Therefore, at the initial stage, Ag^+ released depends mainly on the amount of silver particles embedded on the surface (Damm et al., 2007; Huang & Brazel, 2001; J. Li et al., 2019).

The total cumulative Ag^+ at day 7 are not too much different for all three samples, which indicates that the CNCs contents in the film prior to the green synthesis treatment do not significantly influence the total amount of silver generated on the film. However, in the first 8 hour, both NR/CNCs-3-AgNP120 and NR/CNCs-6-AgNP120 showed higher release than NR/CNCs-12-AgNP120, which could be ascribed to the larger and slightly more silver particles contained in NR/CNCs-3-AgNP120 and NR/CNCs-6-AgNP120. SEM results indicated that nanocomposite films with lower CNCs contents contains larger, and more dispersed silver particles compared to films containing higher CNCs contents. Large silver particles provide more stable reservoir, resulting in higher amounts of Ag^+ being released into the aqueous medium. Consequently, NR/CNCs-3-AgNP120 released much higher Ag^+ at the initial stage of the release process.

After day 1, the release of Ag^+ from NR/CNCs-12-AgNP120 gradually increased and exceeded the other two samples. One possible reason for this was the rapid swelling of the film due to the high contents of hydrophilic CNCs. The swelling process enlarged the pores and created microchannels in the sample, resulting in the better diffusion of Ag^+ and Ag^0 particles from the matrix. Other than the particle size and hydrophilicity of the materials, the rate of initial Ag^+ release was also potentially affected by factors such as silver particle shape, surface passivation of silver particles and silver-CNCs interaction. The acknowledgement of these impact requires further investigations and is beyond the scope of this study.

Figure 4.18 shows the cumulative release of silver particles from the nanocomposite films synthesized with different reaction times (60 min, 120 min). The amount of silver particles being deposited on the surface is proportional to the reaction time of the green synthesis, which indicated

that more effective green synthesis reaction between the nanocomposite films and silver nitrate precursors when the reaction time is increased.

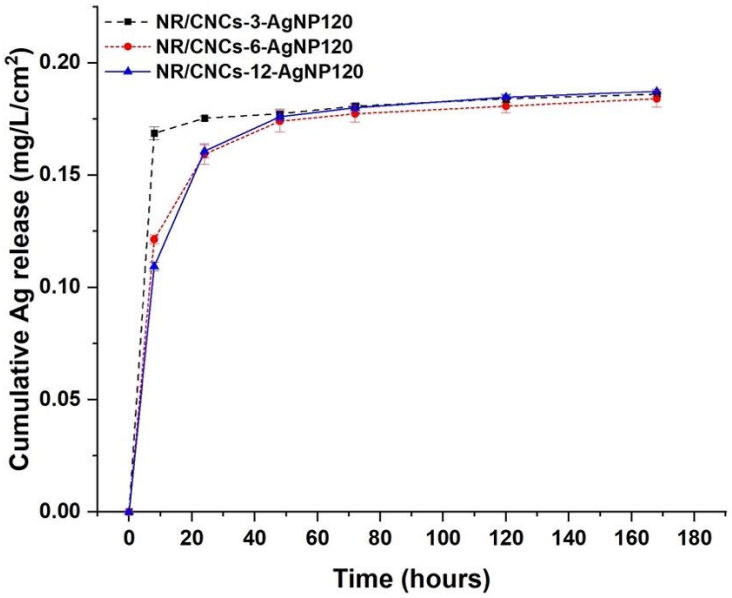

Figure 4.17. The cumulative release of Ag^+ in DI water for silver particles modified nanocomposite films with various contents of CNCs. Scatter plot are experimental data.

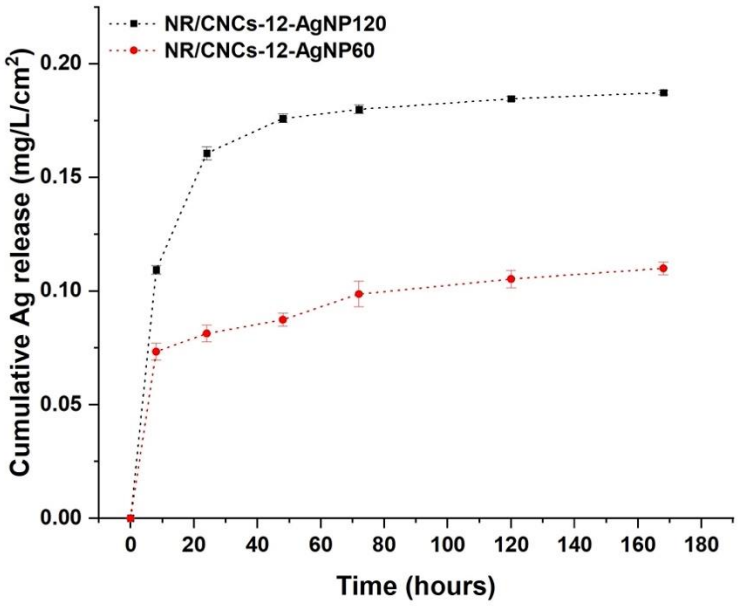

Figure 4.18. The cumulative release of Ag^{+} in DI water for silver particles modified NR/CNCs-12 films processed with different reaction time. The scatter plot is experimental data

4.6 Bacterial adhesion studies

4.6.1 Static condition

To evaluate the antifouling properties of the nanocomposite films, bacteria adhesion assay was conducted. Pristine NR film and nanocomposites films were exposed to liquid medium containing viable gram positive and gram-negative bacteria under static incubation. *Straphylococcus Aureus*, and *Escherichia Coli* were used as model gram positive and gram-negative bacteria, respectively. The antifouling performance of each sample was evaluated by quantifying the bacteria attached on the films by drop plate counting techniques. Figure 4.19 schematically illustrates the proposed anti-adhesion activity of NR/CNCs and NR/CNCs-AgNP nanocomposite films. The anti-adhesion activity of the NR/CNCs films could be mainly attributed

to the release of CNCs from the materials and their flocculation effect against planktonic bacteria. Bacteria flocs or aggregated bacteria experience reduced convective-diffusive transport to the solid surface, and are less prone to surface attachment (Sun et al., n.d., 2012, 2015)

Bacteria adhesion by *E. Coli* and *S. Aureus* in colony forming units (CFU) per unit area of nanocomposite films was depicted Figure 4.20 and Figure 4.21 respectively. Pristine NR film was tested as control. As was demonstrated by the figure, pristine NR had the highest density of bacteria adhered onto the surface. For NR/CNCs nanocomposite films, reduction of bacteria adhesion was observed, which could be ascribed to both the release of the CNCs and the electrostatic repulsion between the CNCs incorporated surfaces and bacteria surfaces. As CNCs particles are negatively charged with the presence of the sulphate and hydroxyl groups, it was expected that the addition of CNCs in the nanocomposite films could increase the surface charge density of the films, resulting in stronger electrostatic repulsion between the bacteria surfaces and nanocomposite films. Both NR/CNCs-6 and NR/CNCs-12 effectively inhibited bacterial adhesion in the first 8 hours of incubation, with 79.6% and 88.5% of bacteria reductions compared to the control, respectively. NR/CNCs-12 exhibited better antifouling performance, which was due to the higher concentration of CNCs being released into aqueous solution at the first 12 hours of immersion. It was noticeable that the antifouling performance of NR/CNCs-6 was less prominent after 24 hours. This could be ascribed to the development of biofilm on the nanocomposite films and the surface conditioning of the films by biofilm associated polymers. Aggregated bacteria and extracellular polymeric substances (EPS) blocked the surface pores and micro-openings of the films, restricting the transport of CNCs from the surface, thus compromising the antifouling effect.

For all NR/CNCs nanocomposite films. the anti-adhesion activity was more effective on *S. Aureus* than *E. Coli*., which can be explained by several reasons. First of all, as was suggested by

(Lekkerkerker & Tuinier, 2011), the depletion efficiency of CNCs on larger colloidal particles depends on the shape of the particles and the geometry of their interactions with CNCs. Due to the remarkable shape difference of the two model bacteria, the CNCs-bacteria interactions are different. Therefore, the required depletant concentration to induce bacterial phase separation are different for these two bacterial systems. In other words, with the same concentration of CNCs in the medium, the bacterial flocculation was triggered at different extent, which explained the variation of the antifouling performance. The difference of bacterial EPS compositions also contributed to the variation of depletion efficiency. Bacterial EPS plays an important role in regulating bacterial aggregations as they can alter the surface charge and hydrophobicity of bacterial surfaces, thereby resulting in a series of different physical and physiochemical interactions. Possible cell-cell interactions include polymer-mediated steric repulsive interactions and polymer bridging attractive interaction. These interactions could significantly impact depletion interaction between bacteria and CNCs, thus resulting in different numbers of bacterial deposited on the surface (An & Friedman, 1998). *E. Coli* bacterium contains high level of negatively charged, colanic acid in its EPS, which make the bacterial surface more hydrophilic. The increase in surface hydrophilicity could induce stronger repulsion of *E. Coli* from the more hydrophilic NR/CNCs nanocomposite films, resulting in slight increase of their deposition on the NR/CNCs nanocomposite films compared to *S. Aureus*.

Modified nanocomposite films incorporated with Ag particles demonstrated excellent anti-adhesion activity. Bacterial adhesions by *E. Coli* and *S. Aureus* were both reduced by over 99% for all samples, which indicated significant inhibition effect against gram positive and gram-negative bacteria. The promising antifouling performance was mainly attributed to the release of silver ions during the two-day incubation, which inactivates bacteria in the incubation medium,

and thereby reducing the bacterial attachment on the surface. NR/CNCs-6-AgNP120 showed slightly better antifouling performance compared to NR/CNCs-12-AgNP120, which was likely due to slightly larger and more silver particles contained in NR/CNCs-6-AgNP120. In addition, Bacteria adhesion by *S. Aureus* was less than *E. Coli* on all samples during the tested time, indicating *S. Aureus* was more susceptible to bactericidal activity of silver particles in the current study. The remarkable difference of their cellular membrane structure might contribute to this phenomenon. Cell walls of typical gram positive bacteria contain three to twenty times more peptidoglycan than gram negative bacteria (Guo & Xu, 2004). The thicker Peptidoglycan makes gram positive bacteria more negatively charged on the surface, which incurs stronger interaction with Ag^{+}, leading to more efficient cell membrane disruption and cell death (Dickson & Koohmaraie, 1989).

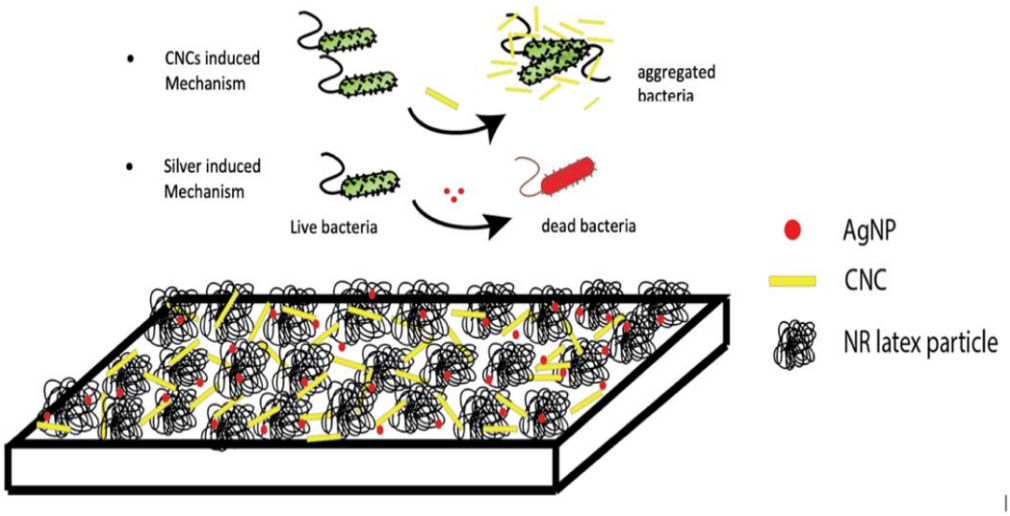

Figure 4.19. Proposed mechanisms of anti-adhesion activity of silver particles modified NR/CNCs nanocomposite films

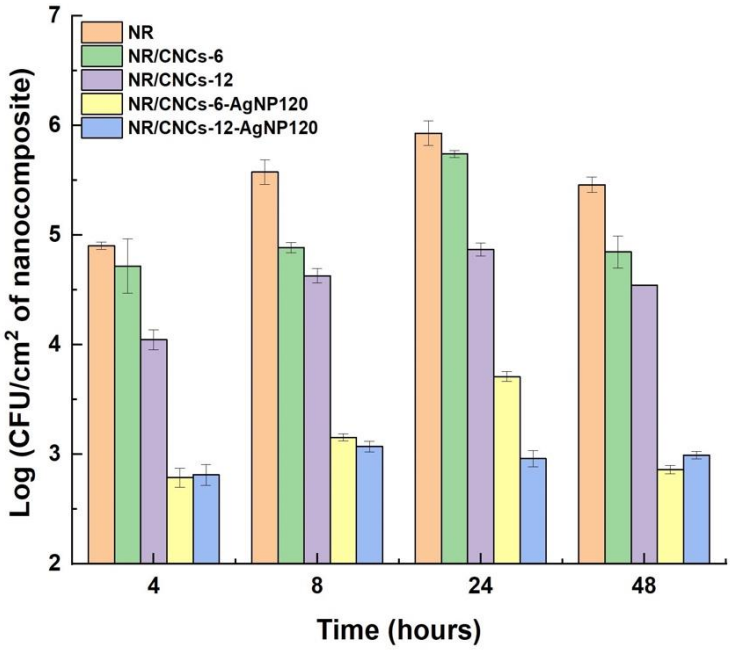

Figure 4.20. Bacteria adhesion on nanocomposite films by *E. Coli* under static conditions at 37 °C

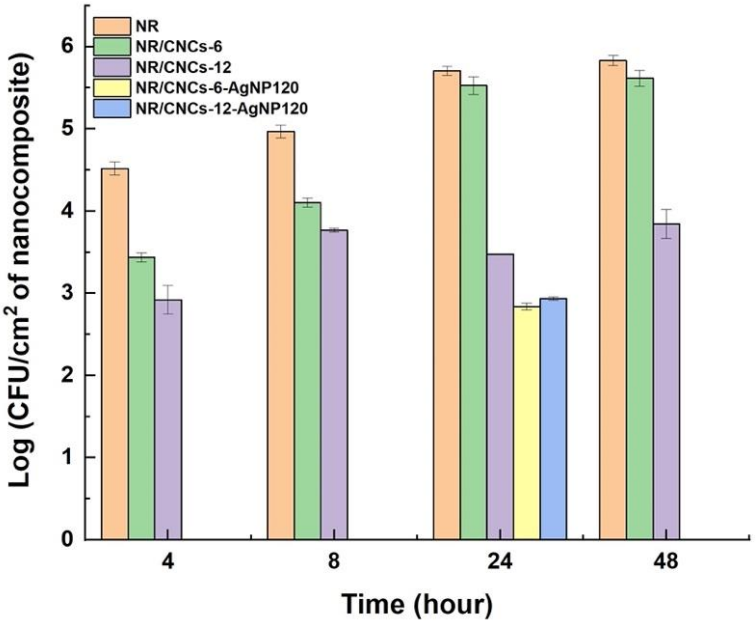

Figure 4.21. Bacteria adhesion on nanocomposite films by *S. Aureus* under static conditions at 37 °C

4.6.1.1 Statistical analysis

Two-way ANOVA (Analysis of Variance) with replications was performed on experimental data of bacteria adhesion test of nanocomposite films at 24 hours incubation, as depicted in table 4.3. Results of bacteria adhesion at fouling period of 24 hours was used for analysis as all results were above detection limit at this fouling time. Each experimental group has four replicates. Both the variance due to the bacteria and the variance due to the materials were statistically significant with P values much less than 0.05. Thus, it can be concluded that the antifouling performance of the nanocomposite films varies by bacteria type. concentration of CNCs, and the presence of silver particles. Variance due to the interaction (bacteria type × materials) was statistically significant, suggesting the antifouling performance of the materials is slightly different for different bacteria type. This has been verified by the results observed. The antifouling performance of NR/CNCs-12-AgNP120 was higher than NR/CNCs-6-AgNP120 in *E. Coli* system but lower in *S. Aureus* system.

Table 4.3. Two-way ANOVA (Analysis of Variance) for the data of bacteria adhesion test (24 hours of fouling) of nanocomposite films

Source of Variation	*SS*	*df*	*MS*	*F*	*P-value*	*F crit*
Variance due to bacteria	2.918	1	2.918	696.41	0.00	4.1708
Variance due to materials	55.65	4	13.91	3320.35	0.00	2.6896
Variance due to interaction	2.631	4	0.657	156.989	0,00	2.6896
Error variance	0.125	30	0.004			
Total	61.33	39				

4.6.2 Continuous flow condition

Figure 4.22 shows the total number of colony forming units on NR/CNCs nanocomposite films, silver particles incorporated nanocomposites films, and pristine NR film under hydrodynamic flow conditions. Synthetic urine containing a constant concentration of viable bacteria (3.3×10^6 cells/mL) was used as flowing medium to simulate the condition in the urinary catheter during urine discharge. 24 ℃ was used as the incubation temperature to perform the experiment. A different incubation temperature (24 ℃) was used for this study. To optimize the experimental designs, the bacteria adhesion on the nanocomposite was evaluated under different temperature (24 ℃, 32℃ and 37℃). The results of the experiments were compared. At higher temperature (32 ℃ and 37 ℃), the total number of bacteria adhered on the samples were

significantly higher than lower temperature (24 ℃) and the difference in the bacteria adhesion was less distinctive as higher temperature allows for faster bacteria accumulation on the surface, which reduced the CNCs release and the exposure of surface charge. Thus, to minimize the implications of surface conditioning and blockage of the surface at the initial stage of CNCs release process, the experiment was conducted at a lower temperature (24 ℃) with slower biofilm formation process. All samples showed anti-adhesion activity against *E. Coli* bacteria. On day 1, bacteria attachment was detected on the NR/CNCs-6 and NR/CNCs-12, with 3.80 to 5.13 logs CFU per cm^2 of material, indicating that the experimental condition provided ideal environment for bacteria growth on the material's surface. Bacteria adhesion was reduced significantly compared to control on NR/CNCs-12 on day 1, with log reductions of 1.32 (95.2%). This result indicated that nanocomposite films inhibited bacterial adhesion more effectively under hydrodynamic flow condition, which could be ascribed to the accelerated release of CNCs and disruption of biofilm formation process when the hydrodynamic shear is introduced into the system. Shear forces accelerated the detachment of CNCs and sessile bacteria from the film, resulting in reduced bacteria deposition (Paul et al., 2012). Additionally, the alkaline nature (pH = 7.80 to 8.00) of the synthetic urine could further promote the release of CNCs from the materials as slightly alkaline conditions could de-aggregate CNCs particles embedded in the nanocomposite films, ultimately accelerating the CNCs diffusion process.

Another factor contributing to the anti-adhesion activity is the enhancement of mechanical properties. Studies have demonstrated that bacteria attachment can be impacted by the substrate stiffness and viscoelastic properties of the materials under hydrodynamic flow condition (Lichter et al., 2008; Song & Ren, 2014; Valentin et al., 2019). The mechanisms of this phenomenon have not been fully understood. However, one explanation can be related to the bacteria-surface

interactions. Soft and viscous surfaces tend to deform more easily when bacteria approach and attach on the surface and this increases their contact surface area and the retention force, leading to stronger bacteria adsorption on the surface. Bacteria contact with rigid surfaces, however, is less likely to trigger surface deformation due to the elastic nature of the materials, and this lead to weaker attachment of bacteria cells (Valentin et al., 2019). As were reported in the previous section, the addition of CNCs in the nanocomposites enhanced stiffness of the films significantly, with the tensile modulus being increased from 0.009 MPa to 2.01 MPa. The reinforcing effect of CNCs resulted in stiffer and more rigid surface formed on the nanocomposite films, which incurs weaker bacteria attachment and lower deposition rate. The speculation of this phenomenon is outside the scope of this study. Thorough characterization of the film surface characteristics and real time monitoring of the adhering bacteria under the dynamic flow conditions should be conducted for further investigation.

The antifouling performance became less prominent with NR/CNCs-12 after day 2, with a log reduction of merely 0.87 (86.5%). The reduced performance can be attributed to the decrease of CNCs release rate between day 2 and day 3. As less CNCs was released during this period, bacteria phase separation in the medium was not effective. On day 5, the antifouling performance of NR/CNCs-12 further reduced, with log reductions of 0.47 (66.1%). It can be expected that after prolonged contact with bacterial foulant medium, the surface became colonized by biofilms and their constituting extracellular polymeric substances, which blocked the pores on the films and restricted the release of CNCs

Bacteria adhesion was under detection limit on all silver particles embedded samples until day 3. After day 3, all samples exhibited excellent anti-adhesion activity against the model *E. Coli* bacteria, demonstrated by bacteria reductions by over 3 log scales (>99.9%). The enhancement of

antifouling performance compared to NR/CNCs films suggested that with the incorporated silver particles and nanoparticles, antibacterial property was successfully introduced into the nanocomposite systems. The anti-adhesion efficiency decreased with prolonged fouling by flowing medium on day 5 and day 7, with log reduction being reduced from 3.65 to 3.20, and 3.88 to 3.10 for NR/CNCs-6-AgNP120 and NR/CNCs-12-AgNP120, respectively. This result is consistent with the silver release study. The antibacterial performance of the modified nanocomposite films depends strongly on the release of Ag^{+} and its bactericidal activity in flow medium. As the silver release rate continually decreased from day 3 to day 7, the antibacterial activity was reduced, leading to increased bacteria adhesion (Dilshad et al., 2020; Guzman et al., 2012).

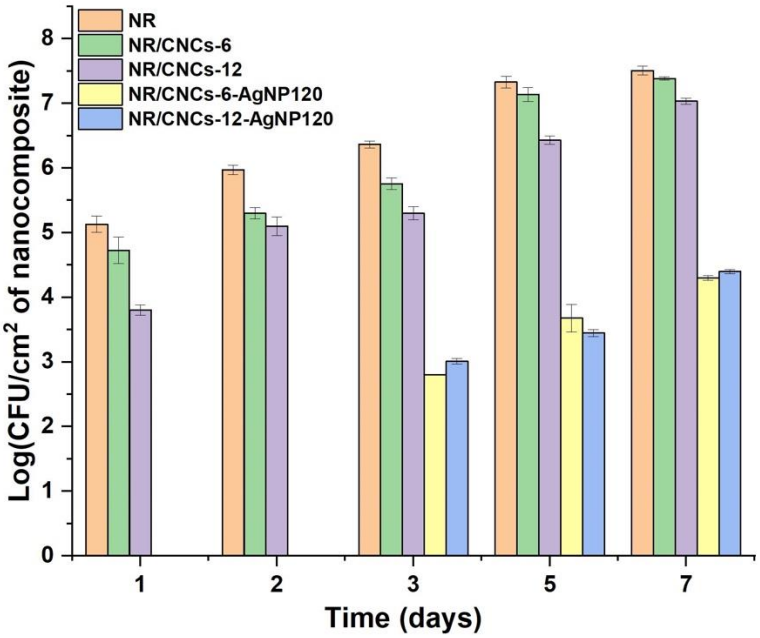

Figure 4.22. Bacterial adhesion on nanocomposite films by *E. Coli* under continuous flow conditions at 24 ℃

Chapter 5 SUMMARY AND CONCLUSIONS

5.1 Conclusion

In this study, mechanically strong natural rubber/CNCs nanocomposite films were prepared by casting/evaporation method to create a non-degradable polymeric system for sustained CNCs release in aqueous solutions. The filler-matrix interactions, the surface characteristics, the mechanical and thermomechanical properties, and the CNCs release capacity in the aqueous solutions were investigated. TEM revealed that CNCs particles do not interact with latex particles in a trended manner. However, they formed, dense, congregated networks at the presence of NR latex particles. The average length and width of the individual CNC particles are 103±26 nm and 10±5 nm (n=50), respectively. Natural rubber latex particles appear as spherical particles with hairy shell structure. Incorporation of CNCs into the NR latex matrix at high concentration increases the tendency of CNCs to aggregate. The release of CNCs in the aqueous solutions was studied using fluorescein labeling techniques. For accurately quantifying CNCs in the aqueous mediums, DTAF fluorescein was chemically grafted onto the CNCs particles, and the fluorescein grafted CNCs were used to prepare the nanocomposite samples. To mathematically model the CNCs release process, first-order release kinetics were adapted with lag time parameter, which signifies the time delay for the release process. Lag time decreased with increasing CNCs contents in the materials as relatively higher NR content in the nanocomposite films hinders water permeation into the films, which restricts the release of CNCs. Both slightly acidic and slightly alkaline conditions facilitate the release of CNCs. Acidic conditions cause the erosion of natural rubber latex, which promotes the detachment of CNCs from NR matrix. At slightly alkaline condition, CNCs have better dispersibility due to the deprotonation of surface groups. CNCs are

thus prone to diffuse into the aqueous medium through osmotic pressure, which increases the total cumulative release. Higher ionic strength of the aqueous medium can inhibit the CNCs release process as the presence of salts causes the charge screening of CNCs particles, which destabilizes colloidal CNCs. Consequently, the release of CNCs were limited due to the compromised dispersibility of CNCs in the aqueous medium.

Silver particles embedded NR/CNCs nanocomposite films were produced using green synthesis approach with modifications. On the surface of the films, silver particles appeared as clustered, randomly distributed particles. Both reducing the CNCs contents in the films and increasing the reaction time for green synthesis could result in the increase of silver particles size on the samples. All silver particles embedded nanocomposite films were able to release silver ions in the deionized water for a time range of seven days.

With different concentrations of CNCs incorporated in the films, bacterial adhesion was inhibited by various extent. Under static condition, bacteria adhesions of *E. Coli* and *S. Aureus* were reduced on NR/CNCs-12 by as much as 90% and 95% compared to the control, respectively. The release of CNCs mainly contributed to this phenomenon. Under the continuous flow condition, NR/CNCs nanocomposite films demonstrated slightly better antifouling performance ascribed to the accelerated CNCs release, the increased substrate stiffness, and the disturbance of bacteria attachment by the hydrodynamic shear force. For silver particles modified films, bacteria adhesion was reduced by over 99% compared to the control under static condition and over 99.9% under continuous flow condition. The antifouling performance was attributed to the release of silver ions and their subsequent bactericidal activity in the aqueous solutions.

5.2 Future Recommendations

5.2.1 Understanding of the CNCs release processes

More characterizations of the NR/CNC nanocomposite films are needed to further understand the CNCs release processes under immersion with aqueous mediums. Possible characterizations include crystallinity analysis, characterizations of fluorescein grafted CNCs.

1) Surface porosity study should be performed to understand the structure-functions relationship between the CNCs release kinetics and surface pore characteristics of the films
2) Fluorescein grafting of CNCs can be further studied. Important properties such as grafting density, degree of substitution should be investigated using fluorescence spectroscopy to further understand grafting properties of DTAF dye. Low grafting density is favoured in the current study as the low degree of substitution will allows the preservation of CNCs' intrinsic surface chemistry. The preservation of surface chemistry could further reduce the undesirable physio-chemical interactions between DTAF-g-CNCs and the matrix, thus minimizing the complications of the release study. Furthermore, CNCs release test should be conducted using other fluorescein to verify the results in the current study. Potential covalent grafting dyes include FITC (fluorescein-5'isothiocynate) and Rodamine B isothiocynate.

5.2.2 Understanding of the mechanisms of antifouling activity

The incorporation of CNCs in the NR latex leads to changes of a variety of surface properties, including surface microstructure, porosity, hydrophobicity and surface charge density and distribution. These factors can affect the bacterial attachment on the nanocomposite films. The

roles of these properties on the anti-adhesion activity should be studied separately. Potential studies include contact angle analysis, and surface charge analysis

1) Contact angle measurements reveals the hydrophobicity of the solid surface, which is one of the critical factors affecting the bacteria initial adhesion. Surface hydrophobicity study can be conducted to understand its impact on the materials' antifouling performance
2) The charge density and distribution on the surface of the nanocomposite films can be further analyzed. With these properties known alongside with bacteria zeta potential, interaction energy models can be developed to understand the behavior of nanocomposite films interacting with bacteria (Sun et al., 2015).

5.2.3 Modifications to the processing techniques

The nanostructure and surface roughness of the nanocomposite films are essential properties that affect the bacteria initial adhesion. Processing the film by casting and evaporation method can result in inconsistent surface structure and roughness, which alters the nanocomposites' performance to regulate bacteria adhesion. Therefore, modified processing techniques are needed to ensure uniform surface properties. Combination of two of more processing techniques such as spin coating, dip coating, and layer by layer coating can be used.

5.2.4 Optimization of the CNCs release process

To effectively prevent the biofilm formation on indwelling catheters, sustained, and long-term release of the CNCs was typically required for period of more than 14 days. In the current study, less than 20% of the total CNCs used in the nanocomposite were released during first seven days and the remaining CNCs was not effectively released from the inner portion of the films due to the barrier effect of NR. Research should be conducted to improve transport of CNCs from inner portion of the films. One achievable approach is to incorporate hydrophilic polymers into the

nanocomposite as co-matrices. The addition of the hydrophilic components in the NR matrix can potentially increase the water absorption and promote erosion of the film to release CNCs (Pichayakorn et al., 2012). For example, carboxymethyl cellulose (CMC) can be added into the nanocomposite as secondary matrix material to partially replace the natural rubber latex. CMC is a highly water-soluble and possesses anionic charges. Its incorporation increase the water sorption capacity of the nanocomposite significantly (Bajpai & Giri, 2002). CMC is bindable to CNCs and therefore can act as carrier for CNCs release (He et al., 2021).

Furthermore, shorter lag time of CNCs release process is desired as immediate antifouling effect is required for the efficient biofilm inhibition. This can be achieved by introducing smart polymeric systems into the nanocomposite system. Potential selections of materials include temperature-responsive, pH-responsive, and ionic strength-responsive polymers. Appropriate polymers can be chosen based on the physiochemical condition of the medium. This will allow for fast and on-time dissociation of smart polymers/CNCs complex (An et al., 2001; Zhao & Moore, 2001).

5.2.5 Optimization of the silver release

To develop efficient silver containing antibacterial systems, it is critical to kill most bacteria with minimal amounts of silver and maintain bactericidal activity for longest period. In order to achieve this, silver ions must be released in a slow and progressive manner to maintain low but sufficient concentration to inhibit bacteria growth (Le Ouay & Stellacci, 2015). The silver release study indicates that the rate of the Ag^+ release gradually diminish after the burst release. Effective controls over the release kinetics and surface chemistry are thus required. This can be achieved by control of silver particles size and particle shape, CNCs contents in the nanocomposite films, and the green synthesis conditions. The impact of the processing conditions and silver

nanoparticles properties on the antibacterial efficiency needs further investigations. One of the potential approaches to effectively control the silver particles distributions and particles size is the introduction of capping agents or stabilizers (Dilshad et al., 2020; Dong et al., 2010). A possible candidate capping agent is tempo oxidized CNCs. Tempo-oxidized CNCs contains carboxyl groups, which can inhibit the adsorption of silver ions through steric hindrance. This prevents the nucleation of silver nanoparticles and potentially promotes the formation of smaller, and homogeneously distributed silver particles on the films (Hoeng et al., 2015)

Nevertheless, silver particles should be synthesized in a more effective controlled manner. More research needs to be conducted to further study the kinetics and mechanisms of silver nanoparticles release in aqueous solutions with various physiochemical conditions

5.2.6 Antifouling performance of nanocomposite films in immersed human urine

In this study, synthetic urine was used as the foulant for evaluation of the nanocomposites' antifouling properties. As was indicated by the current and previous studies, The pH, ionic strength, and the chemical compositions of the aqueous medium have significant impacts on the CNCs release behaviors and the bacterial interaction in the colloidal systems (Gong et al., 2021; Sun et al., 2015). Aqueous solutions with slightly alkaline condition or/and lower ionic strength tend to enhance the dispersity of CNCs in the aqueous medium, ultimately promoting release of CNCs and the bacterial aggregation induced by CNCs. Compared to synthetic urine, healthy human urine contains a large variety (> 90) of organic compounds, with high composition of citrate, urea, creatine, uric acid, and oxalate. The presence of these charge molecules could lead to conflicting effects on bacterial aggregation. On one hand, higher osmolality could induce the aggregation of CNCs in the colloidal system as the shortened distance between CNCs particles at the high concentration of organic particles promote the self-association of CNCs. This can reduce the

depletion potential of CNCs in the bacterial system. In addition, the presence of excess level of ions, particularly cations, could induce conformational changes of the surface polymers on the bacterial cells, increasing the polymer rigidity. Electrostatic repulsion is thus enhanced between bacteria, which reduces their aggregation (Chen & Walker, 2007). On the other hand, negatively charged compounds adsorbing onto the CNCs and bacterial surface could potentially increase the zeta potential of CNCs in the dispersion, ultimately enhancing the depletion attractions of bacteria. The clinical development of the disinfecting technology in this research replies on the efficient bacteria flocculation at the presence of CNCs in real human urine. Thus, future research should focus on the impact of human urine components (uric acid, oxalate, etc.) on the depletion potentials of CNCs particles.

Reference

Abitbol, T., Palermo, A., Moran-Mirabal, J. M., & Cranston, E. D. (2013). Fluorescent labeling and characterization of cellulose nanocrystals with varying charge contents. *Biomacromolecules*, *14*(9), 3278–3284. https://doi.org/10.1021/bm400879x

Aielo, P. B., Borges, F. A., Romeira, K. M., Miranda, M. C. R., Arruda, L. B. D., Paulo, P. N., Drago, B. D. C., & Herculano, R. D. (2014). Evaluation of sodium diclofenac release using natural rubber latex as carrier. *Materials Research*, *17*, 146–152. https://doi.org/10.1590/S1516-14392014005000010

Allison, S. D. (2008). Analysis of initial burst in PLGA microparticles. *Expert Opinion on Drug Delivery*, *5*(6), 615–628. https://doi.org/10.1517/17425247.5.6.615

An, Y. H., & Friedman, R. J. (1998). Concise review of mechanisms of bacterial adhesion to biomaterial surfaces. *Journal of Biomedical Materials Research*, *43*(3), 338–348. https://doi.org/10.1002/(SICI)1097-4636(199823)43:3<338::AID-JBM16>3.0.CO;2-B

An, Y. H., Webb, D., Gutowska, A., Mironov, V. A., & Friedman, R. J. (2001). Regaining chondrocyte phenotype in thermosensitive gel culture. *Anatomical Record*, *263*(4), 336–341. https://doi.org/10.1002/ar.1114

Arias, A., Heuzey, M. C., Huneault, M. A., Ausias, G., & Bendahou, A. (2015). Enhanced dispersion of cellulose nanocrystals in melt-processed polylactide-based nanocomposites. *Cellulose*, *22*(1), 483–498. https://doi.org/10.1007/s10570-014-0476-z

Bajpai, A. K., & Giri, A. (2002). Swelling dynamics of a macromolecular hydrophilic network and evaluation of its potential for controlled release of agrochemicals. *Reactive and Functional Polymers*, *53*(2–3), 125–141. https://doi.org/10.1016/S1381-5148(02)00168-2

Barth, A., & Zscherp, C. (2002). What vibrations tell us about proteins. *Quarterly Reviews of Biophysics*, *35*(4), 369–430. https://doi.org/10.1017/S0033583502003815

Beck-Candanedo, S., Viet, D., & Gray, D. G. (2006). Induced phase separation in low-ionic-strength cellulose nanocrystal suspensions containing high-molecular-weight blue dextrans. *Langmuir*, *22*(21), 8690–8695. https://doi.org/10.1021/la061310j

Bera, R. K., Mandal, S. M., & Raj, C. R. (2014). Antimicrobial activity of fluorescent Ag nanoparticles. *Letters in Applied Microbiology*, *58*(6), 520–526. https://doi.org/10.1111/lam.12222

Bras, J., Hassan, M. L., Bruzesse, C., Hassan, E. A., El-Wakil, N. A., & Dufresne, A. (2010). Mechanical, barrier, and biodegradability properties of bagasse cellulose whiskers reinforced natural rubber nanocomposites. *Industrial Crops and Products*, *32*(3), 627–633. https://doi.org/10.1016/j.indcrop.2010.07.018

Bras, J., Viet, D., Bruzzese, C., & Dufresne, A. (2011). Correlation between stiffness of sheets prepared from cellulose whiskers and nanoparticles dimensions. *Carbohydrate Polymers*, *84*(1), 211–215. https://doi.org/10.1016/j.carbpol.2010.11.022

Broaders, K. E., Pastine, S. J., Grandhe, S., & Fréchet, J. M. J. (2011). Acid-degradable solid-walled microcapsules for pH-responsive burst-release drug delivery. *Chemical*

Communications, *47*(2), 665–667. https://doi.org/10.1039/c0cc04190d

Cao, L., Yuan, D., Fu, X., & Chen, Y. (2018). Green method to reinforce natural rubber with tunicate cellulose nanocrystals via one-pot reaction. *Cellulose*, *25*(8), 4551–4563. https://doi.org/10.1007/s10570-018-1877-1

Chen, G., & Walker, S. L. (2007). Role of solution chemistry and ion valence on the adhesion kinetics of groundwater and marine bacteria. *Langmuir*, *23*(13), 7162–7169. https://doi.org/10.1021/la0632833

Damm, C., Münstedt, H., & Rösch, A. (2007). Long-term antimicrobial polyamide 6/silver-nanocomposites. *Journal of Materials Science*, *42*(15), 6067–6073. https://doi.org/10.1007/s10853-006-1158-5

Damodaran, V. B., & Murthy, S. N. (2016). Bio-inspired strategies for designing antifouling biomaterials. *Biomaterials Research*, *20*(1), 1–11. https://doi.org/10.1186/s40824-016-0064-4

Danna, C. S., Cavalcante, D. G. S. M., Gomes, A. S., Kerche-Silva, L. E., Yoshihara, E., Osorio-Román, I. O., Salmazo, L. O., Rodríguez-Pérez, M. A., Aroca, R. F., & Job, A. E. (2016). Silver Nanoparticles Embedded in Natural Rubber Films: Synthesis, Characterization, and Evaluation of in Vitro Toxicity. *Journal of Nanomaterials*, *2016*. https://doi.org/10.1155/2016/2368630

Darouiche, R. O., & Hull, R. A. (2012). Bacterial interference for prevention of urinary tract infection. *Clinical Infectious Diseases*, *55*(10), 1400–1407.

https://doi.org/10.1093/cid/cis639

Dastjerdi, Z., Cranston, E. D., & Dubé, M. A. (2017). Synthesis of Poly(n-butyl acrylate/methyl methacrylate)/CNC Latex Nanocomposites via In Situ Emulsion Polymerization. *Macromolecular Reaction Engineering*, *11*(6), 1–8. https://doi.org/10.1002/mren.201700013

de Barros, N. R., Miranda, M. C. R., Borges, F. A., de Mendonça, R. J., Cilli, E. M., & Herculano, R. D. (2016). Oxytocin Sustained Release Using Natural Rubber Latex Membranes. *International Journal of Peptide Research and Therapeutics*, *22*(4), 435–444. https://doi.org/10.1007/s10989-016-9523-y

Dias Murbach, H., Jaques Ogawa, G., Azevedo Borges, F., Romeiro Miranda, M. C., Lopes, R., Roberto De Barros, N., Guedes Mazalli, A. V., Gonçalves Da Silva, R., Ferreira Cinman, J. L., De Camargo Drago, B., & Donizetti Herculano, R. (2014). Ciprofloxacin release using natural rubber latex membranes as carrier. *International Journal of Biomaterials*, *2014*. https://doi.org/10.1155/2014/157952

Dickson, J. S., & Koohmaraie, M. (1989). Cell surface charge characteristics and their relationship to bacterial attachment to meat surfaces. *Applied and Environmental Microbiology*, *55*(4), 832–836. https://doi.org/10.1128/aem.55.4.832-836.1989

Dilshad, E., Bibi, M., Sheikh, N. A., Tamrin, K. F., Mansoor, Q., Maqbool, Q., & Nawaz, M. (2020). Synthesis of functional silver nanoparticles and microparticles with modifiers and evaluation of their antimicrobial, anticancer, and antioxidant activity. *Journal of Functional Biomaterials*, *11*(4). https://doi.org/10.3390/jfb11040076

Dizaj, S. M., Lotfipour, F., Barzegar-Jalali, M., Zarrintan, M. H., & Adibkia, K. (2014). Antimicrobial activity of the metals and metal oxide nanoparticles. *Materials Science and Engineering C*, *44*, 278–284. https://doi.org/10.1016/j.msec.2014.08.031

Dobias, J., & Bernier-Latmani, R. (2013). Silver release from silver nanoparticles in natural waters. *Environmental Science and Technology*, *47*(9), 4140–4146. https://doi.org/10.1021/es304023p

Dong, X., Ji, X., Jing, J., Li, M., Li, J., & Yang, W. (2010). Synthesis of triangular silver nanoprisms by stepwise reduction of sodium borohydride and trisodium citrate. *Journal of Physical Chemistry C*, *114*(5), 2070–2074. https://doi.org/10.1021/jp909964k

Donizetti, R., Pereira, C., Ereno, C., Catanzaro, S., Kinoshita, A., & Oliveira, C. (2009). Natural Rubber Latex Used as Drug Delivery System in Guided Bone Regeneration (GBR) 2 . Experimental Section. *Materials Research*, *12*(2), 253–256.

Du, L., Arnholt, K., Ripp, S., Sayler, G., Wang, S., Liang, C., Wang, J., & Zhuang, J. (2015). Biological toxicity of cellulose nanocrystals (CNCs) against the luxCDABE-based bioluminescent bioreporter Escherichia coli 652T7. *Ecotoxicology*, *24*(10), 2049–2053. https://doi.org/10.1007/s10646-015-1555-0

Duchesne, L. C., & Larson, D. W. (1989). Cellulose and the Evolution of Plant Life. *BioScience*, *39*(4), 238–241. https://doi.org/10.2307/1311160

Dufresne, A. (2000). *Plasticized Starch/Tunicin Whiskers Nanocomposites. 1. Structural Analysis*. 8344–8353.

Dufresne, A. (2013). Nanocellulose: A new ageless bionanomaterial. *Materials Today*, *16*(6), 220–227. https://doi.org/10.1016/j.mattod.2013.06.004

Dufresne, A. (2017). 7. Processing of nanocellulose-based materials. In *Nanocellulose*. https://doi.org/10.1515/9783110480412-008

Eboigbodin, K. E., Newton, J. R. A., Routh, A. F., & Biggs, C. A. (2005). Role of nonadsorbing polymers in bacterial aggregation. *Langmuir*, *21*(26), 12315–12319. https://doi.org/10.1021/la051740u

Favier, V., Chanzy, H., & Cavaillé, J. Y. (1995). Polymer Nanocomposites Reinforced by Cellulose Whiskers. *Macromolecules*, *28*(18), 6365–6367. https://doi.org/10.1021/ma00122a053

Flauzino Neto, W. P., Mariano, M., da Silva, I. S. V., Silvério, H. A., Putaux, J. L., Otaguro, H., Pasquini, D., & Dufresne, A. (2016). Mechanical properties of natural rubber nanocomposites reinforced with high aspect ratio cellulose nanocrystals isolated from soy hulls. *Carbohydrate Polymers*, *153*, 143–152. https://doi.org/10.1016/j.carbpol.2016.07.073

Foster, E. J., Moon, R. J., Agarwal, U. P., Bortner, M. J., Bras, J., Camarero-Espinosa, S., Chan, K. J., Clift, M. J. D., Cranston, E. D., Eichhorn, S. J., Fox, D. M., Hamad, W. Y., Heux, L., Jean, B., Korey, M., Nieh, W., Ong, K. J., Reid, M. S., Renneckar, S., … Youngblood, J. (2018). Current characterization methods for cellulose nanomaterials. *Chemical Society Reviews*, *47*(8), 2609–2679. https://doi.org/10.1039/c6cs00895j

Foster, L. L., Yusa, S. I., & Kuroda, K. (2019). Solution-mediated modulation of pseudomonas

aeruginosa biofilm formation by a cationic synthetic polymer. *Antibiotics*, *8*(2). https://doi.org/10.3390/antibiotics8020061

Francolini, I., Vuotto, C., Piozzi, A., & Donelli, G. (2017). Antifouling and antimicrobial biomaterials: an overview. *Apmis*, *125*(4), 392–417. https://doi.org/10.1111/apm.12675

Fu, Y., & Kao, W. J. (2010). Drug release kinetics and transport mechanisms of non-degradable and degradable polymeric delivery systems. *Expert Opinion on Drug Delivery*, *7*(4), 429–444. https://doi.org/10.1517/17425241003602259

Garcia de Rodriguez, N. L., Thielemans, W., & Dufresne, A. (2006). Sisal cellulose whiskers reinforced polyvinyl acetate nanocomposites. *Cellulose*, *13*(3), 261–270. https://doi.org/10.1007/s10570-005-9039-7

Gong, X., Liu, T., Zhang, H., Liu, Y., & Boluk, Y. (2021). Release of Cellulose Nanocrystal Particles from Natural Rubber Latex Composites into Immersed Aqueous Media. *ACS Applied Bio Materials*, *4*(2), 1413–1423. https://doi.org/10.1021/acsabm.0c01310

Grolimund, D., & Borkovec, M. (1999). Long-term release kinetics of colloidal particles from natural porous media. *Environmental Science and Technology*, *33*(22), 4054–4060. https://doi.org/10.1021/es990194m

Guidelli, É. J., Kinoshita, A., Ramos, A. P., & Baffa, O. (2013). Silver nanoparticles delivery system based on natural rubber latex membranes. *Journal of Nanoparticle Research*, *15*(4). https://doi.org/10.1007/s11051-013-1536-2

Guidelli, E. J., Ramos, A. P., Zaniquelli, M. E. D., & Baffa, O. (2011). Green synthesis of colloidal

silver nanoparticles using natural rubber latex extracted from Hevea brasiliensis. *Spectrochimica Acta - Part A: Molecular and Biomolecular Spectroscopy*, *82*(1), 140–145. https://doi.org/10.1016/j.saa.2011.07.024

Guo, T., & Xu, Z. R. (2004). Antibacterial effect of copper-montmorillonite on oral bacteria under anaerobic conditions. *Chinese Journal of Biomedical Engineering*, *23*(3), 259–264.

Gupta, P., Sarkar, S., Das, B., Bhattacharjee, S., & Tribedi, P. (2016). Biofilm, pathogenesis and prevention—a journey to break the wall: a review. *Archives of Microbiology*, *198*(1), 1–15. https://doi.org/10.1007/s00203-015-1148-6

Guzman, M., Dille, J., & Godet, S. (2012). Synthesis and antibacterial activity of silver nanoparticles against gram-positive and gram-negative bacteria. *Nanomedicine: Nanotechnology, Biology, and Medicine*, *8*(1), 37–45. https://doi.org/10.1016/j.nano.2011.05.007

Habibi, Y., Lucia, L. A., & Rojas, O. J. (2010). Cellulose nanocrystals: Chemistry, self-assembly, and applications. *Chemical Reviews*, *110*(6), 3479–3500. https://doi.org/10.1021/cr900339w

Harris, R. H., & Mitchell, R. (1973). *THE ROLE OF POLYMERS IN MICROBIAL AGGREGATION*. 27–50.

Hasan, A. S., Socha, M., Lamprecht, A., Ghazouani, F. El, Sapin, A., Hoffman, M., Maincent, P., & Ubrich, N. (2007). Effect of the microencapsulation of nanoparticles on the reduction of burst release. *International Journal of Pharmaceutics*, *344*(1–2), 53–61. https://doi.org/10.1016/j.ijpharm.2007.05.066

He, Y., Li, H., Fei, X., & Peng, L. (2021). Carboxymethyl cellulose/cellulose nanocrystals immobilized silver nanoparticles as an effective coating to improve barrier and antibacterial properties of paper for food packaging applications. *Carbohydrate Polymers*, *252*(August 2020), 117156. https://doi.org/10.1016/j.carbpol.2020.117156

Helbert, W., Cavaillé, J. Y., & Dufresne, A. (1996). Thermoplastic nanocomposites filled with wheat straw cellulose whiskers. Part I: Processing and mechanical behavior. *Polymer Composites*, *17*(4), 604–611. https://doi.org/10.1002/pc.10650

Herculano, R. D., Guimarães, S. A. C., Belmonte, G. C., Duarte, M. A. H., De Oliveira Júnior, O. N., Kinoshita, A., & De Oliveira Graeff, C. F. (2010). Metronidazole release using Natural Rubber Latex as matrix. *Materials Research*, *13*(1), 57–61. https://doi.org/10.1590/S1516-14392010000100013

Hoeng, F., Denneulin, A., Neuman, C., & Bras, J. (2015). Charge density modification of carboxylated cellulose nanocrystals for stable silver nanoparticles suspension preparation. *Journal of Nanoparticle Research*, *17*(6), 1–14. https://doi.org/10.1007/s11051-015-3044-z

Horwitz, D., McCue, T., Mapes, A. C., Ajami, N. J., Petrosino, J. F., Ramig, R. F., & Trautner, B. W. (2015). Decreased microbiota diversity associated with urinary tract infection in a trial of bacterial interference. *Journal of Infection*, *71*(3), 358–367. https://doi.org/10.1016/j.jinf.2015.05.014

Huang, X., & Brazel, C. S. (2001). On the importance and mechanisms of burst release in matrix-controlled drug delivery systems. *Journal of Controlled Release*, *73*(2–3), 121–136. https://doi.org/10.1016/S0168-3659(01)00248-6

Jenkins, P., & Snowden, M. (1996). Depletion flocculation in colloidal dispersions. *Advances in Colloid and Interface Science*, *68*(1–3), 57–96. https://doi.org/10.1016/s0001-8686(96)90046-9

Joanicot, M., Wong, K., Maquet, J., Chevalier, Y., Pichot, C., Graillat, C., Lindner, P., Rios, L., & Cabane, B. (1990). Ordering of latex particles during film formation. *Progress in Colloid and Polymer Science*, *81*, 175–183. https://doi.org/10.1007/bfb0115548

Kedzior, S. A., Kiriakou, M., Niinivaara, E., Dubé, M. A., Fraschini, C., Berry, R. M., & Cranston, E. D. (2018). Incorporating Cellulose Nanocrystals into the Core of Polymer Latex Particles via Polymer Grafting. *ACS Macro Letters*, *7*(8), 990–996. https://doi.org/10.1021/acsmacrolett.8b00334

Kenawy, E. R., Worley, S. D., & Broughton, R. (2007). The chemistry and applications of antimicrobial polymers: A state-of-the-art review. *Biomacromolecules*, *8*(5), 1359–1384. https://doi.org/10.1021/bm061150q

Khoshkava, V., & Kamal, M. R. (2014). Effect of drying conditions on cellulose nanocrystal (CNC) agglomerate porosity and dispersibility in polymer nanocomposites. *Powder Technology*, *261*, 288–298. https://doi.org/10.1016/j.powtec.2014.04.016

Kosmidis, K., Rinaki, E., Argyrakis, P., & Macheras, P. (2003). Analysis of Case II drug transport with radial and axial release from cylinders. *International Journal of Pharmaceutics*, *254*(2), 183–188. https://doi.org/10.1016/S0378-5173(03)00030-9

Krishnaraj, C., Jagan, E. G., Rajasekar, S., Selvakumar, P., Kalaichelvan, P. T., & Mohan, N.

(2010). Synthesis of silver nanoparticles using Acalypha indica leaf extracts and its antibacterial activity against water borne pathogens. *Colloids and Surfaces B: Biointerfaces*, *76*(1), 50–56. https://doi.org/10.1016/j.colsurfb.2009.10.008

Langer, R. (1990). *New Methods of Drug Delivery*. *1595*(1985), 1527–1534.

Larsen, M. U., Seward, M., & Shapley, N. C. (2008). Biocompatible nanoparticles trigger rapid bacteria clustering. *AIChE Annual Meeting, Conference Proceedings*. https://doi.org/10.1021/bp.179

Lawrence, E. L., & Turner, I. G. (2005). Materials for urinary catheters: A review of their history and development in the UK. *Medical Engineering and Physics*, *27*(6), 443–453. https://doi.org/10.1016/j.medengphy.2004.12.013

Le Ouay, B., & Stellacci, F. (2015). Antibacterial activity of silver nanoparticles: A surface science insight. *Nano Today*, *10*(3), 339–354. https://doi.org/10.1016/j.nantod.2015.04.002

Lekkerkerker, H. N. W., & Tuinier, R. (2011). Colloids and the Depletion Interaction. In *Lecture Notes in Physics* (Vol. 833). https://doi.org/10.1007/978-94-007-1223-2_1

Lewis, K. (2007). Persister cells, dormancy and infectious disease. *Nature Reviews Microbiology*, *5*(1), 48–56. https://doi.org/10.1038/nrmicro1557

Li, J., Kang, L., Wang, B., Chen, K., Tian, X., Ge, Z., Zeng, J., Xu, J., & Gao, W. (2019). Controlled Release and Long-Term Antibacterial Activity of Dialdehyde Nanofibrillated Cellulose/Silver Nanoparticle Composites. *ACS Sustainable Chemistry and Engineering*, *7*(1), 1146–1158. https://doi.org/10.1021/acssuschemeng.8b04799

Li, Q., Mahendra, S., Lyon, D. Y., Brunet, L., Liga, M. V., Li, D., & Alvarez, P. J. J. (2008). Antimicrobial nanomaterials for water disinfection and microbial control: Potential applications and implications. *Water Research*, *42*(18), 4591–4602. https://doi.org/10.1016/j.watres.2008.08.015

Liang, Y., Hilal, N., Langston, P., & Starov, V. (2007). Interaction forces between colloidal particles in liquid: Theory and experiment. *Advances in Colloid and Interface Science*, *134–135*, 151–166. https://doi.org/10.1016/j.cis.2007.04.003

Lichter, J. A., Thompson, M. T., Delgadillo, M., Nishikawa, T., Rubner, M. F., & Van Vliet, K. J. (2008). Erratum: Substrata mechanical stiffness can regulate adhesion of viable bacteria (Biomacromolecules (2008) vol 9 (1574-1576)). *Biomacromolecules*, *9*(10), 2967. https://doi.org/10.1021/bm8009335

Liu, H., Wang, D., Song, Z., & Shang, S. (2011). Preparation of silver nanoparticles on cellulose nanocrystals and the application in electrochemical detection of DNA hybridization. *Cellulose*, *18*(1), 67–74. https://doi.org/10.1007/s10570-010-9464-0

Lokanathan, A. R., Uddin, K. M. A., Rojas, O. J., & Laine, J. (2014). Cellulose nanocrystal-mediated synthesis of silver nanoparticles: Role of sulfate groups in nucleation phenomena. *Biomacromolecules*, *15*(1), 373–379. https://doi.org/10.1021/bm401613h

Loo, C. Y., Young, P. M., Lee, W. H., Cavaliere, R., Whitchurch, C. B., & Rohanizadeh, R. (2012). Superhydrophobic, nanotextured polyvinyl chloride films for delaying Pseudomonas aeruginosa attachment to intubation tubes and medical plastics. *Acta Biomaterialia*, *8*(5), 1881–1890. https://doi.org/10.1016/j.actbio.2012.01.015

Lopez, A. I., Kumar, A., Planas, M. R., Li, Y., Nguyen, T. V., & Cai, C. (2011). Biofunctionalization of silicone polymers using poly(amidoamine) dendrimers and a mannose derivative for prolonged interference against pathogen colonization. *Biomaterials*, *32*(19), 4336–4346. https://doi.org/10.1016/j.biomaterials.2011.02.056

Mallakpour, S., & Naghdi, M. (2018). Polymer/SiO2 nanocomposites: Production and applications. In *Progress in Materials Science* (Vol. 97, Issue June 2017). https://doi.org/10.1016/j.pmatsci.2018.04.002

Maneerung, T., Tokura, S., & Rujiravanit, R. (2008). Impregnation of silver nanoparticles into bacterial cellulose for antimicrobial wound dressing. *Carbohydrate Polymers*, *72*(1), 43–51. https://doi.org/10.1016/j.carbpol.2007.07.025

Mariano, M., El Kissi, N., & Dufresne, A. (2014). Cellulose nanocrystals and related nanocomposites: Review of some properties and challenges. *Journal of Polymer Science, Part B: Polymer Physics*, *52*(12), 791–806. https://doi.org/10.1002/polb.23490

Mariano, M., El Kissi, N., & Dufresne, A. (2016). Cellulose nanocrystal reinforced oxidized natural rubber nanocomposites. *Carbohydrate Polymers*, *137*, 174–183. https://doi.org/10.1016/j.carbpol.2015.10.027

Mekonnen, T. H., Ah-Leung, T., Hojabr, S., & Berry, R. (2019). Investigation of the co-coagulation of natural rubber latex and cellulose nanocrystals aqueous dispersion. *Colloids and Surfaces A: Physicochemical and Engineering Aspects*, *583*(August), 123949. https://doi.org/10.1016/j.colsurfa.2019.123949

Mi, L., & Jiang, S. (2014). Integrated Antimicrobial and Nonfouling Zwitterionic Polymers. *Angewandte Chemie International Edition*, *53*(7), 1746-1754.

Miranda, M. C. R., Prezotti, F. G., Borges, F. A., Barros, N. R., Cury, B. S. F., Herculano, R. D., & Cilli, E. M. (2017). Porosity effects of natural latex (Hevea brasiliensis) on release of compounds for biomedical applications. *Journal of Biomaterials Science, Polymer Edition*, *28*(18), 2117–2130. https://doi.org/10.1080/09205063.2017.1377024

Mooibroek, H., & Cornish, K. (2000). Alternative sources of natural rubber. *Applied Microbiology and Biotechnology*, *53*(4), 355–365. https://doi.org/10.1007/s002530051627

Morelli, C. L., Belgacem, M. N., Branciforti, M. C., Salon, M. C. B., Bras, J., & Bretas, R. E. S. (2016). Nanocomposites of PBAT and Cellulose Nanocrystals Modified by in situ Polymerization and Melt Extrusion. *Polymer Engineering and Science*. https://doi.org/10.1002/pen

Nacey, J., & Delahunt, B. (1993). The evolution and development of the urinary catheter. *The Australian and New Zealand Journal of Surgery*, *63*(10), 815–819. https://doi.org/10.1111/j.1445-2197.1993.tb00347.x

Nawamawat, K., Sakdapipanich, J. T., Ho, C. C., Ma, Y., Song, J., & Vancso, J. G. (2011). Surface nanostructure of Hevea brasiliensis natural rubber latex particles. *Colloids and Surfaces A: Physicochemical and Engineering Aspects*, *390*(1–3), 157–166. https://doi.org/10.1016/j.colsurfa.2011.09.021

Ngo, T.-D., Danumah, C., & Ahvazi, B. (2018). Production of Cellulose Nanocrystals at InnoTech

Alberta. *Nanocellulose and Sustainability*, 269–287. https://doi.org/10.1201/9781351262927-12

Noronha, V. T., Camargos, C. H. M., Jackson, J. C., Souza Filho, A. G., Paula, A. J., Rezende, C. A., & Faria, A. F. (2021). Physical Membrane-Stress-Mediated Antimicrobial Properties of Cellulose Nanocrystals. *ACS Sustainable Chemistry and Engineering*, *9*(8), 3203–3212. https://doi.org/10.1021/acssuschemeng.0c08317

Oliveira, A. D. de, & Beatrice, C. A. G. (2019). Polymer Nanocomposites with Different Types of Nanofiller. In *Nanocomposites Recent Evolutions* (pp. 103–128). https://doi.org/10.1016/j.colsurfa.2011.12.014

Pal, S., Tak, Y. K., & Song, J. M. (2007). Does the antibacterial activity of silver nanoparticles depend on the shape of the nanoparticle? A study of the gram-negative bacterium Escherichia coli. *Applied and Environmental Microbiology*, *73*(6), 1712–1720. https://doi.org/10.1128/AEM.02218-06

Pasquini, D., Teixeira, E. de M., Curvelo, A. A. da S., Belgacem, M. N., & Dufresne, A. (2010). Extraction of cellulose whiskers from cassava bagasse and their applications as reinforcing agent in natural rubber. *Industrial Crops and Products*, *32*(3), 486–490. https://doi.org/10.1016/j.indcrop.2010.06.022

Paul, E., Ochoa, J. C., Pechaud, Y., Liu, Y., & Liné, A. (2012). Effect of shear stress and growth conditions on detachment and physical properties of biofilms. *Water Research*, *46*(17), 5499–5508. https://doi.org/10.1016/j.watres.2012.07.029

Phan-Xuan, T., Thuresson, A., Skepö, M., Labrador, A., Bordes, R., & Matic, A. (2016). Aggregation behavior of aqueous cellulose nanocrystals: the effect of inorganic salts. *Cellulose*, *23*(6), 3653–3663. https://doi.org/10.1007/s10570-016-1080-1

Phanthong, P., Reubroycharoen, P., Hao, X., Xu, G., Abudula, A., & Guan, G. (2018). Nanocellulose: Extraction and application. *Carbon Resources Conversion*, *1*(1), 32–43. https://doi.org/10.1016/j.crcon.2018.05.004

Pichayakorn, W., Suksaeree, J., Boonme, P., Amnuaikit, T., Taweepreda, W., & Ritthidej, G. C. (2012). Nicotine transdermal patches using polymeric natural rubber as the matrix controlling system: Effect of polymer and plasticizer blends. *Journal of Membrane Science*, *411–412*, 81–90. https://doi.org/10.1016/j.memsci.2012.04.017

Pugliara, A., Makasheva, K., Despax, B., Bayle, M., Carles, R., Benzo, P., BenAssayag, G., Pécassou, B., Sancho, M. C., Navarro, E., Echegoyen, Y., & Bonafos, C. (2015). Assessing bio-available silver released from silver nanoparticles embedded in silica layers using the green algae Chlamydomonas reinhardtii as bio-sensors. *Science of the Total Environment*, *565*, 863–871. https://doi.org/10.1016/j.scitotenv.2016.02.141

Rai, M., Yadav, A., & Gade, A. (2009). Silver nanoparticles as a new generation of antimicrobials. *Biotechnology Advances*, *27*(1), 76–83. https://doi.org/10.1016/j.biotechadv.2008.09.002

Rhim, J. W., & Lee, J. H. (2004). Effect of CaCl2 treatment on mechanical and moisture barrier properties of sodium alginate and soy protein-based films. *Food Science and Biotechnology*.

Roosjen, A., Van Der Mei, H. C., Busscher, H. J., & Norde, W. (2004). Microbial adhesion to

poly(ethylene oxide) brushes: Influence of polymer chain length and temperature. *Langmuir*, *20*(25), 10949–10955. https://doi.org/10.1021/la0484691

Sadaka, F., Campistron, I., Laguerre, A., & Pilard, J. F. (2012). Controlled chemical degradation of natural rubber using periodic acid: Application for recycling waste tyre rubber. *Polymer Degradation and Stability*, *97*(5), 816–828. https://doi.org/10.1016/j.polymdegradstab.2012.01.019

Sanguansap, K., Suteewong, T., Saendee, P., Buranabunya, U., & Tangboriboonrat, P. (2005). Composite natural rubber based latex particles: A novel approach. *Polymer*, *46*(4 SPEC. ISS.), 1373–1378. https://doi.org/10.1016/j.polymer.2004.11.074

Seabra, A. B., & Durán, N. (2015). Nanotoxicology of metal oxide nanoparticles. *Metals*, *5*(2), 934–975. https://doi.org/10.3390/met5020934

Siepmann, J., & Siepmann, F. (2008). Mathematical modeling of drug delivery. *International Journal of Pharmaceutics*, *364*(2), 328–343. https://doi.org/10.1016/j.ijpharm.2008.09.004

Singha, P., Locklin, J., & Handa, H. (2017). A review of the recent advances in antimicrobial coatings for urinary catheters. *Acta Biomaterialia*, *50*, 20–40. https://doi.org/10.1016/j.actbio.2016.11.070

Siqueira, G., Abdillahi, H., Bras, J., & Dufresne, A. (2010). High reinforcing capability cellulose nanocrystals extracted from Syngonanthus nitens (Capim Dourado). *Cellulose*, *17*(2), 289–298. https://doi.org/10.1007/s10570-009-9384-z

Siqueira, G., Bras, J., & Dufresne, A. (2010). New process of chemical grafting of cellulose

nanoparticles with a long chain isocyanate. *Langmuir*, *26*(1), 402–411. https://doi.org/10.1021/la9028595

Song, F., & Ren, D. (2014). Stiffness of cross-linked poly(dimethylsiloxane) affects bacterial adhesion and antibiotic susceptibility of attached cells. *Langmuir*, *30*(34), 10354–10362. https://doi.org/10.1021/la502029f

Stoodley, P., Sauer, K., Davies, D. G., & Costerton, J. W. (2002). Biofilms as complex differentiated communities. *Annual Review of Microbiology*, *56*, 187–209. https://doi.org/10.1146/annurev.micro.56.012302.160705

Sun, X., Danumah, C., Liu, Y., & Boluk, Y. (2012). Flocculation of bacteria by depletion interactions due to rod-shaped cellulose nanocrystals. *Chemical Engineering Journal*, *198–199*, 476–481. https://doi.org/10.1016/j.cej.2012.05.114

Sun, X., Lu, Q., Boluk, Y., & Liu, Y. (n.d.). Impact of Cellulose Nanocrystals on the Aggregation and Initial Adhesion of Pseudomonas fluorescens Bacteria. In *Encyclopedia of Nanotechnology*. https://doi.org/10.1007/978-94-017-9780-1_101043

Sun, X., Shao, Y., Boluk, Y., & Liu, Y. (2015). The impact of cellulose nanocrystals on the aggregation and initial adhesion to a solid surface of Escherichia coli K12: Role of solution chemistry. *Colloids and Surfaces B: Biointerfaces*, *136*, 570–576. https://doi.org/10.1016/j.colsurfb.2015.09.042

Suwan, T., Khongkhunthian, S., & Okonogi, S. (2019). Silver nanoparticles fabricated by reducing property of cellulose derivatives. *Drug Discoveries & Therapeutics*, *13*(2), 70–79.

https://doi.org/10.5582/ddt.2019.01021

Tian, M., Zhen, X., Wang, Z., Zou, H., Zhang, L., & Ning, N. (2017). Bioderived Rubber-Cellulose Nanocrystal Composites with Tunable Water-Responsive Adaptive Mechanical Behavior. *ACS Applied Materials and Interfaces*, *9*(7), 6482–6487. https://doi.org/10.1021/acsami.6b16308

Treweek, G. P., & Morgan, J. J. (1977). The mechanism of E. coli aggregation by polyethyleneimine. *Colloid and Interface Science*, *60*(2), 258–273.

Umscheid, C. A., Mitchell, M. D., Doshi, J. A., Agarwal, R., Williams, K., & Brennan, P. J. (2011). Estimating the Proportion of Healthcare-Associated Infections That Are Reasonably Preventable and the Related Mortality and Costs. *Infection Control & Hospital Epidemiology*, *32*(2), 101–114. https://doi.org/10.1086/657912

Unagollaa, J. M., & Jayasuriyaa, A. C. (2018). Drug Transport Mechanisms and In Vitro Release Kinetics of Vancomycin Encapsulated Chitosan-Alginate Polyelectrolyte Microparticles as a Controlled Drug Delivery System. *European Jouranl of Pharmaceutical Science*, 199–209. https://doi.org/10.1016/j.physbeh.2017.03.040

Valentin, J. D. P., Qin, X. H., Fessele, C., Straub, H., van der Mei, H. C., Buhmann, M. T., Maniura-Weber, K., & Ren, Q. (2019). Substrate viscosity plays an important role in bacterial adhesion under fluid flow. *Journal of Colloid and Interface Science*, *552*, 247–257. https://doi.org/10.1016/j.jcis.2019.05.043

Visakh, P. M., Thomas, S., Oksman, K., & Mathew, A. P. (2011). Cellulose Nanofibres and

Cellulose Nanowhiskers Based Natural Rubber Composites: Diffusion, Sorption, and Permeation of Aromatic Organic Solvents. *Journal of Applied Polymer Science*, 1614–1623. https://doi.org/10.1002/app

Wang, L., Hu, C., & Shao, L. (2017). The antimicrobial activity of nanoparticles: Present situation and prospects for the future. *International Journal of Nanomedicine*, *12*, 1227–1249. https://doi.org/10.2147/IJN.S121956

Xiong, R., Lu, C., Zhang, W., Zhou, Z., & Zhang, X. (2013). Facile synthesis of tunable silver nanostructures for antibacterial application using cellulose nanocrystals. *Carbohydrate Polymers*, *95*(1), 214–219. https://doi.org/10.1016/j.carbpol.2013.02.077

Xu, S. H., Gu, J., Luo, Y. F., & Jia, D. M. (2012). Effects of partial replacement of silica with surface modified nanocrystalline cellulose on properties of natural rubber nanocomposites. *Express Polymer Letters*, *6*(1), 14–25. https://doi.org/10.3144/expresspolymlett.2012.3

Yang, L., Liu, Y., Wu, H., Song, Z., Høiby, N., Molin, S., & Givskov, M. (2012). Combating biofilms. *FEMS Immunology and Medical Microbiology*, *65*(2), 146–157. https://doi.org/10.1111/j.1574-695X.2011.00858.x

Yin, Q., Wang, D., Jia, H., Ji, Q., Wang, L., Li, G., & Yin, B. (2018). Water-induced modulus changes of bio-based uncured nanocomposite film based on natural rubber and bacterial cellulose nanocrystals. *Industrial Crops and Products*, *113*(February), 240–248. https://doi.org/10.1016/j.indcrop.2018.01.040

Yonashiro Marcelino, M., Azevedo Borges, F., Martins Costa, A. F., De Lacorte Singulani, J.,

Ribeiro, N. V., Barcelos Costa-Orlandi, C., Garms, B. C., Soares Mendes-Giannini, M. J., Herculano, R. D., & Fusco-Almeida, A. M. (2018). Antifungal activity of fluconazole-loaded natural rubber latex against Candida albicans. *Future Microbiology*, *13*(3), 359–367. https://doi.org/10.2217/fmb-2017-0154

Zhang, C., Dan, Y., Peng, J., Turng, L. S., Sabo, R., & Clemons, C. (2014). Thermal and mechanical properties of natural rubber composites reinforced with cellulose nanocrystals from southern pine. *Advances in Polymer Technology*, *33*(S1), 1–7. https://doi.org/10.1002/adv.21448

Zhao, B., & Moore, J. S. (2001). Fast pH- and ionic strength-responsive hydrogels in microchannels. *Langmuir*, *17*(16), 4758–4763. https://doi.org/10.1021/la001709m